Applied Physics Reviews

REVIEW ARTICLE | JULY 09 2024

Modeling quantum optical phenomena using transition currents

Aviv Karnieli ; Nicholas Rivera ; Valerio Di Giulio ; Ady Arie ; F. Javier García de Abajo ; Ido Kaminer

Appl. Phys. Rev. 11, 031305 (2024)
https://doi.org/10.1063/5.0156353

Applied Physics Reviews REVIEW pubs.aip.org/aip/are

Modeling quantum optical phenomena using transition currents

Cite as: Appl. Phys. Rev. **11**, 031305 (2024); doi: 10.1063/5.0156353
Submitted: 28 April 2023 · Accepted: 5 February 2024 ·
Published Online: 9 July 2024

View Online Export Citation CrossMark

Aviv Karnieli,[1,2,a] Nicholas Rivera,[3] Valerio Di Giulio,[4] Ady Arie,[5] F. Javier García de Abajo,[4,6] and Ido Kaminer[2]

AFFILIATIONS

[1]Raymond and Beverly Sackler School of Physics and Astronomy, Tel Aviv University, Ramat Aviv, 69978 Tel Aviv, Israel
[2]Andrew and Erna Viterbi Department of Electrical and Computer Engineering, Technion—Israel Institute of Technology, Haifa 32000, Israel
[3]Department of Physics, Harvard University, Cambridge, Massachusetts 02138, USA
[4]ICFO-Institut de Ciencies Fotoniques, The Barcelona Institute of Science and Technology, 08860 Castelldefels, Barcelona, Spain
[5]School of Electrical Engineering, Fleischman Faculty of Engineering, Tel Aviv University, 69978 Tel Aviv, Israel
[6]ICREA-Institució Catalana de Recerca i Estudis Avançats, Passeig Lluís Companys 23, 08010 Barcelona, Spain

[a)]**Author to whom correspondence should be addressed:** avivkarl@gmail.com

ABSTRACT

Spontaneous light emission is central to a vast range of physical systems and is a founding pillar for the theory of light–matter interactions. In the presence of complex photonic media, the description of spontaneous light emission usually requires advanced theoretical quantum optics tools such as macroscopic quantum electrodynamics, involving quantized electromagnetic fields. Although rigorous and comprehensive, the complexity of such models can obscure the intuitive understanding of many quantum-optical phenomena. Here, we review a method for calculating spontaneous emission and other quantum-optical processes without making explicit use of quantized electromagnetic fields. Instead, we introduce the concept of transition currents, comprising charges in matter that undergo transitions between initial and final quantum states. We show how predictions that usually demand advanced methods in quantum electrodynamics or quantum optics can be reproduced by feeding these transition currents as sources to the classical Maxwell equations. One then obtains the relevant quantum observables from the resulting classical field amplitudes, without washing out quantum optical effects. We show that this procedure allows for a straightforward description of quantum phenomena, even when going beyond the dipole approximation and single emitters. As illustrative examples, we calculate emission patterns and Purcell-enhanced emission rates in both bound-electron and free-electron systems. For the latter, we derive cathodoluminescence emission and energy-loss probabilities of free electrons interacting with nanostructured samples. In addition, we calculate quantum-beat phenomena in bound-electron systems and wave function-dependent optical coherence in free-electron systems. Remarkably, the transition-current formalism captures more complex phenomena, such as many-body interference effects and super-radiance of both bound- and free-electron systems, second-order processes such as two-photon emission, and quantum recoil corrections to free-electron radiation. We review a variety of light–matter interactions in fields ranging from electron microscopy to nanophotonics and quantum optics, for which the transition-current theoretical formalism facilitates practical simulations and a deeper understanding of novel applications.

TABLE OF CONTENTS

I. INTRODUCTION

Spontaneous emission provides a source of insight into light–matter interactions in atomic, molecular,[1–39] and condensed-matter[40–56] systems. Although the fundamental principles of spontaneous emission have been well understood for some time,[57,58] ongoing research explores intriguing variations of this process, including novel light emitters,[3] multipolar transitions beyond the dipole approximation,[2,6,8–15] quantum emission rates through the Purcell effect,[5,16–20,32–39] and exotic variants in nonlinear processes like two-photon emission[13,21–27] and high-harmonic generation.[28,30] Solid-state emitters[40–56] serve as novel single-photon sources[40,48–52] and allow probing the rich physics of excitons.[40,41,46,47,53–56] Additionally, spontaneous emission by free charged particles[59–91] finds applications in particle detection,[63,65] radiation sources,[60,70,82–84] electron microscopy,[61,68,74,77–81,90] and the study of fundamental quantum physics.[64,69,85–89]

The comprehensive understanding of these spontaneous emission phenomena is credited to quantum electrodynamics (QED), where second-quantized electromagnetic field operators are employed.[27,31,92–94] However, it has been recognized that quantizing the electromagnetic field into photons or photonic quasiparticles,[27] though sufficient for describing spontaneous emission, is not entirely necessary.[94,95] Moreover, the conventional QED approach becomes particularly cumbersome when dealing with complex optical media requiring a macroscopic treatment[27,93] [Figs. 1(a) and 1(b)]. Nonetheless, it is important to note that much of the underlying physics can be explained by Maxwell's equations—classical electrodynamics offers a simpler approach to calculating radiation emission by considering the fields emanating from a current source. Notably, ample computational tools are available for such calculations, even in complex structures. This classical perspective proves advantageous for research in various fields, such as nanophotonics,[96] electron beam physics,[90] and quantum optics.[92,94]

Consequently, there is a constant uncertainty between the contrasting ways for calculating radiation emission: cumbersome methods in QED that are usually only practically applicable in simple material configurations, vs the ample tools in classical electrodynamics that apply even in complex environments. Remarkably, there exists a rigorous and intuitive way to find a common ground: the "transition-current formalism" (TCF) of spontaneous emission.[29,97,98] This method can be applied to take the best of both worlds—enabling quantitative QED predictions in complex material configurations by using the established tools of classical electrodynamics.

In this work, we review the TCF for calculating quantum optical phenomena in complex settings. While this method was used in a few pioneering works,[29,97,98] its potential was not fully appreciated by the wider community. This has recently become more relevant than ever, as there is a growing need for a versatile predictive theory in light–matter interactions and quantum optics in arbitrary electromagnetic platforms. For this purpose, we provide a tutorial of the theoretical formalism and complement it with examples of application to explain several phenomena in a variety of light–matter interaction platforms.

The TCF offers an exact description of radiation emission, utilizing electromagnetic field amplitudes from current sources associated with transitions in quantized matter. This method accurately accounts for phenomena like spontaneous emission, photon correlations, and decay rates of systems such as bound electrons in atoms, molecules, and condensed matter, as well as cathodoluminescence (CL) and electron energy-loss spectroscopy (EELS) from free electrons. Additionally, it applies to light emission from many-body systems, and even applies for second-order processes like two-photon emission.

Further, the TCF allows an intuitive understanding while rigorously accounting for quantum interference effects in light emission. Reproducing the same results as in perturbative QED (see Fig. 1), this formalism relies on solving the classical Maxwell equations, decoupling the electromagnetic environment from the sources of radiation (e.g., quantum emitters). This approach accurately captures quantum optical aspects from the emitter, while established classical treatments are employed to determine the radiation field amplitudes.

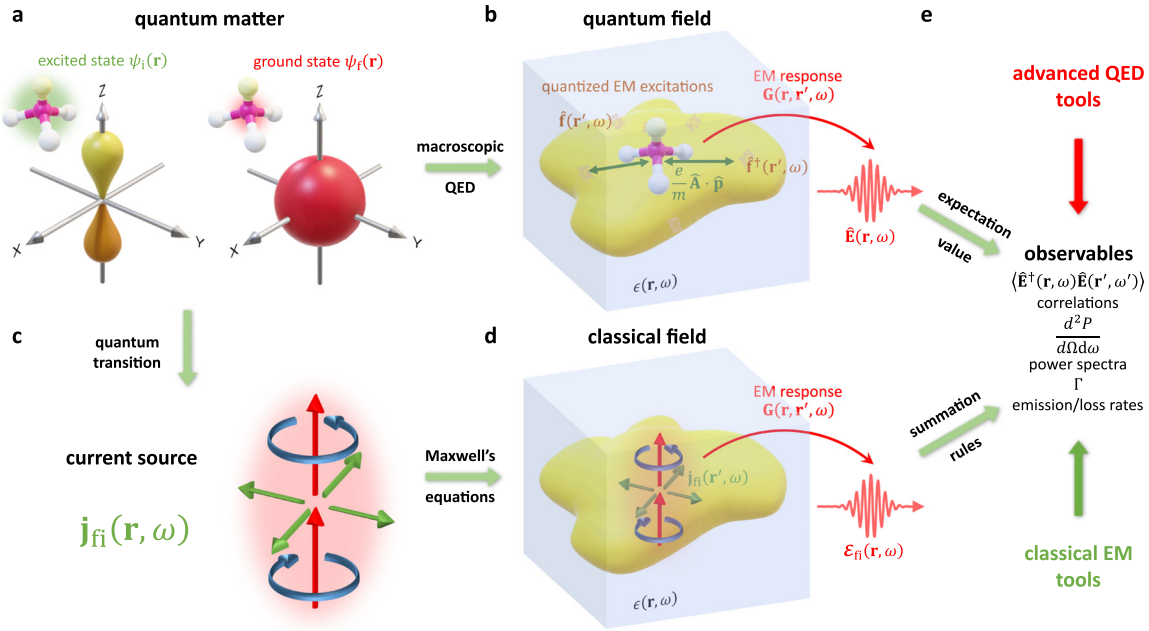

FIG. 1. The transition-current formalism (TCF): concept and equivalence to conventional QED. (a) A quantum emitter can undergo a transition between an initial (e.g., excited) state and a final (e.g., ground) state, with known wave functions. (b) A conventional QED approach for calculating the spontaneous emission transition relies on macroscopic QED for quantitative predictions in arbitrary photonic environments. This approach requires calculating matrix elements between initial and final states from the interaction Hamiltonian, namely, $(e/m)\widehat{\mathbf{A}}\cdot\widehat{\mathbf{p}}$ in the linearized minimal coupling scheme. The electromagnetic field operators $\widehat{\mathbf{A}}$ and $\widehat{\mathbf{E}}$ are quantized in terms of local optical excitation operators $\widehat{\mathbf{f}}(\mathbf{r},\omega)$, which are related to the electric field operator $\widehat{\mathbf{E}}$ at every point in space via the dyadic Green function $\mathbf{G}(\mathbf{r},\mathbf{r}',\omega)$, constituting the electromagnetic response of the medium. (c) The TCF bypasses the cumbersome calculations of conventional QED. This approach defines a current source function $\mathbf{j}_{fi}(\mathbf{r},\omega)$ that captures the transition between the initial and final states. (d) This function is then directly fed as the source of the classical Maxwell equations. The field amplitude solution $\boldsymbol{\mathcal{E}}_{fi}$ can be obtained from the current source using the (classical) dyadic Green function. The final quantum predictions can all be derived using the set of $\boldsymbol{\mathcal{E}}_{fi}$ and $\mathbf{j}_{fi}$ for all the relevant initial and final states. In this picture, one need not explicitly consider the notion of the photon—arriving at the same predictions without a quantized electromagnetic field. (e) The same observables can be derived either using macroscopic QED or transition currents. In macroscopic QED, the expectation value of the field operators is calculated via the rules of quantum theory, considering entanglement with the emitting matter, and tracing out its degrees of freedom. Conversely, the TCF enables the derivation of the same observables using a simple summation of the different classical fields $\boldsymbol{\mathcal{E}}_{fi}$ over the relevant initial and final states.

II. THE TRANSITION-CURRENT FORMALISM: BASIC INGREDIENTS

A. The foundations of the transition-current formalism: Quantum-optical emission from the classical Maxwell equations

Research of spontaneous emission in complex electromagnetic media has mainly concentrated on modifying emission rates (e.g., via the Purcell effect[16]) and molding radiation patterns. Various structures like optical cavities,[34–37,97,99] photonic crystals,[17,38,39,52,100–103] nanoplasmonic structures,[19,29,104–108] metamaterials,[109–114] and two-dimensional materials[43,45,53,115–120] have been probed for enhancing or suppressing spontaneous emission. Analytical calculations are often limited to scenarios that admit closed-form expressions for the medium response and the electromagnetic Green function.[96]

An alternative approach to considering the complex optical environment involves numerical simulations of radiation patterns using solvers of Maxwell's equations. This approach often treats quantum transitions of emitters like atoms, molecules, or free electrons as classical sources. For example, emitters are often modeled as point-dipole sources,[19,97,121] while in areas such as electron microscopy and high-harmonic generation, electron wave functions are described by classical current densities.[66,72,91] However, these simplified semiclassical methods[29,30,91,97,104,121–132] have limited validity,[69,123,124,126,127,129–131] particularly when multiple coherent quantum transitions are present.[32,33,124,133–139] This simplification is also problematic when emitter wave functions extend spatially[40,46,69,123] and become comparable to the emitted wavelength, impacting phenomena such as quantum path interference,[33] quantum decoherence,[140] emission due to delocalized wave functions,[40,46] and quantum recoil corrections.[64,141] These quantum aspects gain importance in phenomena such as quantum beats from multi-level emitters,[32,33,124,133–136,142,143] multipolar transitions in atoms,[2,6,144] spontaneous emission from quantum dots,[40,46] high-harmonic generation,[28,30,123,145] super-radiance,[146–148] and radiation from free electrons.[64,68,69,90,149–151]

To correctly model quantum-mechanical light emission using classical fields, we first need to describe the radiation sources in terms of classical current densities. We consider a generic system in which matter (bound- or free-electron systems) is described by the Hamiltonian $\widehat{H}_{\text{mat}}$, and the electromagnetic field by the Hamiltonian $\widehat{H}_{\text{F}}$. The interaction between them is described by the linear part of the minimal coupling interaction Hamiltonian, $\widehat{H}_{\text{int}} = \frac{e}{m}\widehat{\mathbf{A}}\cdot\widehat{\mathbf{p}}$, where $\widehat{\mathbf{A}}$ denotes the electromagnetic vector potential, $\widehat{\mathbf{p}}$ is the electronic momentum operator (hereon, $\widehat{\cdot}$ denotes an operator), and e and m are the electron charge and mass, respectively. Other forms of the interaction Hamiltonian are considered in Sec. II B, but for now, we exemplify the concept using this ubiquitous form of interaction.

We can associate current densities with the "transition" of the electronic system from an initial state $|\mathrm{i}\rangle$ to a final state $|\mathrm{f}\rangle$. To keep the correspondence with the transition matrix element for emission of a photon in mode $\mathbf{u}_{\boldsymbol{\kappa}}(\mathbf{r})$ that is proportional to $\int d^3\mathbf{r}\psi_{\mathrm{f}}^{*}\mathbf{u}_{\boldsymbol{\kappa}}\cdot(-i\hbar\boldsymbol{\nabla})\psi_{\mathrm{i}}$, this c-number current density, or "transition current," is given by

$$\mathbf{j}_{\mathrm{fi}}(\mathbf{r},t)=\frac{e}{m}\psi_{\mathrm{f}}^{*}(\mathbf{r},t)(-i\hbar\boldsymbol{\nabla})\psi_{\mathrm{i}}(\mathbf{r},t), \tag{1}$$

where $\psi_{\mathrm{i(f)}}(\mathbf{r},t)$ is the wave function of the initial (final) state of the electronic system. As we shall see in Sec. II B, the c-number amplitude $\mathbf{j}_{\mathrm{fi}}(\mathbf{r},t)$ is no other than the matrix element, between states $|\mathrm{i}\rangle$ and $|\mathrm{f}\rangle$, of the current density operator $\widehat{\mathbf{j}}(\mathbf{r})$, which by itself is an observable.

The frequency-domain c-number electric field amplitude is then related to the Fourier transform of the transition current density of Eq. (1) via

$$\boldsymbol{\mathcal{E}}_{\mathrm{fi}}(\mathbf{r},\omega)=i\mu_0\omega\int d^3\mathbf{r}'\mathbf{G}(\mathbf{r},\mathbf{r}',\omega)\mathbf{j}_{\mathrm{fi}}(\mathbf{r}',\omega), \tag{2}$$

where $\mathbf{G}(\mathbf{r},\mathbf{r}',\omega)$ denotes the dyadic electromagnetic Green tensor of the optical medium in question, on which we elaborate in an ensuing section. Therefore, $\boldsymbol{\mathcal{E}}_{\mathrm{fi}}$ is a classical field amplitude associated with the emission of light due to a single transition of the emitter system from state $|\mathrm{i}\rangle$ to state $|\mathrm{f}\rangle$.

The TCF is applicable in more general configurations. For example, oftentimes emitters are prepared in a coherent superposition of different initial states. Such initial quantum coherence can lead to "which path" interference between different emission channels, resulting from non-zero matrix elements from multiple initial states to a common final state. This leads to a coherence that may be inherited by the emitted light [as is the case with quantum beats,[55,56,124,152,153] for example; see Fig. 2(a)]. Since the emitter-light system is inherently

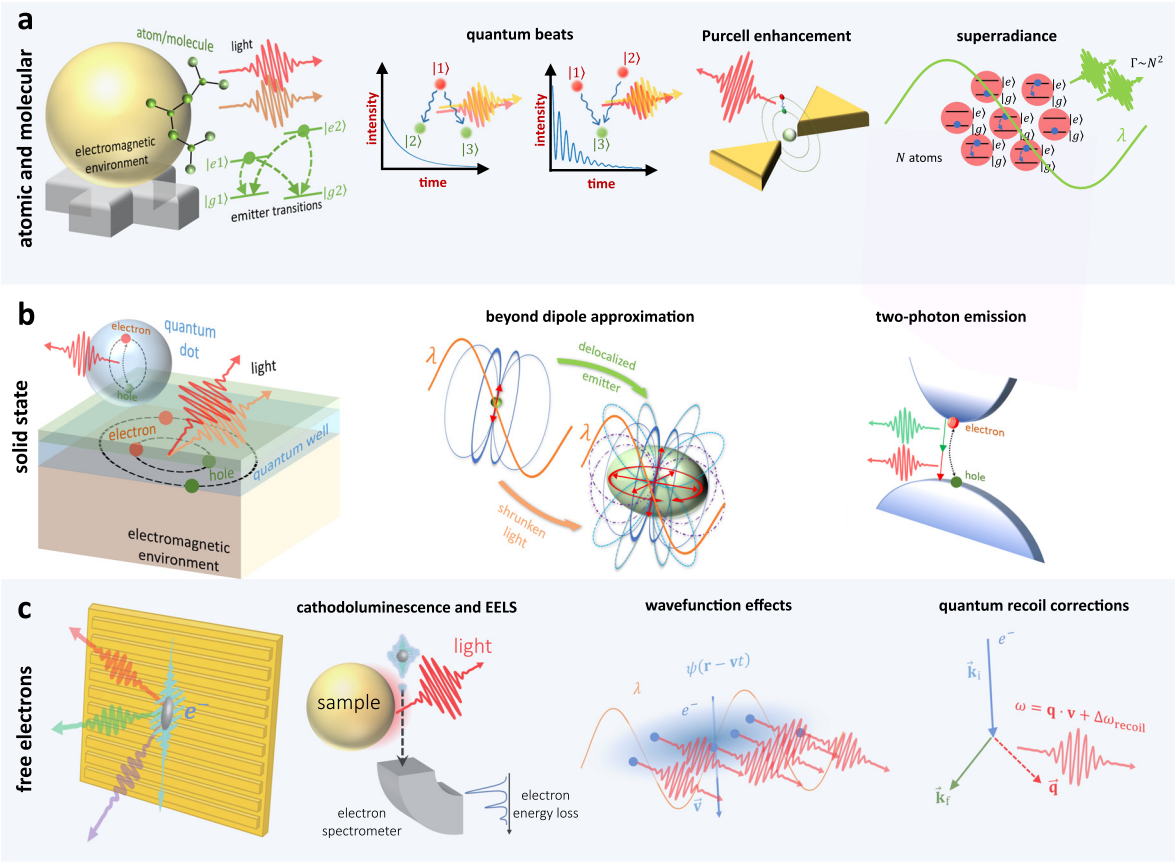

FIG. 2. Applications of the transition-current formalism (TCF) in different physical systems. (a) Atoms and molecules: Examples of effects that can be directly described by the TCF include quantum beats, the Purcell effect and super-radiance. Atoms and molecules are characterized by discrete transitions, and they are often placed near nanophotonic structures, situations of special relevance to the TCF. (b) Solid state emitters: Examples of effects that can be directly described by the TCF include beyond-dipole phenomena and two-photon emission processes. Solid state emitters include, for example, quantum dots and quantum wells, and they can host bound states of electrons and holes called excitons, that upon recombination may emit light. Such emitters are often located in the vicinity of dielectric and metallic interfaces, situations in which the transition-current approach is especially beneficial. (c) Free electrons: Examples of effects that can be directly described by the TCF include interactions of a free electron and a periodic nanostructure resulting in the emission of light—the so-called Smith–Purcell effect, and, more generally, cathodoluminescence and electron energy loss spectroscopy. Other effects include quantum optical decoherence and quantum coherence transfer in free-electron light emission, and quantum recoil corrections in free-electron radiation that change the spectrum of the emitted light. Free-electron emission processes are unique as electrons cannot emit light in free space; however, they can do so when interacting with optical near fields of an electromagnetic environment at any arbitrary spectral range, exactly the situations in which the transition-current approach is applicable.

entangled by the interaction, quantum decoherence[140] plays a major role. Decoherence occurs, for example, when a single emitter finds itself in more than one final state, and when only the light is measured (i.e., only one subsystem of the composite system is measured). In particular, decoherence determines the ability of different modes of the emitted light to interfere coherently. Thus, decoherence has direct implications already on measurables such as the degree of first-order coherence of the electric field.

These effects are often cited as one of the hallmarks of the field of quantum optics.[94] In the language of quantum optics,[154] the degree of first-order coherence is a physical observable that is given by the expectation value of a product of two electromagnetic field "operators" $\hat{\mathbf{E}}$: as in $\langle \hat{\mathbf{E}}^{\dagger}(\mathbf{r},\omega)\hat{\mathbf{E}}(\mathbf{r}',\omega')\rangle$, where $\langle\cdot\rangle$ denotes a quantum expectation value. However, the TCF allows us to recover the same physical observable without the complexity of using the quantum-optical notation of field operators, as described below and illustrated in Fig. 3.

It turns out that, to correctly account for quantum interference between different transitions, and simultaneously capture the effects of decoherence, the field autocorrelation function should be expressed as a coherent summation of the c-number amplitudes $\boldsymbol{\mathcal{E}}_{\mathrm{fi}}$ over initial emitter states, together with an incoherent summation over available final states,

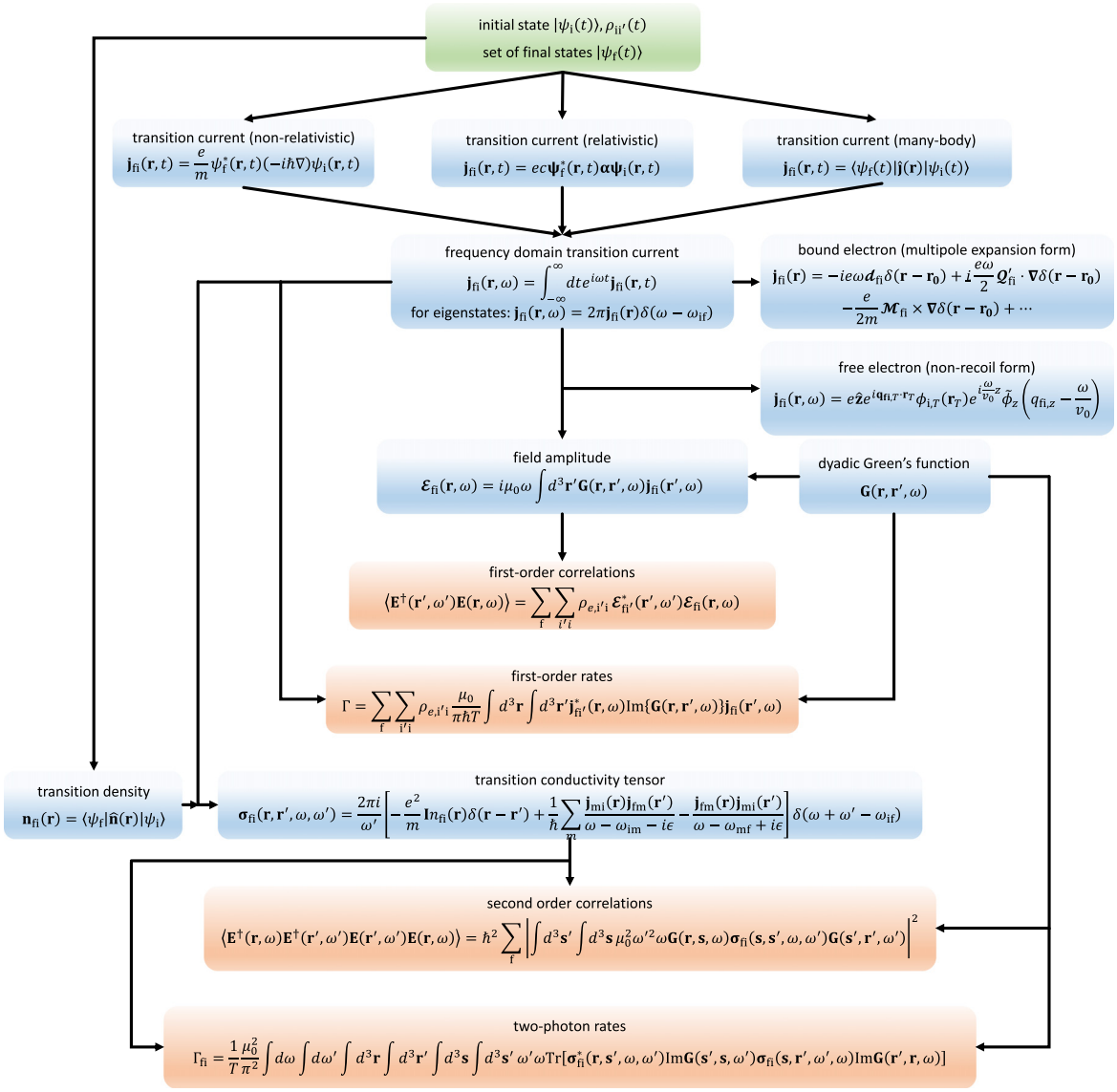

FIG. 3. Flowchart of the transition-current framework. The initial and final quantum states of the emitter define the transition currents, in their various forms, regimes, and system types (e.g., bound and free electrons). Moving to the frequency domain, one can derive the field amplitudes using the dyadic Green function. From there, the first-order correlations, transition rates, and emission patterns could be directly derived. To calculate two-photon processes, one defines the transition conductivity tensor, followed by the use of the dyadic Green function to obtain second-order correlations and two-photon emission rates.

$$\left\langle \widehat{\mathbf{E}}^{\dagger}(\mathbf{r},\omega)\widehat{\mathbf{E}}(\mathbf{r}',\omega')\right\rangle = \sum_{\mathrm{i,i'}}\sum_{\mathrm{f}} \rho_{\mathrm{e}}(\mathrm{i},\mathrm{i}')\boldsymbol{\mathcal{E}}^{*}_{\mathrm{fi}}(\mathbf{r},\omega)\boldsymbol{\mathcal{E}}_{\mathrm{fi}'}(\mathbf{r}',\omega'), \quad (3)$$

where $\rho_{\mathrm{e}}(\mathrm{i},\mathrm{i}')$ denotes the initial density matrix of the emitter. The intuition behind Eq. (3) stems from the above observations: initial states can interfere coherently, and their coefficients are given by the entries of the initial density matrix in the emitter. Moreover, distinct orthogonal final states cannot contribute to coherence, and therefore, they are summed incoherently (i.e., traced-out). In the supplementary material, Secs. SI2–SI3, we prove that the above rule, together with Maxwell's equations, reproduces the results obtained from time-dependent perturbation theory in QED as well as macroscopic QED.

B. Different forms of the transition current

The transition current presented in Eq. (1) is its most common form in previous literature. In this section, we present other forms that are relevant for the different implementations of the TCF. These examples show that the TCF is a general framework that can be directly applied to different interaction Hamiltonians. The results of this subsection are summarized in Table I.

For example, when including the electron spin angular momentum operator $\widehat{\mathbf{S}}$ and the magnetic field $\widehat{\mathbf{B}}$, described by the interaction Hamiltonian $\widehat{H}_{\mathrm{int}} = \frac{e}{m}\widehat{\mathbf{A}}\cdot\widehat{\mathbf{p}} + \frac{e}{m}\widehat{\mathbf{S}}\cdot\widehat{\mathbf{B}}$, the transition current is

$$\mathbf{j}_{\mathrm{fi}}(\mathbf{r},t) = \frac{e}{m}\psi^{*}_{\mathrm{f}}(\mathbf{r},t)(-i\hbar\boldsymbol{\nabla})\psi_{\mathrm{i}}(\mathbf{r},t) + \frac{e}{m}\boldsymbol{\nabla}\left[\psi^{*}_{\mathrm{f}}(\mathbf{r},t)\psi_{\mathrm{i}}(\mathbf{r},t)\right]\times\mathbf{S}_{\mathrm{fi}}, \quad (4)$$

where $\mathbf{S}_{\mathrm{fi}} = \langle \mathrm{f}|\widehat{\mathbf{S}}|\mathrm{i}\rangle$ is the matrix element of the spin operator. We shall use this form for calculating the emission from the hydrogen atom. If one wishes instead to use the symmetrized version of the nonrelativistic interaction Hamiltonian, namely, $\widehat{H}_{\mathrm{int}} = \frac{e}{2m}\widehat{\mathbf{A}}\cdot\widehat{\mathbf{p}} + \frac{e}{2m}\widehat{\mathbf{p}}\cdot\widehat{\mathbf{A}}$, the transition current reads

$$\mathbf{j}_{\mathrm{fi}}(\mathbf{r},t) = \frac{e}{2m}\psi^{*}_{\mathrm{f}}(\mathbf{r},t)(-i\hbar\boldsymbol{\nabla})\psi_{\mathrm{i}}(\mathbf{r},t) - \frac{e}{2m}(-i\hbar\boldsymbol{\nabla})\psi^{*}_{\mathrm{f}}(\mathbf{r},t)\psi_{\mathrm{i}}(\mathbf{r},t). \quad (5)$$

For most cases, the symmetrized form Eq. (5) could be reduced to the asymmetric form in Eq. (1) whenever the permittivity $\epsilon(\mathbf{r})$ is a slowly varying function of position in the vicinity of the emitter. The generalized Coulomb gauge, $\boldsymbol{\nabla}\cdot\left[\epsilon(\mathbf{r})\widehat{\mathbf{A}}\right] = 0$ ensures that, to a good approximation, $\left[\widehat{\mathbf{A}},\widehat{\mathbf{p}}\right] = 0$ at the emitter location, even in more general optical environments.

For relativistic particles, the interaction Hamiltonian emerging from the Dirac equation is $\widehat{H}_{\mathrm{int}} = ec\boldsymbol{\alpha}\cdot\widehat{\mathbf{A}}$, and the transition current becomes

$$\mathbf{j}_{\mathrm{fi}}(\mathbf{r},t) = ec\boldsymbol{\psi}^{\dagger}_{\mathrm{f}}(\mathbf{r},t)\boldsymbol{\alpha}\boldsymbol{\psi}_{\mathrm{i}}(\mathbf{r},t), \quad (6)$$

where $\boldsymbol{\psi}_{\mathrm{i(f)}}(\mathbf{r},t)$ are the initial (final) spinor wave functions and $\boldsymbol{\alpha}$ the Dirac α matrix. Mitigating the complexity of working with spinor wave functions for a relativistic treatment, the scalar Klein–Gordon wave functions with positive energy,

$$E(\mathbf{k}) = \sqrt{\hbar^2k^2c^2 + m^2c^4}, \quad (7)$$

and the interaction Hamiltonian $\widehat{H}_{\mathrm{int}} = \frac{e}{m\gamma}\widehat{\mathbf{A}}\cdot\widehat{\mathbf{p}}$ with the Lorentz factor γ, can be employed, yielding

$$\mathbf{j}_{\mathrm{fi}}(\mathbf{r},t) = \frac{e}{m\gamma}\psi^{*}_{\mathrm{f}}(\mathbf{r},t)(-i\hbar\boldsymbol{\nabla})\psi_{\mathrm{i}}(\mathbf{r},t). \quad (8)$$

Finally, when using second quantization to describe the emission by a many-particle system, it is common to consider the current operator, which takes the form

$$\widehat{\mathbf{j}}(\mathbf{r}) = \frac{e\hbar}{2im}\widehat{\psi}^{\dagger}(\mathbf{r})\boldsymbol{\nabla}\widehat{\psi}(\mathbf{r}) - \frac{e\hbar}{2im}\left(\boldsymbol{\nabla}\widehat{\psi}^{\dagger}(\mathbf{r})\right)\widehat{\psi}(\mathbf{r}), \quad (9)$$

where $\widehat{\psi}(\mathbf{r})$ denotes the position-space annihilation operator. We can identify the transition current as the matrix element of the current operator

$$\mathbf{j}_{\mathrm{fi}}(\mathbf{r},t) = \langle \mathrm{f}(t)|\widehat{\mathbf{j}}(\mathbf{r})|\mathrm{i}(t)\rangle, \quad (10)$$

where $|\mathrm{i}(t)\rangle = e^{-i\widehat{H}_{\mathrm{mat}}t/\hbar}|\mathrm{i}\rangle$ and $|\mathrm{f}(t)\rangle = e^{-i\widehat{H}_{\mathrm{mat}}t/\hbar}|\mathrm{f}\rangle$ are the many-body initial and final states. Treating the current as an operator also leads to the useful identity

$$\sum_{\mathrm{i,i'}}\sum_{\mathrm{f}} \rho_{\mathrm{e}}(\mathrm{i},\mathrm{i}')\mathbf{j}^{*}_{\mathrm{fi}}(\mathbf{r},\omega)\mathbf{j}_{\mathrm{fi}'}(\mathbf{r}',\omega') = \mathrm{tr}\left\{\widehat{\rho}_{\mathrm{e}}\widehat{\mathbf{j}}^{\dagger}(\mathbf{r},\omega)\widehat{\mathbf{j}}(\mathbf{r}',\omega')\right\} \equiv \left\langle \widehat{\mathbf{j}}^{\dagger}(\mathbf{r},\omega)\widehat{\mathbf{j}}(\mathbf{r}',\omega')\right\rangle, \quad (11)$$

TABLE I. Different forms of the transition current. We consider the position-dependent current density $\mathbf{j}_{\mathrm{fi}}(\mathbf{r})$ defined in Eq. (13) for transitions between energy eigenstates having energies E_{f} and E_{i}, where $\mathbf{j}_{\mathrm{fi}}(\mathbf{r},\omega) = 2\pi\delta\left(\omega - \frac{E_{\mathrm{i}}-E_{\mathrm{f}}}{\hbar}\right)\mathbf{j}_{\mathrm{fi}}(\mathbf{r})$ and $\mathbf{j}_{\mathrm{fi}}(\mathbf{r},t) = e^{-i(E_{\mathrm{i}}-E_{\mathrm{f}})t/\hbar}\mathbf{j}_{\mathrm{fi}}(\mathbf{r})$ are, respectively, the frequency- and time-dependent current densities.

Minimal coupling	$\mathbf{j}_{\mathrm{fi}}(\mathbf{r}) = \frac{e}{m}\psi^{*}_{\mathrm{f}}(\mathbf{r})(-i\hbar\boldsymbol{\nabla})\psi_{\mathrm{i}}(\mathbf{r})$
Atomic	$\mathbf{j}_{\mathrm{fi}}(\mathbf{r}) = \frac{e}{m}\psi^{*}_{\mathrm{f}}(\mathbf{r})(-i\hbar\boldsymbol{\nabla})\psi_{\mathrm{i}}(\mathbf{r}) + \frac{e}{m}\boldsymbol{\nabla}\left[\psi^{*}_{\mathrm{f}}(\mathbf{r})\psi_{\mathrm{i}}(\mathbf{r})\right]\times\mathbf{S}_{\mathrm{fi}}$
Point-like emitter	$\mathbf{j}_{\mathrm{fi}}(\mathbf{r}) = -ie\omega\boldsymbol{d}_{\mathrm{fi}}\delta(\mathbf{r}-\mathbf{r}_0) + i\frac{e\omega}{2}\boldsymbol{\mathcal{Q}}'_{\mathrm{fi}}\cdot\boldsymbol{\nabla}\delta(\mathbf{r}-\mathbf{r}_0) - \frac{e}{2m}\mathcal{M}_{\mathrm{fi}}\times\boldsymbol{\nabla}\delta(\mathbf{r}-\mathbf{r}_0) + \cdots$
Symmetric minimal coupling	$\mathbf{j}_{\mathrm{fi}}(\mathbf{r}) = \frac{e}{2m}\psi^{*}_{\mathrm{f}}(\mathbf{r})(-i\hbar\boldsymbol{\nabla})\psi_{\mathrm{i}}(\mathbf{r}) - \frac{e}{2m}(-i\hbar\boldsymbol{\nabla})\psi^{*}_{\mathrm{f}}(\mathbf{r})\psi_{\mathrm{i}}(\mathbf{r})$
Dirac	$\mathbf{j}_{\mathrm{fi}}(\mathbf{r}) = ec\boldsymbol{\psi}^{\dagger}_{\mathrm{f}}(\mathbf{r})\boldsymbol{\alpha}\boldsymbol{\psi}_{\mathrm{i}}(\mathbf{r})$
Klein–Gordon	$\mathbf{j}_{\mathrm{fi}}(\mathbf{r}) = \frac{e}{m\gamma}\psi^{*}_{\mathrm{f}}(\mathbf{r})(-i\hbar\boldsymbol{\nabla})\psi_{\mathrm{i}}(\mathbf{r})$
Many-body	$\mathbf{j}_{\mathrm{fi}}(\mathbf{r}) = \langle \mathrm{f}\|\widehat{\mathbf{j}}(\mathbf{r})\|\mathrm{i}\rangle$ with $\widehat{\mathbf{j}}(\mathbf{r}) = \frac{e\hbar}{2im}\widehat{\psi}^{\dagger}(\mathbf{r})\boldsymbol{\nabla}\widehat{\psi}(\mathbf{r}) - \frac{e\hbar}{2im}\left(\boldsymbol{\nabla}\widehat{\psi}^{\dagger}(\mathbf{r})\right)\widehat{\psi}(\mathbf{r})$

relating the electric field correlations to the current correlations via Eqs. (2) and (3) as

$$\left\langle \widehat{\mathbf{E}}^{\dagger}(\mathbf{r},\omega)\widehat{\mathbf{E}}(\mathbf{r}',\omega')\right\rangle = \mu_0^2\omega^2\int d^3\mathbf{R}\int d^3\mathbf{R}'\mathbf{G}^*(\mathbf{R},\mathbf{r},\omega) \times \mathbf{G}(\mathbf{r}',\mathbf{R}',\omega')\left\langle \widehat{\mathbf{j}}^{\dagger}(\mathbf{R},\omega)\widehat{\mathbf{j}}(\mathbf{R}',\omega')\right\rangle. \quad (12)$$

To clarify tensor notation, the above equation is to be understood as an outer product of the two vector electric fields, such the $\mathbf{G}^*$ contracts with $\widehat{\mathbf{J}}^{\dagger}$ and $\mathbf{G}$ contracts with $\widehat{\mathbf{J}}$. Finally, we introduce two useful notations for transitions between energy eigenstates. First, the position-dependent transition current, $\mathbf{j}_{\mathrm{fi}}(\mathbf{r})$, which relates to the frequency-domain transition current $\mathbf{j}_{\mathrm{fi}}(\mathbf{r},\omega)$ via

$$\mathbf{j}_{\mathrm{fi}}(\mathbf{r},\omega) = 2\pi\delta\left(\omega - \frac{E_i - E_f}{\hbar}\right)\mathbf{j}_{\mathrm{fi}}(\mathbf{r}), \quad (13)$$

and its spatial Fourier transform,

$$\boldsymbol{j}_{\mathrm{fi}}(\mathbf{q}) = \int d^3\mathbf{r}e^{-i\mathbf{q}\cdot\mathbf{r}}\mathbf{j}_{\mathrm{fi}}(\mathbf{r}), \quad (14)$$

which becomes useful for the description of far fields.

C. Transition currents beyond the dipole approximation

The TCF covers all transition multipolar orders,[155] enabling unified calculations of emission by delocalized quantum emitters beyond the dipole approximation. Strong magnetic transition-dipole moments in rare-earth ions[156] sparked interest in atomic transitions beyond the dipole approximation. Contemporary studies investigated Purcell enhancement of magnetic transitions in nanophotonics[6,9,10,12] (see Fig. 4), while plasmonic structures with strong field confinement were explored for enhancing multipolar transitions.[8,11,14,15] Short light wavelengths were shown to grant access to multipolar forbidden transitions of atomic emitters.[13] Substantial multipolar corrections to spontaneous emission were observed in large quantum dots[40,46,98,157–159] (Fig. 5). Furthermore, the dipolar approximation has been predicted to breakdown in inter-subband transitions in quantum wells with graphene plasmons, leading to enhanced emission rates and transition frequency shifts.[45,160]

In the supplementary material, Secs. SI4–SI5, we show that for a nonrelativistic current with a Pauli spin term [Eq. (4)] the transition current up to the first order in q is given by

$$\boldsymbol{j}_{\mathrm{fi}}(\mathbf{q}) = -ie\omega\boldsymbol{d}_{\mathrm{fi}} - \frac{e\omega^2}{2c}\mathcal{Q}'_{\mathrm{fi}}\cdot\hat{\mathbf{q}} - \frac{ie\omega}{2mc}\mathcal{M}_{\mathrm{fi}}\times\hat{\mathbf{q}} + \cdots, \quad (15)$$

where $\boldsymbol{d}_{\mathrm{fi}}$, $\mathcal{Q}'_{\mathrm{fi}}$, and $\mathcal{M}_{\mathrm{fi}}$ are, respectively, the transition electric dipole, the electric quadrupole and the magnetic dipole moments of the quantum emitter. Note that the notation $\mathcal{Q}'_{\mathrm{fi}}$ stands for the non-traceless tensor $\mathcal{Q}'_{\mathrm{fi}} = \int d^3\mathbf{r}\psi_f^*(\mathbf{r})\mathbf{r}\mathbf{r}\psi_i(\mathbf{r})$, which, although being more accurate for the above description, differs from the conventional traceless definition of the electric quadrupole tensor $\mathcal{Q}_{\mathrm{fi}} = \int d^3\mathbf{r}\psi_f^*(\mathbf{r}) \times \left(\mathbf{r}\mathbf{r} - \frac{1}{3}r^2\mathbf{I}\right)\psi_i(\mathbf{r})$. These definitions are interchangeable when

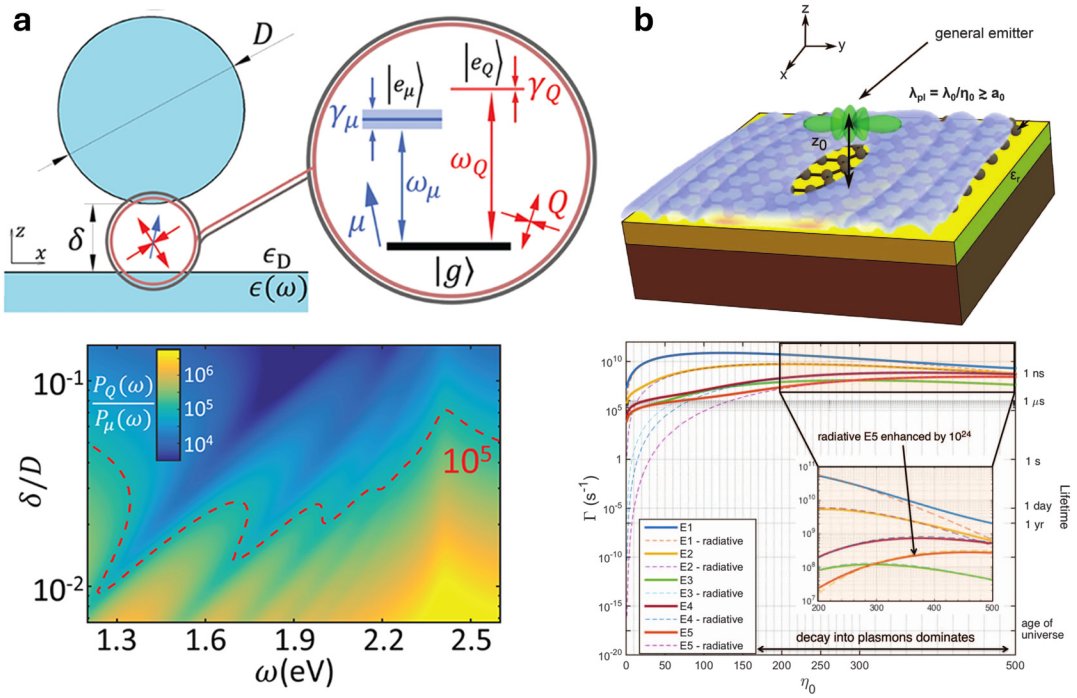

FIG. 4. Spontaneous emission beyond the dipole approximation in atomic and molecular emitters. (a) Theoretical study of comparable dipolar and quadrupolar transitions from three-level quantum emitters inside a plasmonic particle-on-mirror nanocavity.[15] Bottom: ratio between the Purcell factors of the quadrupole and dipole contributions. Reproduced with permission from Cuartero-González *et al.*, ACS Photonics **5**, 3415 (2018). Copyright 2018 American Chemical Society. (b) Accessing dipole-forbidden transitions of atoms by shrinking the wavelength of the emitted light.[13] Bottom: Transition rates of forbidden hydrogen transitions as a function of the confinement factor (ratio between the free-space and plasmonic wavelength). Reproduced with permission from Rivera *et al.*, Science **353**, 263 (2016). Copyright 2016 AAAS.

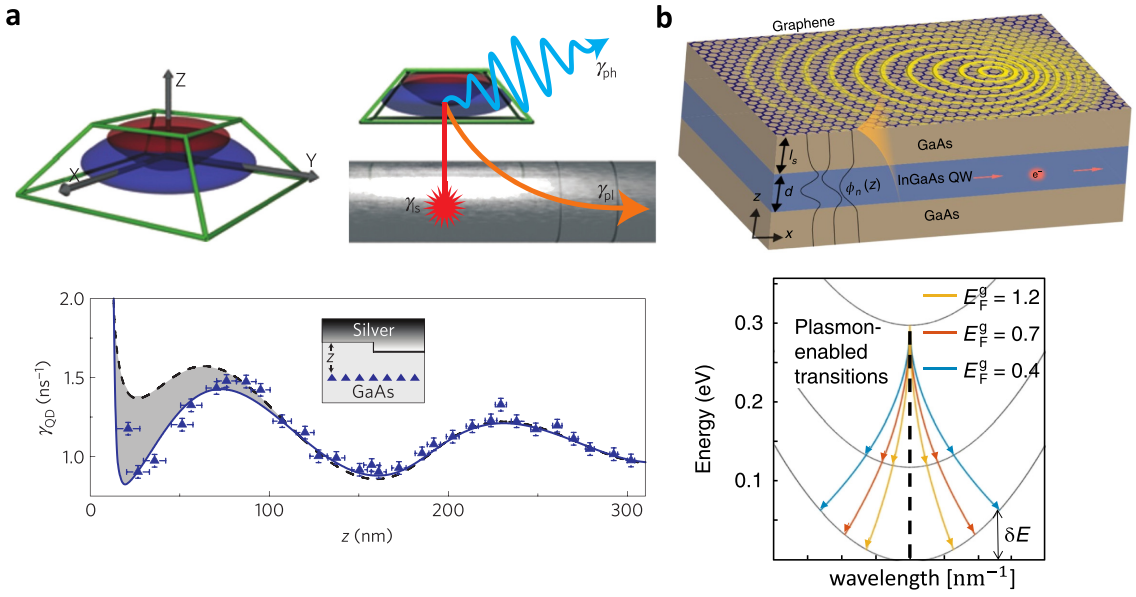

FIG. 5. Spontaneous emission beyond the dipole approximation in solid state emitters. (a) Experimental demonstration of modified emission rates of mesoscopic quantum dots near plasmonic nanostructures.[40] Bottom: measured deviation of the emission rate of a mesoscopic quantum dot from the dipole approximation, as a function of emitter-interface distance. Reproduced with permission from Andersen *et al.*, Nat. Phys. **7**, 215 (2011). Copyright 2011 Springer Nature. (b) The presence of graphene plasmons can shift emission frequency and enhance emission rates in quantum-well emitters, with corrections beyond the dipole approximation.[45] Bottom: controllable transition frequencies of quantum wells enabled by graphene plasmons and by tunable Fermi energy. Reproduced with permission from Kurman *et al.*, Nat. Photonics **12**, 423 (2018). Copyright 2018 Springer Nature.

considering emission in free space because a transverse polarization satisfies $\widehat{\boldsymbol{\epsilon}} \cdot \left(\boldsymbol{\mathcal{Q}}'_{\mathrm{fi}} - \boldsymbol{\mathcal{Q}}_{\mathrm{fi}}\right) \cdot \widehat{\mathbf{q}} = 0$.

From the above expansion and using $\int d^3\mathbf{q} e^{i\mathbf{q}\cdot\mathbf{r}}\mathbf{q} = -i\nabla\delta(\mathbf{r})$, one can also infer the expansion of the position space transition current up to first order in ∇, given by

$$\mathbf{j}_{\mathrm{fi}}(\mathbf{r}) = -ie\omega\boldsymbol{d}_{\mathrm{fi}}\delta(\mathbf{r}-\mathbf{r}_0) + i\frac{e\omega}{2}\boldsymbol{\mathcal{Q}}'_{\mathrm{fi}}\cdot\nabla\delta(\mathbf{r}-\mathbf{r}_0) - \frac{e}{2m}\mathcal{M}_{\mathrm{fi}} \times \nabla\delta(\mathbf{r}-\mathbf{r}_0) + \cdots. \tag{16}$$

The expression above is valid for a localized emitter at a position $\mathbf{r}_0$ whose size is much smaller than the emission wavelength. These point-like emitters may possess electric dipole, electric quadrupole, magnetic dipole moments, and so on, all of which are contained in the position space transition current. The leading expansion orders are summarized in Table II. Equations (15) and (16) show that the transition current indeed encapsulates all the relevant information for a localized emitter. This is, of course, also true for delocalized emitters whose length scales may exceed the emitted wavelength, such as free electrons or excitons. For such systems the expansion of Eq. (16) may become inaccurate, thus necessitating the full functional form of $\mathbf{j}_{\mathrm{fi}}(\mathbf{r})$.

D. Transition currents of free charged particles

Complementing the sections above on bound-electron systems, we focus now on the application of the TCF to explain spontaneous light emission and energy-loss rates in free-electron systems. Prior to delving into the details, we discuss the experimental context in which spontaneous light emission by free electrons serves as a diagnostic tool in electron microscopy.

A large deal of work has been devoted to researching on the interaction between free electrons and nanophotonic structures using electron microscopes (Fig. 6). Free-electron beams function as high-resolution probes, characterizing nanoscale optical systems. Electron energy loss spectroscopy[61,79–81] (EELS) can be used to measure the electromagnetic local density of optical states (LDOS) and reconstruct near-field profiles[61,79,81] of, for example, plasmonic nanoparticles.[61,79–81] Complementary to EELS, cathodoluminescence (CL) spectroscopy methods have evolved,[75–78] capitalizing on light emission from the free-electron–sample interaction. Enhanced techniques such as angle- and polarization-resolved spectroscopy[76–78,161] yield richer insights, including, for example, the coherent interference of multiple plasmonic modes induced by the electron beam.[77]

CL-based light sources have been extensively studied since the discovery of the Cherenkov effect[59] and phenomena such as the Smith–Purcell effect,[71] transition radiation,[162] diffraction radiation,[163] and undulator radiation.[164] Recent research demonstrates the versatility and controllability of these sources, enabling light emission with tailored spectral and spatial profiles.[70,84,165–171] For an in-depth

TABLE II. Multipolar expansion of the transition current. The transition-current functions $\mathbf{j}_{\mathrm{fi}}(\mathbf{r})$ and $\boldsymbol{j}_{\mathrm{fi}}(\mathbf{q})$ can be expanded to leading orders in $\mathbf{q}\cdot\mathbf{r}$, where the strongest multipole is commonly retained to derive emission rates, as in Eqs. (76), (81), and (82). In cases where several multipolar orders have a comparable strength, the TCF recovers the coherent contributions from all multipoles, as in Eq. (83).

Multipole	Position space	Momentum space
Electric dipole	$-ie\omega\boldsymbol{d}_{\mathrm{fi}}\delta(\mathbf{r}-\mathbf{r}_0)$	$-ie\omega\boldsymbol{d}_{\mathrm{fi}}$
Magnetic dipole	$-\frac{e}{2m}\mathcal{M}_{\mathrm{fi}}\times\nabla\delta(\mathbf{r}-\mathbf{r}_0)$	$-\frac{ie\omega}{2mc}\mathcal{M}_{\mathrm{fi}}\times\widehat{\mathbf{q}}$
Electric quadrupole	$i\frac{e\omega}{2}\boldsymbol{\mathcal{Q}}'_{\mathrm{fi}}\cdot\nabla\delta(\mathbf{r}-\mathbf{r}_0)$	$-\frac{e\omega^2}{2c}\boldsymbol{\mathcal{Q}}'_{\mathrm{fi}}\cdot\widehat{\mathbf{q}}$

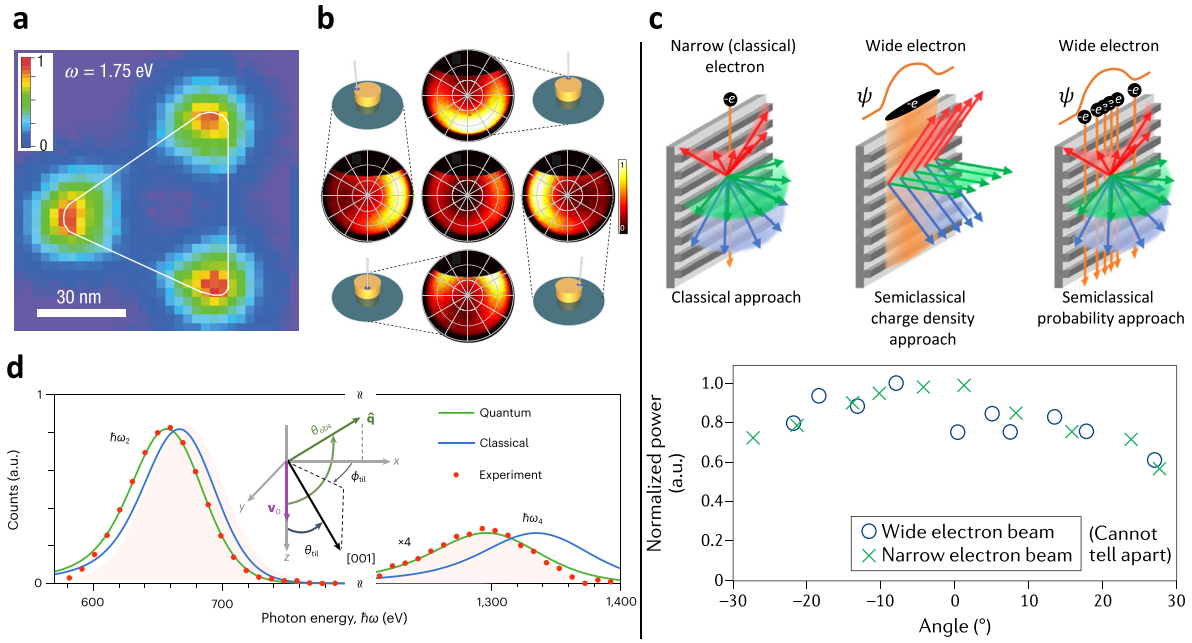

FIG. 6. Spontaneous light emission by free electrons: from classical to quantum. (a) Electron energy-loss spectroscopy (EELS) mapping of plasmonic modes.[61] Reproduced with permission from Nelayah *et al.*, Nat. Phys. **3**, 348 (2007). Copyright 2007 Springer Nature. (b) Directional emission from a plasmonic nanoparticle excited by a free electron, as a function of position, imaged by angle-resolved cathodoluminescence (CL) spectroscopy.[77] Reproduced with permission from Coenen *et al.*, Nat. Commun. **5**, 3250 (2014). Copyright 2014 Springer Nature. (c) Experimental and theoretical evidence for the independence of Smith–Purcell light emission from a uniform grating on the free-electron transverse wave function.[69] Bottom: radiation pattern of Smith–Purcell light as a function of the azimuthal observation angle, showing no dependence on electron wave function transverse size. Reproduced with permission from Remez *et al.*, Phys. Rev. Lett. **123**, 060401 (2019). Copyright 2019 the American Physical Society. (d) first experimental demonstration of the theoretically predicted quantum recoil[141] in free-electron light emission in the x-ray regime.[178] Reproduced with permission from Huang *et al.*, Nat. Photonics **17**, 224 (2023). Copyright 2023 Springer Nature.

exploration of free-electron interactions in nanophotonics, we refer to Refs. 68, 74, 90, 168, and 171.

Fundamentally, free-electron-driven spontaneous light emission reveals quantum effects beyond classical Maxwell's equations, including electron wave-function effects,[69,74,172–176] quantum coherence transfer,[85,87,176] quantum recoil corrections,[64,141,177,178] and electron-electron entanglement.[86] These aspects are further examined in separate sections below. Notably, the formalism introduced here conveniently encapsulates all these features within transition currents.

We now proceed to describe the transition currents for free electrons. When considering spontaneous emission from free electrons, one can write the most general initial wave function as

$$\psi_{\mathrm{i}}(\mathbf{r},t) = e^{i\mathbf{k}_0\cdot\mathbf{r} - i\frac{E_{\mathbf{k}_0}}{\hbar}t}\phi_{\mathrm{i}}(\mathbf{r},t), \tag{17}$$

where $\mathbf{k}_0$ and $E_{\mathbf{k}_0}$ are the carrier wave-vector and energy, and the wave fuction envelope is

$$\phi_{\mathrm{i}}(\mathbf{r},t) = \int \frac{d^3\delta\mathbf{k}_{\mathrm{i}}}{(2\pi)^3}\psi(\mathbf{k}_0+\delta\mathbf{k}_{\mathrm{i}})e^{i\delta\mathbf{k}_{\mathrm{i}}\cdot(\mathbf{r}-\mathbf{v}_0 t) - i\left(\frac{\hbar}{2m\gamma^3}\delta\mathbf{k}_{\mathrm{i}}^2+\cdots\right)t}, \tag{18}$$

is a (not necessarily paraxial) envelope. In writing the above wave function, we have expanded the relativistic free-electron dispersion relation

$$E(\mathbf{k}_0+\delta\mathbf{k}) = E(\mathbf{k}_0) + \hbar\mathbf{v}_0\cdot\delta\mathbf{k} + \frac{\hbar^2}{2m\gamma^3}\delta\mathbf{k}^2 + \cdots, \tag{19}$$

where $\mathbf{v}_0 = \hbar\mathbf{k}_0/m\gamma$ is the electron velocity, and, in particular, $E_{\mathbf{k}_0} - E_{\mathbf{k}_{\mathrm{f}}} = -\left(E_{\mathbf{k}_0+(\mathbf{k}_{\mathrm{f}}-\mathbf{k}_0)} - E_{\mathbf{k}_0}\right) = \hbar\mathbf{v}_0\cdot(\mathbf{k}_0-\mathbf{k}_{\mathrm{f}}) - \frac{\hbar^2}{2m\gamma^3}(\mathbf{k}_0-\mathbf{k}_{\mathrm{f}})^2$. Using the Klein–Gordon transition current (or, equivalently, the Dirac form neglecting spin effects), we find

$$\mathbf{j}_{\mathrm{fi}}(\mathbf{r},t) = e\frac{e^{i(\mathbf{k}_0-\mathbf{k}_{\mathrm{f}})\cdot(\mathbf{r}-\mathbf{v}_0 t)+i\left[\frac{\hbar}{2m\gamma^3}(\mathbf{k}_0-\mathbf{k}_{\mathrm{f}})^2+\cdots\right]t}}{\sqrt{V}}\left(\mathbf{v}_0 - \frac{\hbar}{m\gamma}\nabla\right)\phi_{\mathrm{i}}(\mathbf{r},t), \tag{20}$$

where we have used a plane wave $\psi_{\mathrm{f}}(\mathbf{r},t) = \frac{1}{\sqrt{V}}e^{i\mathbf{k}_{\mathrm{f}}\cdot\mathbf{r} - i\frac{E_{\mathrm{f}}}{\hbar}t}$ for the final state. In the paraxial approximation, we consider a dominant carrier wave-vector and neglect the derivative of the envelope function $\nabla\phi_{\mathrm{i}}$ as compared to the carrier wave vector $\mathbf{k}_0$. This simplifies the transition current to

$$\mathbf{j}_{\mathrm{fi}}(\mathbf{r},t) = e\mathbf{v}_0\frac{e^{i(\mathbf{k}_0-\mathbf{k}_{\mathrm{f}})\cdot(\mathbf{r}-\mathbf{v}_0 t)+i\left[\frac{\hbar}{2m\gamma^3}(\mathbf{k}_0-\mathbf{k}_{\mathrm{f}})^2+\cdots\right]t}}{\sqrt{V}}\phi_{\mathrm{i}}(\mathbf{r},t), \tag{21}$$

which still contains corrections due to electron wavepacket diffraction, dispersion, and recoil. Equation (21) can be used to calculate quantum recoil corrections to the coherent CL spectrum, as recently predicted for the Smith–Purcell effect[141] and observed experimentally.[178]

Taking $\hbar \to 0$ in the exponentials in Eqs. (19)–(21), simultaneously neglects recoil corrections (the so-called "nonrecoil" approximation) as well as diffraction and dispersion; this approximation is justified under common CL and EELS experimental conditions.[90] The transition current then further simplifies to

$$\mathbf{j}_{\mathrm{fi}}(\mathbf{r},t) = e\mathbf{v}_0 \frac{e^{i(\mathbf{k}_0-\mathbf{k}_\mathrm{f})\cdot(\mathbf{r}-\mathbf{v}_0 t)}}{\sqrt{V}} \phi_\mathrm{i}(\mathbf{r}-\mathbf{v}_0 t), \tag{22}$$

in that case, $\mathbf{j}_{\mathrm{fi}}(\mathbf{r},\omega) = e\widehat{\mathbf{z}} e^{i\mathbf{q}_{\mathrm{fi},T}\cdot\mathbf{r}_T}\phi_{\mathrm{i},T}(\mathbf{r}_T)e^{i\frac{\omega}{v_0}z}\tilde{\phi}_z\left(q_{\mathrm{fi},z}-\frac{\omega}{v_0}\right)/\sqrt{V}$ [with $\mathbf{q}_{\mathrm{fi}} = \mathbf{k}_0 - \mathbf{k}_\mathrm{f}$ and where we assumed that the electron wavepacket can be decomposed into transverse and longitudinal parts, with $\tilde{\phi}_z(k)$ denoting the spatial Fourier transform of $\phi_z(z)$] resulting in the current-current correlation for a single electron of the following form

$$\left\langle \widehat{\mathbf{j}}^\dagger(\mathbf{r},\omega)\widehat{\mathbf{j}}(\mathbf{r}',\omega')\right\rangle = e^2\widehat{\mathbf{z}}\widehat{\mathbf{z}} e^{i\left(\frac{\omega'}{v_0}z'-\frac{\omega}{v_0}z\right)}\delta(\mathbf{r}_T-\mathbf{r}'_T)\int dZ e^{i\frac{\omega-\omega'}{v_0}Z}\left|\phi_\mathrm{i}(\mathbf{r}_T,Z)\right|^2, \tag{23}$$

which encapsulates wave function effects both on the power spectrum[69,173,176] and on the spectral coherence of the emitted light,[85,87] as we shall discuss below.

As a final remark, we note that the classical, point-particle limit is recovered for $\left|\phi_\mathrm{i}(\mathbf{r}_T,z)\right|^2 = \delta(\mathbf{r}_T-\mathbf{r}_{T0})\delta(z)$, for which we have

$$\begin{aligned}\left\langle \widehat{\mathbf{j}}^\dagger(\mathbf{r},\omega)\widehat{\mathbf{j}}(\mathbf{r}',\omega')\right\rangle &= e^2\widehat{\mathbf{z}}\widehat{\mathbf{z}} e^{i\left(\frac{\omega'}{v_0}z'-\frac{\omega}{v_0}z\right)}\delta(\mathbf{r}'_T-\mathbf{r}_{T0})\delta(\mathbf{r}_T-\mathbf{r}_{T0})\\ &= \mathbf{j}_\mathrm{c}^*(\mathbf{r},\omega)\mathbf{j}_\mathrm{c}(\mathbf{r}',\omega'),\end{aligned} \tag{24}$$

where the classical current density for a point electron is given by

$$\mathbf{j}_\mathrm{c}(\mathbf{r},\omega) = e\widehat{\mathbf{z}} e^{i\frac{\omega}{v_0}z}\delta(\mathbf{r}_T-\mathbf{r}_{T0}). \tag{25}$$

E. Relevant properties of the dyadic Green function

The cornerstone of the TCF, Eq. (2), centers on the dyadic Green function, which encapsulates the electromagnetic response of material structures, linking the electric field at point $\mathbf{r}$ and frequency ω to a co-located current source at $\mathbf{r}'$. Within the framework of this formalism, the dyadic Green function serves multiple purpose: it is applicable across diverse media, encompassing loss and nonlocal effects,[93] and is amenable to analytical solutions or numerical electromagnetic simulations, depending on the complexity of the system. Here, we outline the origins of the dyadic Green function and its diverse forms. We provide a concise overview without an exhaustive exploration of its properties and calculation methods, which are extensively detailed elsewhere.[93,96,179]

In general, a Green function represents the response of a linear system to a point source. In our case, a point source of radiation is represented by a dipole moment $\mathbf{d}(\omega)$ placed at some position $\mathbf{r}_0$; since this is a vectorial quantity—as is the electromagnetic field at point $\mathbf{r}$—the response function should be a rank-2 tensor, which we denote as $\mathbf{G}(\mathbf{r},\mathbf{r}_0,\omega)$. Given this observation, we write the electric field emanating from this dipole source as

$$\boldsymbol{\mathcal{E}}(\mathbf{r},\omega) = e\mu_0\omega^2\mathbf{G}(\mathbf{r},\mathbf{r}_0,\omega)\mathbf{d}(\omega), \tag{26}$$

where the pre-factor appears due to dimensionality conventions. For an arbitrary current source $\mathbf{j}(\mathbf{r},\omega)$, one may envision the summation over many point-like infinitesimal dipole sources $\mathbf{d}(\mathbf{r},\omega) = d^3\mathbf{r}\,\mathbf{j}(\mathbf{r},\omega)/(-ie\omega)$. Turning the summation into integration, we obtain the relation presented in Eq. (2):

$$\boldsymbol{\mathcal{E}}(\mathbf{r},\omega) = i\mu_0\omega\int d^3\mathbf{r}'\mathbf{G}(\mathbf{r},\mathbf{r}',\omega)\mathbf{j}(\mathbf{r}',\omega). \tag{27}$$

The dyadic Green function of a local, isotropic, non-magnetic, lossy, and dispersive medium of permittivity $\epsilon(\mathbf{r},\omega)$ satisfies the equation[27,93,96]

$$\boldsymbol{\nabla}\times\boldsymbol{\nabla}\times\mathbf{G}(\mathbf{r},\mathbf{r}',\omega) - \frac{\omega^2}{c^2}\epsilon(\mathbf{r},\omega)\mathbf{G}(\mathbf{r},\mathbf{r}',\omega) = \mathbf{I}\delta(\mathbf{r}-\mathbf{r}'), \tag{28}$$

where $\mathbf{I}$ is the unit dyad. In addition, we select solutions of this equation that vanish at infinite distances from the interaction region, in the spirit of the retarded response convention, in which the electromagnetic frequency-dependent quantities have their poles in the negative imaginary part of the complex ω plane. Generalizations exist[27,93] for nonlocal [$\epsilon(\mathbf{r},\omega)\to\epsilon(\mathbf{r},\mathbf{r}',\omega)$] anisotropic [scalar $\epsilon(\mathbf{r},\omega)\to$ tensor $\boldsymbol{\epsilon}(\mathbf{r},\omega)$] and magnetic [$\mu_0\to\mu(\mathbf{r},\omega)$] media, though we shall not consider them here. There are several cases in which the dyadic Green function admits a closed-form solution, such as in a uniform medium:[96]

$$\mathbf{G}^{(0)}(\mathbf{r},\mathbf{r}',\omega) = \frac{e^{ikR}}{4\pi R}\left[\left(1+\frac{ikR-1}{k^2R^2}\right)\mathbf{I} + \frac{3-3ikR-k^2R^2}{k^2R^2}\frac{\mathbf{RR}}{R^2}\right], \tag{29}$$

where $k = n(\omega)\omega/c$ is the wave vector in the uniform medium of refractive index $n(\omega)$, and $\mathbf{R} = \mathbf{r}-\mathbf{r}'$ with $R = |\mathbf{R}|$. Other cases include stratified media in planar, cylindrical and spherical geometries.[93,180] In Sec. III A, we present a far-field approximation for the uniform medium and planar dielectric boundary cases to calculate radiation patterns. In addition, the vacuum near-field approximation, valid for $kr\to 0$ and given by

$$\mathbf{G}^{(0)}_{\mathrm{NF}}(\mathbf{r},\mathbf{r}',\omega) = \frac{3\mathbf{RR}/R^2-\mathbf{I}}{4\pi k^2R^3}, \tag{30}$$

can be useful for the calculation of emission and energy loss rates from emitters positioned in the vicinity of an optical sample embedded in vacuum (or any uniform medium).

One can also approximate an unknown Green function $\mathbf{G}(\mathbf{r},\mathbf{r}',\omega)$ in the presence of a permittivity perturbation $\delta\boldsymbol{\epsilon}(\mathbf{r},\omega)$ inside a medium of a known Green function $\mathbf{G}_0(\mathbf{r},\mathbf{r}',\omega)$. Denoting $\mathbf{G}(\mathbf{r},\mathbf{r}',\omega) = \mathbf{G}_0(\mathbf{r},\mathbf{r}',\omega) + \mathbf{G}_\mathrm{S}(\mathbf{r},\mathbf{r}',\omega)$, one writes the scattering part $\mathbf{G}_\mathrm{S}(\mathbf{r},\mathbf{r}',\omega)$ as a Dyson series:[93]

$$\begin{aligned}\mathbf{G}_\mathrm{S}(\mathbf{r},\mathbf{r}',\omega) = {}& \frac{\omega^2}{c^2}\int \mathrm{d}^3\mathbf{s}\mathbf{G}_0(\mathbf{r},\mathbf{s},\omega)\delta\boldsymbol{\epsilon}(\mathbf{s},\omega)\mathbf{G}_0(\mathbf{s},\mathbf{r}',\omega)\\ &+\left(\frac{\omega^2}{c^2}\right)^2\int \mathrm{d}^3\mathbf{s}\int \mathrm{d}^3\mathbf{s}'\mathbf{G}_0(\mathbf{r},\mathbf{s},\omega)\delta\boldsymbol{\epsilon}(\mathbf{s},\omega)\\ &\times\mathbf{G}_0(\mathbf{s},\mathbf{s}',\omega)\delta\boldsymbol{\epsilon}(\mathbf{s}',\omega)\mathbf{G}_0(\mathbf{s}',\mathbf{r}',\omega)+\cdots.\end{aligned} \tag{31}$$

For a nanoparticle of polarizability $\boldsymbol{\alpha}(\omega)$ located at some $\mathbf{r}_0$, Eq. (31) reduces to a closed-form result for the scattering part of the Green function (proved in Sec. SI12 of the supplementary material):

$$\mathbf{G}_\mathrm{S}(\mathbf{r},\mathbf{r}',\omega) = \mu_0\omega^2\mathbf{G}_0(\mathbf{r},\mathbf{r}_0,\omega)\boldsymbol{\alpha}(\omega)\mathbf{G}_0(\mathbf{r}_0,\mathbf{r}',\omega). \tag{32}$$

We shall employ Eq. (32) for cathodoluminescence and electron energy loss calculations in Secs. VI A and VI B, respectively.

Finally, in lossless and weakly dispersive media, Eq. (28) (with the right-hand side replaced by zero) is satisfied by the eigenmodes $\mathbf{u}_{\boldsymbol{\kappa}}(\mathbf{r})$ of the system, with eigenfrequencies $\omega_{\boldsymbol{\kappa}}$, as defined by the eigensystem equation

$$\boldsymbol{\nabla}\times\boldsymbol{\nabla}\times\mathbf{u}_{\boldsymbol{\kappa}}(\mathbf{r}) - \frac{\omega_{\boldsymbol{\kappa}}^2}{c^2}\epsilon(\mathbf{r},\omega_{\boldsymbol{\kappa}})\mathbf{u}_{\boldsymbol{\kappa}}(\mathbf{r}) = 0. \tag{33}$$

The eigenmodes then satisfy the generalized orthogonality condition

$$\int d^3\mathbf{r}\frac{1}{2\omega_{\boldsymbol{\kappa}}}\frac{d}{d\omega}\left[\omega^2\epsilon(\mathbf{r},\omega)\right]\Big|_{\omega_{\boldsymbol{\kappa}}}\mathbf{u}^*_{\boldsymbol{\kappa}}(\mathbf{r})\mathbf{u}_{\boldsymbol{\kappa}'}(\mathbf{r}) = \delta_{\boldsymbol{\kappa}\boldsymbol{\kappa}'}. \tag{34}$$

In order to link the eigenmodes to the dyadic Green function, we follow Ref. 96 and substitute the dyad $\mathbf{G}(\mathbf{r},\mathbf{r}',\omega)=\sum_{\boldsymbol{\kappa}}\mathbf{u}_{\boldsymbol{\kappa}}(\mathbf{r})\mathbf{A}_{\boldsymbol{\kappa}}(\mathbf{r}')$, where $\mathbf{A}_{\boldsymbol{\kappa}}(\mathbf{r}')$ is to be determined, into Eq. (28). To proceed, we use the approximation for weakly dispersive media

$$\frac{\omega^2\epsilon(\mathbf{r},\omega)-\omega_{\boldsymbol{\kappa}}^2\epsilon(\mathbf{r},\omega_{\boldsymbol{\kappa}})}{\omega^2-\omega_{\boldsymbol{\kappa}}^2}\cong\frac{1}{2\omega_{\boldsymbol{\kappa}}}\frac{d}{d\omega}\left[\omega^2\epsilon(\mathbf{r},\omega)\right]\Big|_{\omega_{\boldsymbol{\kappa}}},\tag{35}$$

where we note that for a nondispersive medium [i.e., for $\epsilon(\mathbf{r},\omega)=\epsilon(\mathbf{r})$] Eq. (35) is an exact equality. Using Eqs. (28) and (35), we arrive at

$$\sum_{\boldsymbol{\kappa}}\frac{\omega^2-\omega_{\boldsymbol{\kappa}}^2}{c^2}\frac{1}{2\omega_{\boldsymbol{\kappa}}}\frac{d}{d\omega}\left[\omega^2\epsilon(\mathbf{r},\omega)\right]\Big|_{\omega_{\boldsymbol{\kappa}}}\mathbf{u}_{\boldsymbol{\kappa}}(\mathbf{r})\mathbf{A}_{\boldsymbol{\kappa}}(\mathbf{r}')=\mathbf{I}\delta(\mathbf{r}-\mathbf{r}').\tag{36}$$

Multiplying both sides of Eq. (36) by $\mathbf{u}_{\boldsymbol{\kappa}}^*(\mathbf{r}')$ from the left and integrating, we find $\mathbf{A}_{\boldsymbol{\kappa}}(\mathbf{r}')=c^2\mathbf{u}_{\boldsymbol{\kappa}}^*(\mathbf{r}')/(\omega^2-\omega_{\boldsymbol{\kappa}}^2)$, resulting in

$$\mathbf{G}_T(\mathbf{r},\mathbf{r}',\omega)=\sum_{\boldsymbol{\kappa}}c^2\frac{\mathbf{u}_{\boldsymbol{\kappa}}(\mathbf{r})\mathbf{u}_{\boldsymbol{\kappa}}^*(\mathbf{r}')}{\omega_{\boldsymbol{\kappa}}^2-\omega^2},\tag{37}$$

where the subscript T was added since the above ansatz procedure[96] in fact reproduces the eigenmode expansion of the transverse part of the dyadic Green function, satisfying the transversality condition of the generalized Coulomb gauge $\nabla_{\mathbf{r}}\cdot[\epsilon(\mathbf{r},\omega)\mathbf{G}_T(\mathbf{r},\mathbf{r}',\omega)]=0$.[182] As shown in Sec. SI33 of the supplementary material, the total Green function is $\mathbf{G}=\mathbf{G}_T+\mathbf{G}_L$, where the longitudinal component $\mathbf{G}_L$ (satisfying $\nabla\times\mathbf{G}_L=0$) can be expressed in terms of the scalar electrostatic Green function.[183] We stress that, for this expansion to exist, the system needs to be lossless, such that eigenmodes are well-defined. The uniform-medium transverse dyadic Green function can also be cast in this form, yielding

$$\mathbf{G}_T^{(0)}(\mathbf{r},\mathbf{r}',\omega)=c^2\int\frac{d^3\mathbf{k}}{(2\pi)^3}\sum_{\sigma}\frac{\widehat{\boldsymbol{\epsilon}}_{\mathbf{k}\sigma}\widehat{\boldsymbol{\epsilon}}_{\mathbf{k}\sigma}e^{i\mathbf{k}\cdot(\mathbf{r}-\mathbf{r}')}}{c^2k^2-\omega^2},\tag{38}$$

where, as we show in Sec. SI33 of the supplementary material, the full Green function is $\mathbf{G}^{(0)}(\mathbf{r},\mathbf{r}',\omega)=\mathbf{G}_T^{(0)}(\mathbf{r},\mathbf{r}',\omega)-(c^2/\omega^2)\nabla_{\mathbf{r}}\otimes\nabla_{\mathbf{r}}'\times(1/4\pi|\mathbf{r}-\mathbf{r}'|)$, which is completely equivalent to Eq. (29).

Importantly, as we show in Sec. SI33 of the supplementary material, we have that $\mathrm{Im}\mathbf{G}(\mathbf{r},\mathbf{r}',\omega)=\mathrm{Im}\mathbf{G}_T(\mathbf{r},\mathbf{r}',\omega)=\sum_{\kappa}(\pi c^2/2\omega_{\kappa})\times\mathbf{u}_{\kappa}(\mathbf{r})\mathbf{u}_{\kappa}^*(r')\delta(\omega-\omega_{\kappa})$ (recovering the identity in Ref. 96) for lossless media and strictly-positive frequencies (see also Eq. 78). This latter observation indicates that all the relevant information for spontaneous emission in lossless dielectrics is encoded in the eigenmode expansion of the transverse part of the Green function.

III. CALCULATION OF RADIATION PATTERNS USING TRANSITION CURRENTS

A. Far-field Green's function

The TCF is versatile for calculating radiation patterns, power spectra, quantum optical coherence, and collective emission effects. Our analysis below focuses on light emission processes leading to propagating radiation fields. Specifically, our attention centers on scenarios where light is collected in the far field on the vacuum side. To achieve this, we derive the far-field limit of the dyadic Green function. Expanding in other types of propagating modes, like guided modes in waveguides, is straightforward using either an eigenmode expansion of the dyadic Green function [Eq. (37)] or numerical simulations. In Secs. V and VI, both analytical results and numerical simulations are employed to compute far-field power spectra for various systems.

Prior to employing numerical simulations for the calculation of the electromagnetic response of arbitrary complex media, we can gain intuition from considering simpler cases that are analytically tractable. As mentioned above, the dyadic Green function has a known closed-form solution in stratified media with either planar, cylindrical or spherical symmetry,[93,179] and describes the field distribution and polarization in all space due to a point dipole at a given point and direction. Here, to analyze some selected analytical examples, we shall consider only the simpler case of the "far-field" dyadic Green function $\mathbf{G}_{\infty}(\mathbf{r},\mathbf{r}',\omega)$[96] which is useful for the calculation of emission spectra in many experiments. The far-field dyadic Green function is well-defined for all media by taking the limit $kr\to\infty$, but rarely admits a closed analytical form. Below, we consider two such unique cases: a uniform medium and a planar boundary. A third case—a nanoparticle—will be briefly discussed in Sec. VI A.

For a uniform medium, the far-field Green function is[96]

$$\mathbf{G}_{\infty}^{(0)}(r\hat{\mathbf{n}},\mathbf{r}',\omega)=\frac{e^{ik(\omega)r}}{4\pi r}(\mathbf{I}-\hat{\mathbf{n}}\hat{\mathbf{n}})e^{-ik(\omega)\hat{\mathbf{n}}\cdot\mathbf{r}'},\tag{39}$$

where $\hat{\mathbf{n}}$ is the unit vector pointing in the direction of the observer in the far field, and r is the distance to that observer. For the field reflected from a boundary, the far-field Green function is given as (see the supplementary material, Secs. SI30–SI31 for derivation):

$$\begin{aligned}\mathbf{G}_{\infty}^{(\mathrm{ref})}(r\hat{\mathbf{n}},\mathbf{r}',\omega)=&\frac{e^{ikr}}{4\pi r}(\mathbf{I}-\hat{\mathbf{n}}\hat{\mathbf{n}})e^{-ik\hat{\mathbf{n}}\cdot\mathbf{r}'}\\&+\frac{e^{ikr}}{4\pi r}\left[\varkappa_s(\theta)\hat{\boldsymbol{\phi}}\hat{\boldsymbol{\phi}}-\varkappa_p(\theta)\hat{\boldsymbol{\theta}}\left(\hat{\boldsymbol{\theta}}+2\sin\theta\hat{\mathbf{z}}\right)\right]e^{-ik\hat{\mathbf{n}}\cdot\mathbf{r}'_{\mathrm{ref}}},\end{aligned}\tag{40}$$

where θ,ϕ and $\hat{\boldsymbol{\theta}},\hat{\boldsymbol{\phi}}$ are, respectively, the far-field polar and azimuthal angles and unit vectors, orthogonal to the observation direction unit vector $\hat{\mathbf{n}}$; $\mathbf{r}'_{\mathrm{ref}}$ denotes the reflected position vector $\mathbf{r}'_{\mathrm{ref}}=(x',y',-z')$; and $\varkappa_s(\theta)$ and $\varkappa_p(\theta)$ are the reflection coefficients for s and p polarizations, respectively.[96] In both scenarios, the convolution integral of Eq. (2) implies that the field amplitude is directly proportional to the spatial Fourier transform of the transition current, given by Eq. (14).

B. Far-field power spectrum

In many spectroscopy experiments, the relevant observable is the radiated power per unit frequency, detected in the far field. For an observer at a distance r and direction $\hat{\mathbf{n}}$ relative to the system, the total emitted power per unit solid angle is proportional to the time-average of the expectation value over a long timescale T

$$\begin{aligned}\frac{dP}{d\Omega}&=2r^2\epsilon_0c\frac{1}{T}\mathrm{Tr}\int dt\left\langle\widehat{\mathbf{E}}^{(-)}(r\hat{\mathbf{n}},t)\widehat{\mathbf{E}}^{(+)}(r\hat{\mathbf{n}},t)\right\rangle\\&=2r^2\epsilon_0c\frac{1}{2\pi T}\mathrm{Tr}\int d\omega\left\langle\widehat{\mathbf{E}}^{\dagger}(r\hat{\mathbf{n}},\omega)\widehat{\mathbf{E}}(r\hat{\mathbf{n}},\omega)\right\rangle,\end{aligned}\tag{41}$$

where we have used Plancherel's theorem, and Tr denotes the tensorial trace $\mathrm{Tr}\{T\}=\sum_{\alpha}T_{\alpha\alpha}$. The far-field power spectrum per unit frequency reads

$$\frac{d^2P}{d\Omega d\omega}=\frac{r^2\epsilon_0c}{\pi T}\mathrm{Tr}\left\langle\widehat{\mathbf{E}}^{\dagger}(r\hat{\mathbf{n}},\omega)\widehat{\mathbf{E}}(r\hat{\mathbf{n}},\omega)\right\rangle.\tag{42}$$

Using Eqs. (11)–(13), we find, when expanding in terms of energy eigenstates (see the supplementary material, Secs. SI6 for derivation),

$$\frac{d^2P}{d\Omega d\omega} = \frac{2r^2\omega^2}{c^3\epsilon_0}\sum_{\mathrm{i,i'}}\sum_{\mathrm{f}}\rho_{\mathrm{e}}(\mathrm{i},\mathrm{i}')\delta\left(\omega - \frac{E_{\mathrm{i}}-E_{\mathrm{f}}}{\hbar}\right)\frac{2\pi}{T}\delta\left(\frac{E_{\mathrm{i}}-E_{\mathrm{i}'}}{\hbar}\right) \times \mathrm{Tr}\int d^3\mathbf{r}''\mathbf{G}^*_\infty(r\hat{\mathbf{n}},\mathbf{r}'',\omega)\int d^3\mathbf{r}'\mathbf{G}_\infty(r\hat{\mathbf{n}},\mathbf{r}',\omega)\mathbf{j}^*_{\mathrm{fi}}(\mathbf{r}'')\mathbf{j}_{\mathrm{fi}'}(\mathbf{r}'). \tag{43}$$

C. Radiation power spectrum of point-like bound-electron emitters

Most bound electron systems are localized with sizes ranging from nanoscale to mesoscopic. This often places them much smaller than or slightly comparable to the emitted wavelength, with exceptions for cases of reduced effective wavelength or extended emitter wave functions. Transition currents from localized emitters raise interest in those displaying multipolar effects beyond the dipole approximation. This is exemplified in Secs. V C–V E for the two simple media mentioned earlier.

Considering a single transition between two energy eigenstates, we substitute the far-field Green tensor for a uniform medium, Eq. (39), into Eq. (43), and obtain

$$\frac{d^2P}{d\Omega d\omega} = \frac{\omega^2}{c^3\epsilon_0 8\pi^2}\delta\left(\omega - \frac{E_{\mathrm{i}}-E_{\mathrm{f}}}{\hbar}\right)\sum_\sigma\left|\hat{\boldsymbol{\epsilon}}_\sigma\cdot\boldsymbol{j}_{\mathrm{fi}}(k\hat{\mathbf{n}})\right|^2. \tag{44}$$

We can envision the transition-current expansion of Eqs. (15) and (16) as summing coherently over all the multipole terms. Using this expansion, we find (see the supplementary material, Secs. SI7 for derivation),

$$\frac{d^2P}{d\Omega d\omega} = \frac{e^2\omega^4}{c^3\epsilon_0 8\pi^2}\delta\left(\omega - \frac{E_{\mathrm{i}}-E_{\mathrm{f}}}{\hbar}\right) \times\sum_\sigma\left|\hat{\boldsymbol{\epsilon}}_\sigma\cdot\left(\boldsymbol{d}_{\mathrm{fi}} - i\frac{\omega}{2c}\boldsymbol{\mathcal{Q}}'_{\mathrm{fi}}\cdot\hat{\mathbf{n}} + \frac{1}{2mc}\mathcal{M}_{\mathrm{fi}}\times\hat{\mathbf{n}} + \cdots\right)\right|^2. \tag{45}$$

Repeating the calculation for the far-field Green function of a boundary, Eq. (40), with the emitter located a height h above the boundary, we find

$$\frac{d^2P}{d\Omega d\omega} = \frac{e^2\omega^4}{c^3\epsilon_0 8\pi^2}\delta\left(\omega - \frac{E_{\mathrm{i}}-E_{\mathrm{f}}}{\hbar}\right) \times\sum_\sigma\left|\hat{\boldsymbol{\epsilon}}_\sigma\cdot\left(\boldsymbol{d}^\sigma_{\mathrm{fi}}(\theta,h) - i\frac{\omega}{2c}\boldsymbol{\mathcal{Q}}'^\sigma_{\mathrm{fi}}(\theta,h)\cdot\hat{\mathbf{n}} + \frac{1}{2mc}\mathcal{M}^\sigma_{\mathrm{fi}}(\theta,h)\times\hat{\mathbf{n}} + \cdots\right)\right|^2, \tag{46}$$

where $\boldsymbol{d}^\sigma_{\mathrm{fi}}(\theta,h) = \boldsymbol{d}_{\mathrm{fi}} + e^{2i\frac{\omega}{c}\cos\theta h}\curlyvee_\sigma(\theta)\boldsymbol{d}^{\mathrm{ref}}_{\mathrm{fi}}$, with $\curlyvee_\sigma(\theta) = -\curlyvee_p(\theta)$ and $\curlyvee_\sigma(\theta) = \curlyvee_s(\theta)$ for $\sigma = p, s$, respectively, and similarly for $\boldsymbol{\mathcal{Q}}'^\sigma_{\mathrm{fi}}$ and $\mathcal{M}^\sigma_{\mathrm{fi}}$. The additional transition dipole, quadrupole and magnetic dipole moments introduced above, $\boldsymbol{d}^{\mathrm{ref}}_{\mathrm{fi}}$, $\boldsymbol{\mathcal{Q}}'^{\mathrm{ref}}_{\mathrm{fi}}$ and $\mathcal{M}^{\mathrm{ref}}_{\mathrm{fi}}$, respectively, correspond to their reflections about the z axis, e.g., $\boldsymbol{d}^{\mathrm{ref}}_{\mathrm{fi}} = \langle\mathrm{f}|\mathbf{r}^{\mathrm{ref}}|\mathrm{i}\rangle$, with $\mathbf{r}^{\mathrm{ref}} = (x,y,-z)$ such that $\boldsymbol{d}^{\mathrm{ref}}_{\mathrm{fi}} = (d_{\mathrm{fi},x}, d_{\mathrm{fi},y}, -d_{\mathrm{fi},z})$. Even for this simple optical environment, an emitter with comparable electric dipole, quadrupole, and magnetic dipole transitions should clearly demonstrate a vastly different power spectrum due to the coherent interference of the multipole transitions. For completeness, we reduce Eqs. (45) and (46) to the textbook example[96] of a single dipole transition oriented along $\hat{\mathbf{z}}$, for which we have

$$\frac{d^2P}{d\Omega d\omega} = \frac{e^2\omega^4}{c^3\epsilon_0 8\pi^2}\sin^2\theta\delta(\omega-\omega_{\mathrm{fi}}) \times\begin{cases}|d_{\mathrm{fi}}|^2, & \text{free space}\\ |d_{\mathrm{fi}}|^2\left|1+e^{2i\frac{\omega}{c}\cos\theta h}\curlyvee_p(\theta)\right|^2, & \text{boundary,}\end{cases} \tag{47}$$

showing how the optical environment alters the radiation pattern, suppressing or enhancing it depending on the material, observation direction and height h (we shall discuss the enhancement and suppression of transition rate in general—the Purcell effect—in Sec. IV B). Finally, we note that the well-known spontaneous emission rate for a dipolar transition in free space $\Gamma_{\mathrm{sp}} = 4\alpha\omega^3_{\mathrm{fi}}|d_{\mathrm{fi}}|^2/3c^2$ can be recovered from Eq. (47). We note that in some sources in the literature,[96] the convention for classical dipoles is to assign $\boldsymbol{d}(t) = \mathrm{Re}\{\boldsymbol{d}e^{-i\omega t}\}$ instead of the convention $\boldsymbol{d}(t) = \boldsymbol{d}e^{-i\omega_{\mathrm{fi}}t} + \boldsymbol{d}^*e^{i\omega_{\mathrm{fi}}t}$ that we employ here; in this case, a factor of $1/2$ is added to the dipole moment and one obtains $\Gamma_{\mathrm{sp}} = \alpha\omega^3_{\mathrm{fi}}|d_{\mathrm{fi}}|^2/3c^2$.

D. Radiation power spectrum of coherent cathodoluminescence: Light emission by a free electron

For a free electron, we begin by employing the paraxial and nonrecoil approximations, which are compatible with most experimental setups (we shall discuss the exceptions in Sec. V C). For this, we insert the corresponding approximated transition current of Eq. (22) into Eq. (42), and assume that the transverse and longitudinal parts of the wave function could be decoupled such that $|\phi_{\mathrm{i}}(\mathbf{r})|^2 = |\phi_{\mathrm{i}T}(\mathbf{r}_T)|^2|\phi_{\mathrm{i}z}(z)|^2$, where $\int dz|\phi_{\mathrm{i}z}(z)|^2 = 1$. We then show in the supplementary material, Sec. SI8 that one has:

$$\frac{d^2P}{d\Omega d\omega} = \frac{r^2\omega^2e^2}{\pi c^3\epsilon_0 T}\int d^2\mathbf{r}_T|\phi_{\mathrm{i},T}(\mathbf{r}_T)|^2\left|\int dz e^{i\frac{\omega}{v_0}z}\mathbf{G}_\infty(r\hat{\mathbf{n}},\mathbf{r}_T,z,\omega)\cdot\hat{\mathbf{z}}\right|^2. \tag{48}$$

The above formula covers almost all conventional scenarios of cathodoluminescence (CL). For the case of Cherenkov radiation, a straightforward substitution of Eq. (39) recovers the well-known power spectrum:

$$\frac{d^2P}{d\Omega d\omega} = \frac{\hbar\omega\alpha\beta}{2\pi}\sin^2\theta\delta\left(\cos\theta - \frac{1}{n\beta}\right). \tag{49}$$

We now turn our attention to an important relation regarding CL from non-localized electron wave functions in the paraxial nonrecoil limit. First, note that for a classical point particle, $|\phi_{\mathrm{i},T}(\mathbf{r}_T)|^2 = \delta(\mathbf{r}_T - \mathbf{r}_{T_0})$ and so, the classical power spectrum is given by

$$\frac{d^2P(\mathbf{r}_{T_0})}{d\Omega d\omega} = \frac{r^2\omega^2e^2}{\pi c^3\epsilon_0 T}\left|\int dz e^{i\frac{\omega}{v_0}z}\mathbf{G}_\infty(r\hat{\mathbf{n}},\mathbf{r}_{T_0},z,\omega)\cdot\hat{\mathbf{z}}\right|^2. \tag{50}$$

The above equation together with Eq. (48) imply that the relation between the emission pattern of a classical point-like free charged particle and that of a quantum free charged particle with transverse

wavepacket $\phi_{i,T}(\mathbf{r}_T)$ is given by an incoherent summation over the probability density $p(\mathbf{r}_T) = |\phi_{i,T}(\mathbf{r}_T)|^2$:

$$\frac{d^2P}{d\Omega d\omega} = \int d^2\mathbf{r}_T |\phi_{i,T}(\mathbf{r}_T)|^2 \frac{d^2P(\mathbf{r}_T)}{d\Omega d\omega}, \tag{51}$$

as derived and experimentally verified in Ref. 69. We stress that this relation holds in the paraxial and nonrecoil approximations, and for the case where only the light is measured (i.e., where the electron final state is traced-out).

As a final remark, we note that in the literature discussing CL, the scattered amplitude $\mathbf{f}(\hat{\mathbf{n}}, \omega)$ is often used to express the far field via

$$\boldsymbol{\mathcal{E}}_\infty(r\hat{\mathbf{n}}, \omega) = \frac{e^{\frac{i\omega}{c}r}}{r}\mathbf{f}(\hat{\mathbf{n}}, \omega). \tag{52}$$

This quantity can be derived from numerical simulations in several manners. For example, if one has knowledge of the near-field $\boldsymbol{\mathcal{E}}_{\mathrm{NF}}$ on a reference plane $\mathbf{s}$ (with surface normal $\hat{\mathbf{s}}$), the angular spectrum representation[96] can be used to obtain

$$\mathbf{f}(\hat{\mathbf{n}}, \omega) = -2\pi i \frac{\omega}{c}\hat{\mathbf{n}} \cdot \hat{\mathbf{s}} \int d^2\mathbf{s} e^{-i\frac{\omega}{c}\hat{\mathbf{n}}\cdot\mathbf{s}} \boldsymbol{\mathcal{E}}_{\mathrm{NF}}(\mathbf{s}). \tag{53}$$

Alternatively, using the boundary-element method,[90,180] the far-field amplitude could be expressed in terms of the boundary currents $\mathbf{h}(\mathbf{s})$ on the vacuum side as

$$\mathbf{f}(\hat{\mathbf{n}}, \omega) = i\frac{\omega}{c} \int d^2\mathbf{s} e^{-i\frac{\omega}{c}\hat{\mathbf{n}}\cdot\mathbf{s}} \left[\mathbf{h}(\mathbf{s}) - \left(\mathbf{h}(\mathbf{s}) \cdot \hat{\mathbf{n}}\right)\hat{\mathbf{n}}\right]. \tag{54}$$

Using the far-field amplitude, one can express the CL probability per unit frequency per unit solid angle using Eqs. (42) and (52) as

$$\frac{d^2p_{\mathrm{CL}}}{d\Omega d\omega} = \frac{T}{\hbar\omega}\frac{d^2P}{d\Omega d\omega} = \frac{r^2\epsilon_0 c}{\pi\hbar\omega}\left|\boldsymbol{\mathcal{E}}_\infty(r\hat{\mathbf{n}}, \omega)\right|^2 = \frac{\epsilon_0 c}{\pi\hbar\omega}\left|\mathbf{f}(\hat{\mathbf{n}}, \omega)\right|^2. \tag{55}$$

E. Quantum-optical coherence transfer and quantum beats

Until now, we have focused on observables like the power spectrum, unrelated to the initial correlations in the emitter quantum state. The transition-current approach captures these effects in observed radiation field properties. Quantum correlations appear in the current-current correlation function $\left\langle \hat{\mathbf{j}}^\dagger(\mathbf{r}, \omega)\hat{\mathbf{j}}(\mathbf{r}', \omega')\right\rangle$, for $\omega \neq \omega'$, linking spectral correlations of the emitted field and currents through Eq. (12). This associates emitter wave function coherence with optical coherence of the emitted light. Below, we explore such quantum coherence transfer: quantum beats in bound-electron systems and coherence transfer in free-electron systems.

Quantum coherence transfer from emitters to the radiation field distinguishes QED from semiclassical electromagnetism.[33,94,124,128–134,137–142] A notable case is quantum beats[94,127,152] [Figs. 7(a) and 7(b)], where an emitter in an initial superposition of excited states decays to a common ground state. Quantum beats are demonstrated in three-level V systems (two excited states and one ground state), but not in three-level Λ systems (one excited state and two distinguishable lower-energy final states) as predicted by QED [Fig. 2(a)]. In contrast, semiclassical electrodynamics predicts quantum beats in both V and Λ systems.[94] The TCF accurately captures the QED prediction using the summation rule over final states in Eq. (3). Recently, there has been a renewed interest in using quantum beats to measure exciton properties in two-dimensional materials.[55,56,153,181,184] These beats can be observed, for example, in the instantaneous radiated power,

$$\begin{aligned}\frac{dP(t)}{d\Omega} &= 2r^2\epsilon_0 c \mathrm{Tr}\left\langle \hat{\mathbf{E}}^{(-)}(r\hat{\mathbf{n}}, t)\hat{\mathbf{E}}^{(+)}(r\hat{\mathbf{n}}, t)\right\rangle \\ &= 2r^2\epsilon_0 c \sum_{\mathrm{ii'}}\sum_{\mathrm{f}} \rho_{\mathrm{e}}(\mathrm{i}, \mathrm{i}') e^{i(\omega_{\mathrm{fi}} - \omega_{\mathrm{fi'}})t} \mathrm{Tr}\left\{\boldsymbol{\mathcal{E}}^*_{\mathrm{fi}}(r\hat{\mathbf{n}}, \omega_{\mathrm{fi}})\boldsymbol{\mathcal{E}}_{\mathrm{fi'}}(r\hat{\mathbf{n}}, \omega_{\mathrm{fi'}})\right\},\end{aligned} \tag{56}$$

with $\omega_{\mathrm{fi}} = (E_{\mathrm{i}} - E_{\mathrm{f}})/\hbar$. Clearly, a pair of initial excited states $|\mathrm{i}\rangle$ and $|\mathrm{i}'\rangle$ will create a beat note in $\omega_{\mathrm{fi}} - \omega_{\mathrm{fi'}}$ only if they transition to a shared final state $|\mathrm{f}\rangle$. This, however, is not a sufficient condition, since states $|\mathrm{i}\rangle$ and $|\mathrm{i}'\rangle$ need also be in a coherent superposition to begin with; a thermal distribution of initial states, for example, will not display this phenomenon. From the first argument, it is clear why a Λ system cannot exhibit quantum beats. The existence of beats is evidence of the quantum coherence transfer from the initial emitter superposition to the optical coherence of the field.

Another scenario of recent interest is the coherence transfer from free-electrons to light[85,87] [Figs. 7(c) and 7(d)]. In Eq. (23), we calculated the current correlations for a single free electron. It can readily be seen that these are proportional to the coherence factor,[74] namely, the longitudinal Fourier transform of the free-electron wave function

$$M_\Omega = \int_{-\infty}^{\infty} dz \left|\phi_i(\mathbf{r}_T, z)\right|^2 e^{\frac{i\Omega}{v}z} dz, \tag{57}$$

with $\Omega = \omega - \omega'$ in Eq. (23). This shows that the shape of the wave function will be fundamentally related to the spectral coherence of the emitted light (e.g., off diagonal terms of the photonic density matrix, where $\omega \neq \omega'$). The quantum spectral coherence of the single electron wave function is then imprinted onto the radiation field, as first discussed in Refs. 85 and 87. This property can be used both in future particle detection schemes to measure wave function size and shape through Cherenkov radiation of naturally occurring charged particles, or in ultrafast electron microscopy, where the coherent modulation of the free-electron wave function can be used to shape the optical coherence of spontaneously emitted photons. Similar conclusions were derived in a different context, to analyze the quantum regime of the free-electron laser.[185–187] We note that the coherence factor in Eq. (57) will play an important role also for the emission from several electrons,[74,86] as well as for CL interference with external light,[188] as will be discussed in Secs. III F and VI C, respectively.

F. Radiation by many-body systems and super-radiance

This section applies the transition-current approach to many-body emitter systems displaying collective emission effects. We illustrate this with bound-electron and free-electron super-radiance calculations. In contrast to single emitters, many-body wave functions hold quantum correlations influencing emission rates and power spectra, effectively captured by transition currents.

First introduced by Dicke,[146] super-radiance involves collective light emission from N indistinguishable emitters.[146,148,189–195]

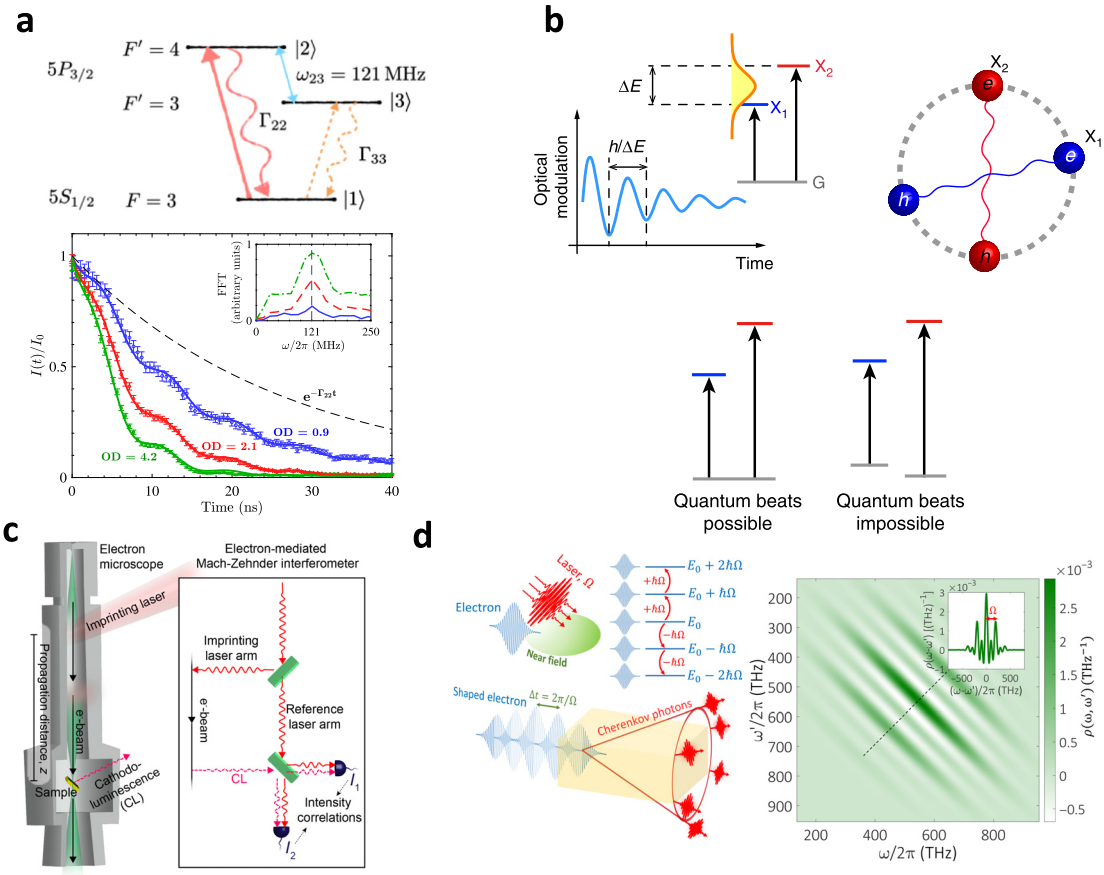

FIG. 7. Coherence transfer between quantum emitters and spontaneously emitted light. (a) and (b) Quantum beats in bound electron systems. (a) Collective quantum beats by a cloud of V-type rubidium atoms.[184] Reproduced with permission from Han *et al.*, Phys. Rev. Lett. **127**, 073604 (2021). Copyright 2021 the American Physical Society. (b) Quantum beats from excitonic superposition states in 2D transition metal dichalcogenides excited by variable laser polarization.[56] Reproduced with permission from Sim *et al.*, Nat. Commun. **9**, 351 (2018). Copyright 2018 Authors, licensed under a Creative Commons Attribution (CC BY) License. (c) and (d) Transfer of free-electron quantum coherence, induced by laser modulation, to optical coherence of subsequently emitted light. Proposed homodyne detection scheme with the modulating laser[87] (c). Reproduced with permission from Kfir *et al.*, Sci. Adv. **7**, eabf6380 (2021). Copyright 2021 AAAS; (d) Proposed measurement of the single-photon spectral density matrix to reveal the quantum optical coherence imprinted on the light.[85] Reproduced with permission from Karnieli *et al.*, Sci. Adv. **7**, eabf8096 (2021). Copyright 2021 AAAS.

This phenomenon has been extensively explored, particularly in bound-electron systems [Figs. 8(a) and 8(b)]. While a fully quantum approach is necessary for bound-electron systems, classical instances of super-radiance are evident in the emission of light from bunches of free electrons.[147,196–200] The quantum regime of free-electron–light interactions has sparked interest, leading to proposed methods for observing super- and subradiant emission from free electrons[74,86] [Figs. 8(c) and 8(d)], some relying on quantum correlations[86,201] not addressed by classical models. Notably, the TCF comprehensively accommodates various manifestations of this phenomenon, as illustrated below for both bound- and free-electron systems.

We begin by noting that Eq. (12) relates the quantum correlations of the field with those of the currents, where the latter operators need to be formulated in second quantization as in Eq. (9). With this in mind, we can write the position-space annihilation operator for electrons as an expansion over an eigenbasis of the matter Hamiltonian $\widehat{H}_{\mathrm{mat}}$ comprising single-particle wave functions $\psi_n(\mathbf{r})$ and corresponding fermionic annihilation operators $\widehat{c}_n$ as

$$\widehat{\psi}(\mathbf{r}) = \sum_n \psi_n(\mathbf{r})\widehat{c}_n. \tag{58}$$

Using Eq. (9) to write the current operator explicitly, one may then derive the current-current correlations. Here we present this procedure for two cases, a many-body free-electron system (here, under the paraxial and nonrecoil approximations), and a many-body bound-electron system based on a collection of two-level systems.

For the free-electron system, denoting $\mathbf{x} = \mathbf{r} - \mathbf{v}_0 t$ and $\mathbf{x}' = \mathbf{r}' - \mathbf{v}_0 t'$, we find (see the supplementary material, Sec. SI9 for derivation)

$$\begin{aligned}\left\langle \widehat{\mathbf{j}}^\dagger(\mathbf{r},\omega)\widehat{\mathbf{j}}(\mathbf{r}',\omega')\right\rangle &= \int dt \int dt' e^{i\omega' t' - i\omega t} e^2 \mathbf{v}_0\mathbf{v}_0 \\ &\times \Big[\underbrace{\left\langle \widehat{\psi}^\dagger(\mathbf{x})\widehat{\psi}^\dagger(\mathbf{x}')\widehat{\psi}(\mathbf{x}')\widehat{\psi}(\mathbf{x})\right\rangle}_{\text{pair correlation}} + \underbrace{\delta(\mathbf{x}-\mathbf{x}')\left\langle \widehat{\psi}^\dagger(\mathbf{x})\widehat{\psi}(\mathbf{x})\right\rangle}_{\text{single electron}}\Big].\end{aligned} \tag{59}$$

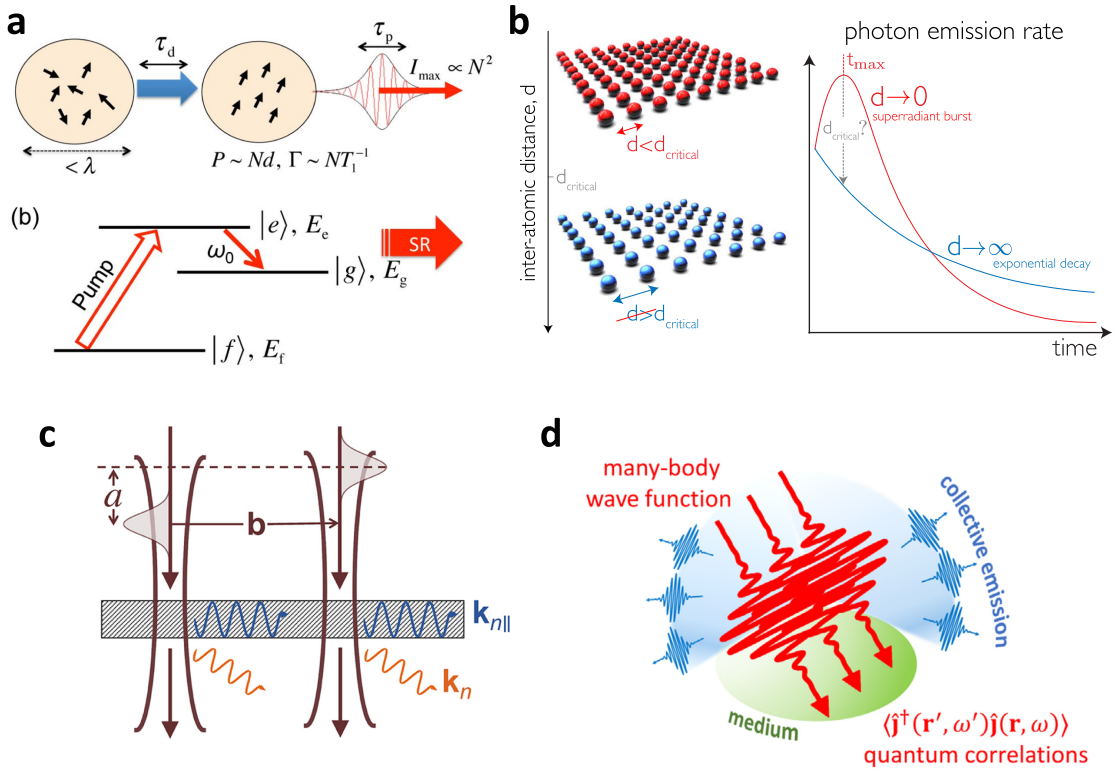

FIG. 8. Emission from many-body systems, showing super-radiance from bound- and from free-electron systems. (a) Typical experimental scheme for observing Dicke super-radiance from a collection of N three-level emitters confined to a volume smaller than the cube of the emitted wavelength, and pumped by a laser. The emitted intensity scales as N^2 and the decay time decreases with N.[192] Reproduced with permission from Cong *et al.*, JOSA B **33**, C80 (2016). Copyright 2016 the Optical Society. (b) Study of Dicke super-radiance in arrays of quantum emitters larger than the emitted wavelength.[193] Reproduced with permission from Masson *et al.*, Nat. Commun. **13**, 131 (2022). Copyright 2022 Authors, licensed under a Creative Commons Attribution (CC BY) License. (c) Interference between free-electron pairs due to temporal delays and spatial separation can manifest in the CL emission intensity.[74] Reproduced with permission from García de Abajo and Di Giulio, ACS Photonics **17**, 36 (2021). Copyright 2021 Authors, licensed under a Creative Commons Attribution (CC BY) License. (d) Super-radiance and subradiance from free electrons due to quantum correlations of the two-electron wave function.[86] Reproduced with permission from Karnieli *et al.*, Phys. Rev. Lett. **127**, 060403 (2021). Copyright 2021 the American Physical Society.

For the single electron, $\left\langle \hat{\psi}^\dagger \hat{\psi}^\dagger \hat{\psi} \hat{\psi} \right\rangle = 0$ identically, and Eq. (23) is recovered. In this case, Eq. (59) shows how the "incoherent" summation over the transverse wave function in Eq. (51) arises for the power spectrum ($\omega = \omega'$) emitted by a single electron. This happens due to the appearance of $\delta(\mathbf{x} - \mathbf{x}')$, suggesting that a point along the electron beam is only emitting coherently with itself. We note that the above conclusion holds under the paraxial approximation, which holds in most conventional instances of CL, and when only the light is being measured (i.e., the electron final state is traced out). If, however, the electron final state is measured, the spatial coherence of the initial state can persist.[89]

For the many-electron case, there are two contributions: the incoherent density term, $\delta(\mathbf{x} - \mathbf{x}')\left\langle \hat{\psi}^\dagger(\mathbf{x})\hat{\psi}(\mathbf{x}) \right\rangle$; and a coherent term $\left\langle \hat{\psi}^\dagger(\mathbf{x})\hat{\psi}^\dagger(\mathbf{x}')\hat{\psi}(\mathbf{x}')\hat{\psi}(\mathbf{x}) \right\rangle$, which permits coherence between points $\mathbf{x}$ and $\mathbf{x}'$. Namely, the coherent term allows for interference between several electrons in the beam. Under certain conditions this can lead to super-radiant CL emission whose power is proportional to N^2, the number of electrons squared, in contrast with the incoherent emission that is proportional to N. This is a well-established effect that has been experimentally demonstrated, for example, in Smith–Purcell radiation in particle accelerators equipped with gratings, in Cherenkov radiation, and undulators in free-electron lasers.[147,196–199]

To exemplify this, we consider the case where the initial many-electron state is separable $|\mathbf{i}\rangle = c^\dagger_{\mathbf{r}_1} c^\dagger_{\mathbf{r}_2} \ldots c^\dagger_{\mathbf{r}_N} |0\rangle$, where $c_{\mathbf{r}_i} = \int d^3\mathbf{r} \phi^*(\mathbf{r} - \mathbf{r}_i)\hat{\psi}(\mathbf{r})$ creates an electron wavepacket centered at $\mathbf{r}_i$; we assume no overlap between wavepackets (dilute beam), such that $\left\{ c_{\mathbf{r}_i}, c^\dagger_{\mathbf{r}_j} \right\} = \delta_{ij}$. This yields $\left\langle \hat{\psi}^\dagger(\mathbf{x})\hat{\psi}(\mathbf{x}) \right\rangle = \sum_i |\phi(\mathbf{x} - \mathbf{r}_i)|^2$ and $\left\langle \hat{\psi}^\dagger(\mathbf{x})\hat{\psi}^\dagger(\mathbf{x}')\hat{\psi}(\mathbf{x}')\hat{\psi}(\mathbf{x}) \right\rangle = \sum_i \sum_{j \neq i} |\phi(\mathbf{x}' - \mathbf{r}_i)|^2 |\phi(\mathbf{x} - \mathbf{r}_j)|^2$. For Cherenkov radiation in a medium of refractive index n, the power spectrum is then

$$\frac{d^2P}{d\Omega d\omega} = \frac{\hbar\omega\alpha\beta}{2\pi} \sin^2\theta \delta\left(\cos\theta - \frac{1}{\beta n}\right)\left[N + N(N-1)S(\omega, \hat{\mathbf{n}})\right], \quad (60)$$

with the structure factor

$$S(\omega,\hat{\mathbf{n}})=\frac{1}{N(N-1)}|M_{n\omega}|^2\sum_i\sum_{j\neq i}e^{i\frac{n\omega}{c}\hat{\mathbf{n}}\cdot(\mathbf{r}_j-\mathbf{r}_i)}, \tag{61}$$

where $M_{n\omega}$ is the coherence factor introduced in Eq. (57). The limit of classical super-radiant CL[147] is recovered by taking $|\phi(\mathbf{r})|^2=\delta(\mathbf{r})$ for which $M_{n\omega}=1$.

N^2- super-radiance can be obtained in two scenarios: (i) when the electron bunch volume is much smaller than λ^3, wherein $S(\omega,\hat{\mathbf{n}})\cong 1$ and (ii) when the electron density is periodically modulated, such that $S(\omega,\hat{\mathbf{n}})\cong 1$ for certain emission frequencies corresponding to the modulation period. Under super-radiance conditions we obtain for the CL emission rate

$$\frac{\Gamma}{\Gamma_0}=N^2. \tag{62}$$

Interestingly, the effect of super-radiant and subradiant CL has yet to be explored experimentally in the electron microscopy regime, where the potential to coherently control the quantum state and correlations between several electrons is much higher than in particle accelerators. In this respect, it was predicted that already for electron pairs, classical correlations such as controlled time delays between electrons[74] can induce interference effects that cause super- and subradiant emission. This analysis thus reproduces the results in Ref. 74 for the arbitrary excitations produced by a collection of N free electrons. Going beyond the example of Eq. (61) introduces the possibility of "quantum correlations" between electron pairs that are manifested in the second order correlations $\left\langle\hat{\psi}^\dagger(\mathbf{x})\hat{\psi}^\dagger(\mathbf{x}')\hat{\psi}(\mathbf{x}')\hat{\psi}(\mathbf{x})\right\rangle$. In this regime, quantum entanglement between electron pairs[86] has been predicted to cause super- and sub-radiance due to quantum interference of the two-body wave function that cannot be accounted for classically.

For comparison, we consider now a bound-electron system of N two-level emitters located at $\mathbf{r}_i$, $i=1,\ldots,N$. We write:

$$\begin{aligned}\hat{\mathbf{j}}(\mathbf{r},\omega)=&2\pi\sum_i\delta(\omega-\omega_{eg})\mathbf{j}_{\mathrm{ge}}(\mathbf{r}-\mathbf{r}_i)\sigma_{-,i}\\&+\delta(\omega+\omega_{eg})\mathbf{j}^*_{\mathrm{ge}}(\mathbf{r}-\mathbf{r}_i)\sigma_{+,i},\end{aligned} \tag{63}$$

where $\mathbf{j}_{\mathrm{ge}}(\mathbf{r})=\frac{e}{m}\psi^*_g(\mathbf{r})(-i\hbar\nabla)\psi_e(\mathbf{r})$ is the c-number transition current density and $\sigma_{-,i}=\hat{c}^\dagger_{g,i}\hat{c}_{e,i}=\sigma^\dagger_{+,i}$ are effective lowering and raising operators for the two-level system i. The power spectrum is then (see the supplementary material, Sec. SI9 for derivation):

$$\begin{aligned}\frac{d^2P}{d\Omega d\omega}=&\frac{\hbar\omega^2\alpha}{2\pi e^2c^2}\delta(\omega-\omega_{\mathrm{eg}})\sum_\sigma\left|\hat{\boldsymbol{\epsilon}}_\sigma\cdot\boldsymbol{j}_{\mathrm{ge}}\left(\frac{\omega}{c}\hat{\mathbf{n}}\right)\right|^2\\&\times\sum_{ij}e^{i\frac{\omega}{c}\hat{\mathbf{n}}\cdot(\mathbf{r}_i-\mathbf{r}_j)}\langle\sigma_{+,i}\sigma_{-,j}\rangle.\end{aligned} \tag{64}$$

Here, a structure factor $\sum_{ij}e^{i\frac{\omega}{c}\hat{\mathbf{n}}\cdot(\mathbf{r}_i-\mathbf{r}_j)}\langle\sigma_{+,i}\sigma_{-,j}\rangle$ appears as well, accounting for the relative phases between emitters radiating from different points. In the limit where the emitters are all confined to a volume much smaller than λ^3 (or when they are periodically spaced), $e^{i\frac{\omega}{c}\hat{\mathbf{n}}\cdot(\mathbf{r}_i-\mathbf{r}_j)}\sim 1$. In this limit, we find that the emission rate is enhanced by

$$\frac{\Gamma}{\Gamma_0}=\sum_{ij}\langle\sigma_{+,i}\sigma_{-,j}\rangle=\langle S_+S_-\rangle, \tag{65}$$

where $S_\pm=\sum_i\sigma_{\pm,i}$ are collective raising and lowering operators.

Unlike super-radiant CL, which could be also explained classically, super-radiant emission from a cloud of indistinguishable emitters, or "Dicke super-radiance," is obtained for quantum-correlated states called symmetric states of $0\leq n\leq N$ initially excited emitters[148]

$$|n\rangle=\sqrt{\frac{n!}{N!(N-n)!}}S_-^{N-n}|ee\ldots e\rangle_N, \tag{66}$$

and thus

$$\frac{\Gamma}{\Gamma_0}=n(N-n+1). \tag{67}$$

The classical product state $|ee\ldots e\rangle_N$ for which $n=N$ yields $\Gamma=N\Gamma_0$. It is only when the system cascades down to the $n=N/2$ symmetric state, does the emission rate scale as N^2.

IV. CALCULATION OF EMISSION RATES USING TRANSITION CURRENTS

A. From transition currents to emission rates

In addition to finding emission patterns, the TCF can be used to intuitively establish the quantum mechanical formulas for "transition rates" directly from the classical Maxwell's equations. Starting from the definition of the work exerted by the current on the field,

$$W_{\mathrm{fi}}=-\int dt\int d^3\mathbf{r}\mathbf{j}_{\mathrm{fi}}(\mathbf{r},t)\boldsymbol{\mathcal{E}}_{\mathrm{fi}}(\mathbf{r},t), \tag{68}$$

we find, by employing Eq. (2), together with Plancherel's theorem, and the reciprocity property of the Green tensor, $G_{\alpha\beta}(\mathbf{r},\mathbf{r}',\omega)=G_{\beta\alpha}(\mathbf{r}',\mathbf{r},\omega)$, that the work is (see the supplementary material, Sec. SI13 for derivation)

$$W_{\mathrm{fi}}=2\mu_0\frac{1}{2\pi}\int d\omega\omega\int d^3\mathbf{r}\int d^3\mathbf{r}'\mathbf{j}^*_{\mathrm{fi}}(\mathbf{r},\omega)\mathrm{Im}\{\mathbf{G}(\mathbf{r},\mathbf{r}',\omega)\}\mathbf{j}_{\mathrm{fi}}(\mathbf{r}',\omega). \tag{69}$$

Defining $P_{\mathrm{fi}}=W_{\mathrm{fi}}/T$ (where T is the interaction time) as the power transmitted to the field, the transition rate per unit frequency is found to be

$$\begin{aligned}\frac{d\Gamma_{\mathrm{fi}}}{d\omega}=&\frac{1}{\hbar\omega}\frac{dP_{\mathrm{fi}}}{d\omega}\\=&\frac{1}{2\pi T}\frac{2}{\hbar\epsilon_0c^2}\int d^3\mathbf{r}\int d^3\mathbf{r}'\mathbf{j}^*_{\mathrm{fi}}(\mathbf{r},\omega)\mathrm{Im}\{\mathbf{G}(\mathbf{r},\mathbf{r}',\omega)\}\mathbf{j}_{\mathrm{fi}}(\mathbf{r}',\omega).\end{aligned} \tag{70}$$

The total rate is then given by the same procedure of summing incoherently over final states, and coherently over initial states (expanded in terms of energy eigenstates), giving

$$\begin{aligned}\Gamma=&\frac{2}{\hbar\epsilon_0c^2}\sum_{\mathrm{f}}\sum_{\mathrm{i,i'}}\rho_{\mathrm{e}}(\mathrm{i},\mathrm{i}')\frac{2\pi}{T}\delta\left(\frac{E_{\mathrm{i}'}-E_{\mathrm{i}}}{\hbar}\right)\\&\times\int d^3\mathbf{r}\int d^3\mathbf{r}'\mathbf{j}^*_{\mathrm{fi}}(\mathbf{r})\mathrm{Im}\{\mathbf{G}(\mathbf{r},\mathbf{r}',\omega_{\mathrm{fi}})\}\mathbf{j}_{\mathrm{fi}'}(\mathbf{r}').\end{aligned} \tag{71}$$

For a single transition between two energy eigenstates $|\mathrm{i}\rangle$ and $|\mathrm{f}\rangle$, we obtain the rate

$$\Gamma_{\mathrm{fi}}=\frac{2}{\hbar\epsilon_0c^2}\int d^3\mathbf{r}\int d^3\mathbf{r}'\mathbf{j}^*_{\mathrm{fi}}(\mathbf{r})\mathrm{Im}\{\mathbf{G}(\mathbf{r},\mathbf{r}',\omega_{\mathrm{fi}})\}\mathbf{j}_{\mathrm{fi}}(\mathbf{r}'), \tag{72}$$

where we have made the replacement $\delta(0) \to T/2\pi$. Equation (71) extends Eq. (72) by allowing coherent interference between different emission channels that end up in the same final state. Since the rate per unit frequency under consideration is at a specific frequency ω, the requirement imposed by the term $\frac{2\pi}{T}\delta\left(\frac{E_{i'}-E_i}{\hbar}\right)$ in Eq. (71) requires energy-level degeneracy for such contributions to be nonzero. Actually, for every finite interaction time, the frequency delta function has a finite spectral width, enabling contributions at ω to $d\Gamma/d\omega$ from different closely-spaced initial energies.

As a final remark, it is instructive to compare the above result to the spontaneous radiation rate,

$$\Gamma_{\mathrm{fi}}^{\mathrm{rad}} = \int d\omega \int d\Omega \frac{1}{\hbar\omega}\frac{d^2P_{\mathrm{fi}}}{d\Omega d\omega}. \tag{73}$$

In a general optical environment, we can expect that $\Gamma_{\mathrm{fi}}^{\mathrm{rad}} \leq \Gamma_{\mathrm{fi}}$, since, in general, nonradiative losses are also possible. The equality is expected for free-space transitions, which are exclusively radiative. We show this by using the imaginary part of the free-space dyadic Green function,

$$\mathrm{Im}\mathbf{G}_0(\mathbf{r},\mathbf{r}',\omega) = \frac{1}{16\pi^2}\frac{\omega}{c}\sum_\sigma \int d\Omega \widehat{\boldsymbol{\epsilon}}_\sigma e^{i\frac{\omega}{c}\widehat{\mathbf{n}}\cdot(\mathbf{r}-\mathbf{r}')}\widehat{\boldsymbol{\epsilon}}_\sigma, \tag{74}$$

and find by virtue of Eq. (72), that the transition rate of an emitter in free space is indeed given by

$$\Gamma_{\mathrm{fi},0} = \frac{\omega_{\mathrm{fi}}}{\hbar c^3\epsilon_0 8\pi^2}\sum_\sigma \int d\Omega \left|\widehat{\boldsymbol{\epsilon}}_\sigma \cdot \boldsymbol{\jmath}_{\mathrm{fi}}\left(\frac{\omega_{\mathrm{fi}}}{c}\widehat{\mathbf{n}}\right)\right|^2 = \Gamma_{\mathrm{fi},0}^{\mathrm{rad}}.$$

B. Purcell enhancements and the local density of optical states

The TCF readily models a hallmark phenomenon influenced by complex optical environments: the Purcell effect. In this section, we present Purcell factors computed by using transition currents and the dyadic Green function. Since its prediction in 1946, the Purcell effect[16] has found widespread use in modifying spontaneous emission rates within intricate optical environments, such as photonic crystals[19,39,101,102,204] and plasmonic nanostructures (Fig. 9).[15,18–20,39,203,205,206] Generally, the "Purcell factor" expresses the ratio of transition rates in the given optical environment to those in free space or a uniform host medium

$$F_{\mathrm{P}} = \frac{\Gamma_{\mathrm{fi}}}{\Gamma_{\mathrm{fi},0}} = \frac{1}{\Gamma_{\mathrm{fi},0}}\frac{2}{\hbar\epsilon_0 c^2}\int d^3\mathbf{r}\int d^3\mathbf{r}'\mathbf{j}_{\mathrm{fi}}^*(\mathbf{r})\mathrm{Im}\{\mathbf{G}(\mathbf{r},\mathbf{r}',\omega_{\mathrm{fi}})\}\mathbf{j}_{\mathrm{fi}}(\mathbf{r}'). \tag{75}$$

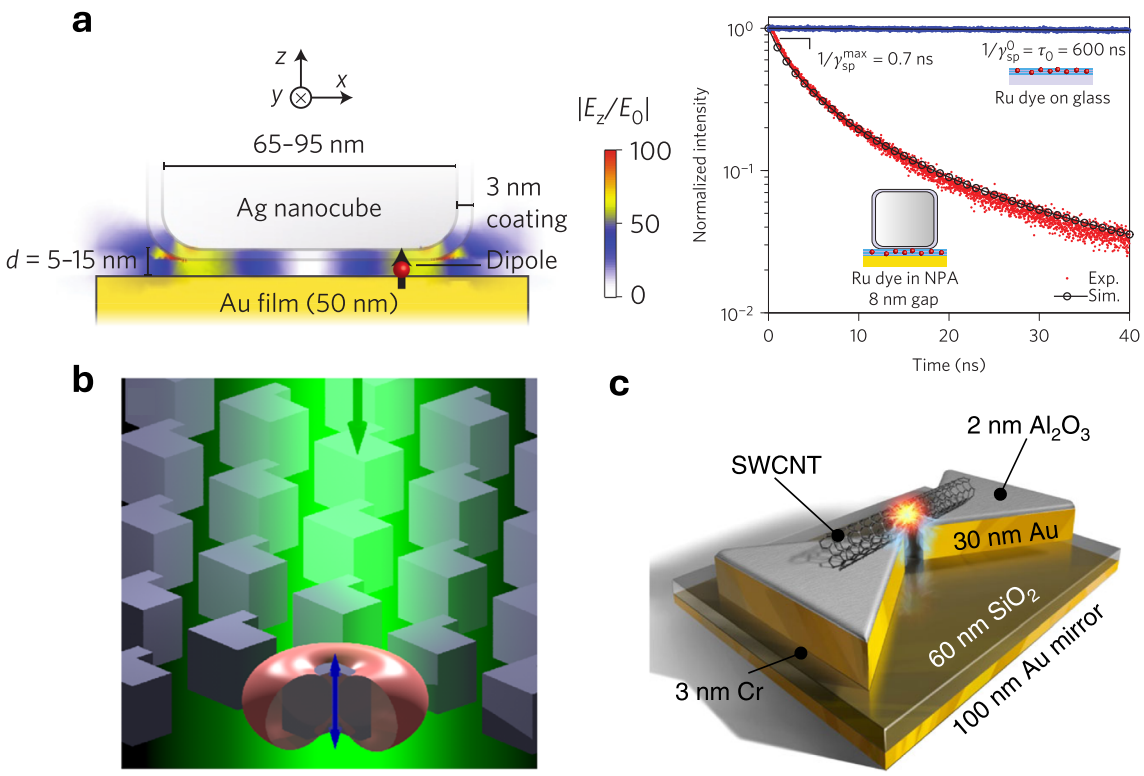

FIG. 9. Purcell enhancement of spontaneous emission: examples in nanophotonic environments. (a) 1000-fold enhancement of the decay rate of fluorescent dye molecules placed between a plasmonic nanocube and a gold film.[18] Reproduced with permission from Akselrod *et al.*, Nat. Photonics **8**, 835 (2014). Copyright 2014 Springer Nature. (b) Metasurfaces hosting embedded emitters allowing far-field engineering and enhancement.[202] Reproduced with permission from Liu *et al.*, Nano Lett. **18**, 6906 (2018). Copyright 2018 American Chemical Society. (c) Purcell enhancement of single-walled carbon nanotube excitons on a plasmonic bowtie.[203] Reproduced with permission from Luo *et al.*, Nat. Commun. **8**, 81 (2017). Copyright 2017 Authors, licensed under a Creative Commons Attribution (CC BY) License.

The more common definition for the Purcell enhancement, however, is that for the special case of a dipole emitter. The dipole transition rate in a general optical environment is obtained for $\mathbf{j}_{\mathrm{fi}}(\mathbf{r}) = -ie\omega \boldsymbol{d}_{\mathrm{fi}}\delta(\mathbf{r}-\mathbf{r}_0)$, giving

$$\Gamma_d = \frac{2e^2\omega^2}{\hbar\epsilon_0 c^2}\boldsymbol{d}_{\mathrm{fi}}^* \cdot \mathrm{Im}\{\mathbf{G}(\mathbf{r}_0,\mathbf{r}_0,\omega)\}\cdot \boldsymbol{d}_{\mathrm{fi}} = \frac{\pi e^2\omega}{\hbar\epsilon_0}|d_{\mathrm{fi}}|^2\rho(\mathbf{r}_0,\omega), \quad (76)$$

where we define

$$\begin{aligned}\rho(\mathbf{r}_0,\omega) &= \frac{2\omega}{\pi c^2}\widehat{\boldsymbol{d}}_{\mathrm{fi}}\cdot \mathrm{Im}\{\mathbf{G}(\mathbf{r}_0,\mathbf{r}_0,\omega_{\mathrm{fi}})\}\cdot\widehat{\boldsymbol{d}}_{\mathrm{fi}} \\ &= \sum\nolimits_{\boldsymbol{\kappa}}\left|\mathbf{u}_{\boldsymbol{\kappa}}(\mathbf{r})\cdot\widehat{\boldsymbol{d}}_{\mathrm{fi}}\right|^2\delta(\omega-\omega_{\mathbf{k}}) \end{aligned} \quad (77)$$

as the "projected local density of optical states" (LDOS). The last equality in Eq. (77) holds for a lossless medium using the eigenmode expansion of the dyadic Green function, Eq. (37), for which we have

$$\mathrm{Im}\{\mathbf{G}(\mathbf{r},\mathbf{r},\omega)\} = \frac{\pi c^2}{2\omega}\sum_{\boldsymbol{\kappa}}\mathbf{u}_{\boldsymbol{\kappa}}(\mathbf{r})\mathbf{u}_{\boldsymbol{\kappa}}^*(\mathbf{r})\delta(\omega-\omega_{\mathbf{k}}). \quad (78)$$

The corresponding Purcell factor is then

$$\begin{aligned}F_{\mathrm{P},d} &= \frac{\rho(\mathbf{r}_0,\omega)}{\rho_0(\mathbf{r}_0,\omega)} = \frac{6\pi c}{\omega}\widehat{\boldsymbol{d}}_{\mathrm{fi}}\cdot\mathrm{Im}\{\mathbf{G}(\mathbf{r}_0,\mathbf{r}_0,\omega_{\mathrm{fi}})\}\cdot\widehat{\boldsymbol{d}}_{\mathrm{fi}} \\ &= \frac{3\pi^2c^3}{\omega^2}\sum_{\boldsymbol{\kappa}}\left|\mathbf{u}_{\boldsymbol{\kappa}}(\mathbf{r}_0)\cdot\widehat{\boldsymbol{d}}_{\mathrm{fi}}\right|^2\delta(\omega-\omega_{\mathbf{k}}), \end{aligned} \quad (79)$$

where we used the value of the LDOS in free space, $\rho_0(\mathbf{r}_0,\omega) = \omega^2/3\pi^2c^3$. By engineering the optical environment such as to maximize the LDOS at a certain position and frequency, one can then enhance spontaneous emission rates by orders of magnitude.

The Purcell factor for a dielectric cavity can be recovered using the eigenmode expression, approximating the delta function by a Lorentzian, where Q is the cavity quality factor, choosing $\omega = \omega_{\boldsymbol{\kappa}}$ for some mode $\mathbf{u}_{\boldsymbol{\kappa}}(\mathbf{r})$, assuming that $\widehat{\boldsymbol{d}}_{\mathrm{fi}}$ is maximally aligned with the field such that $\left|\mathbf{u}_{\boldsymbol{\kappa}}(\mathbf{r})\cdot\widehat{\boldsymbol{d}}_{\mathrm{fi}}\right|^2 = 1/V$ with V denoting the mode volume, and taking $\lambda = \lambda_0/n$ for a host dielectric; these simplifications yield

$$F_{\mathrm{P},d} = \frac{3}{4\pi^2}\frac{Q}{V}\left(\frac{\lambda_0}{n}\right)^3. \quad (80)$$

For a single transition from the eigenstates $|\mathrm{i}\rangle$ to $|\mathrm{f}\rangle$, the Purcell enhancement is a completely classical effect: its dipolar form [Eq. (79)] is completely defined from the electromagnetic response, irrespective of the quantum source. The added value of the TCF in this context is twofold: (1) it enables a generalization of the Purcell factor for delocalized transition currents as in Eq. (75); and (2), it allows for the calculation of the Purcell factor for coherent transitions between several initial states, as in Eq. (71). The former can become especially important when one wishes to engineer an optical environment for mesoscopic emitters, which can break the dipole approximation.

C. Rates of multipolar transitions

For completeness, we employ the position-space multipolar expansion of the transition current for point-like emitters [Eq. (16)], to recover results for higher-order multipole emission rates. This derivation applies to any bound-electron emitter and is especially relevant for intermediate size emitters for which the first few beyond-dipole corrections are substantial. The expression for an electric dipole was presented in Eq. (76). For a magnetic dipole of a two-level point-like system we have a more intricate dependence:[93,96]

$$\Gamma_{\mathcal{M}} = \frac{e^2}{2\hbar\epsilon_0 m^2c^2}\boldsymbol{\mathcal{M}}_{\mathrm{fi}}^*\cdot\left[\vec{\boldsymbol{\nabla}}\times\mathrm{Im}\{\mathbf{G}(\mathbf{r}_0,\mathbf{r}_0,\omega)\}\times\overleftarrow{\boldsymbol{\nabla}}'\right]\cdot\boldsymbol{\mathcal{M}}_{\mathrm{fi}}. \quad (81)$$

Similarly, we derive the electric quadrupole transition[15]

$$\Gamma_{\mathcal{Q}} = \frac{e^2\omega^2}{2\hbar\epsilon_0 c^2}\left(\boldsymbol{\mathcal{Q}}_{\mathrm{fi}}'^*\cdot\vec{\boldsymbol{\nabla}}\right)\mathrm{Im}\{\mathbf{G}(\mathbf{r}_0,\mathbf{r}_0,\omega)\}\left(\overleftarrow{\boldsymbol{\nabla}}'\cdot\boldsymbol{\mathcal{Q}}_{\mathrm{fi}}'\right), \quad (82)$$

where we used the vector calculus identity $\boldsymbol{\mathcal{M}}_{\mathrm{fi}}\times\boldsymbol{\nabla}\delta(\mathbf{r}-\mathbf{r}_0) = -\boldsymbol{\nabla}\times\left[\delta(\mathbf{r}-\mathbf{r}_0)\boldsymbol{\mathcal{M}}_{\mathrm{fi}}\right]$ in addition to integration by parts.

It is important to note that the rates Γ_d, $\Gamma_{\mathcal{M}}$, and $\Gamma_{\mathcal{Q}}$ are all independently valid for emitters that possess a single "dominant" transition multipole (e.g., an electric dipole, magnetic dipole, or electric quadrupole). In the most general scenario, however, an emitter transition that breaks the dipole approximation can possess several multipolar contributions that can be added coherently, and one cannot simply write $\Gamma = \Gamma_d + \Gamma_{\mathcal{M}} + \Gamma_{\mathcal{Q}} + \cdots$, but rather use Eq. (72), which upon insertion of the expansion in Eq. (16), takes the form

$$\begin{aligned}\Gamma_{\mathrm{fi}} = \frac{2}{\hbar\epsilon_0 c^2}\int d^3\mathbf{r}\int d^3\mathbf{r}'\Big[&ie\omega\boldsymbol{d}_{\mathrm{fi}}^*\delta(\mathbf{r}-\mathbf{r}_0) \\ &- i\frac{e\omega}{2}\boldsymbol{\mathcal{Q}}_{\mathrm{fi}}'^*\cdot\boldsymbol{\nabla}\delta(\mathbf{r}-\mathbf{r}_0) - \frac{e}{2m}\boldsymbol{\mathcal{M}}_{\mathrm{fi}}^*\times\boldsymbol{\nabla}\delta(\mathbf{r}-\mathbf{r}_0)+\cdots\Big] \\ &\cdot\mathrm{Im}\mathbf{G}(\mathbf{r},\mathbf{r}',\omega_{\mathrm{fi}})\cdot\Big[-ie\omega\boldsymbol{d}_{\mathrm{fi}}\delta(\mathbf{r}'-\mathbf{r}_0) \\ &+ i\frac{e\omega}{2}\boldsymbol{\mathcal{Q}}_{\mathrm{fi}}'\cdot\boldsymbol{\nabla}'\delta(\mathbf{r}'-\mathbf{r}_0) - \frac{e}{2m}\boldsymbol{\mathcal{M}}_{\mathrm{fi}}\times\boldsymbol{\nabla}'\delta(\mathbf{r}'-\mathbf{r}_0)+\cdots\Big]. \end{aligned} \quad (83)$$

It is therefore clear why the use of the full functional form of the transition current, rather than a decomposition into multipoles, is useful in such situations to capture interference between different multipoles.

D. Electron energy-loss probability

Like the approach for bound-electron systems, the TCF applies to evaluating energy loss rates in free-electron systems. This section concentrates on utilizing transition currents to compute electron energy-loss probabilities during interactions with different optical environments. This is crucial, especially for electron microscopy applications involving EELS measurements.

Under paraxial free-electron conditions, we first note that the more relevant observable is the EELS probability (per unit frequency), rather than the rate. This means that we define

$$\frac{dp_{\mathrm{EELS}}}{d\omega} = \int d^3\mathbf{k}_{\mathrm{f}}\frac{1}{\hbar\omega}\frac{dW_{\mathrm{fi}}}{d\omega}, \quad (84)$$

where, in Eq. (84) we assume that the electron final momentum state $|\mathbf{k}_{\mathrm{f}}\rangle$ is not resolved, hence the trace out over the final momentum. We then obtain, using Eq. (69) and again assuming that the transverse and longitudinal part of the wave function can be decoupled as

$|\phi_i(\mathbf{r})|^2 = |\phi_{iT}(\mathbf{r}_T)|^2 |\phi_{iz}(z)|^2$, where $\int dz |\phi_{iz}(z)|^2 = 1$, the relation (see the supplementary material, Sec. SI14 for derivation)

$$\frac{dp_{\mathrm{EELS}}}{d\omega} = \frac{e^2}{\pi\epsilon_0\hbar c^2}\int d^2\mathbf{r}_T |\phi_{i,T}(\mathbf{r}_T)|^2 \int dz' \times \int dz e^{\frac{i\omega}{v}(z'-z)} \mathrm{Im}\{G_{zz}(\mathbf{r}_T, z; \mathbf{r}_T, z', \omega)\}. \quad (85)$$

Thus, recovering the result reported in Refs. 90 and 207. For a point particle, such that $|\phi_{i,T}(\mathbf{r}_T)|^2 = \delta(\mathbf{r}_T - \mathbf{r}_{T0})$, this result simplifies to the classical limit[90]

$$\frac{dp_{\mathrm{EELS}}}{d\omega}(\mathbf{r}_{T0}) = \frac{e^2}{\pi\hbar\epsilon_0 c^2}\int dz' \int dz e^{\frac{i\omega}{v}(z'-z)} \mathrm{Im}\{G_{zz}(\mathbf{r}_{T0}, z; \mathbf{r}_{T0}, z', \omega)\}. \quad (86)$$

The main application enabled by Eq. (86) is the fact that free electrons can serve as nanometer-scale spatial and meV-resolution spectral probes for a variant of the LDOS projected along $\hat{\mathbf{z}}$ and Fourier-transformed along the electron trajectory, given as

$$\rho'(\mathbf{r}_{T0}, \omega) = \frac{2\omega}{\pi c^2}\int dz' \int dz e^{\frac{i\omega}{v}(z'-z)} \hat{\mathbf{z}} \cdot \mathrm{Im}\{\mathbf{G}(\mathbf{r}_{T0}, z; \mathbf{r}_{T0}, z'; \omega)\} \cdot \hat{\mathbf{z}}, \quad (87)$$

with $dp_{\mathrm{EELS}}/d\omega = (e^2/2\hbar\omega\epsilon_0)\rho'(\mathbf{r}_{T0}, \omega)$, as first shown in Ref. 208. This fundamental relation between LDOS and EELS explains why this technique can retrieve local optical properties[61,79,81] (see Fig. 6).

As a final remark, we connect the EELS probability result to the theory of quantum photon-induced near-field electron microscopy[88,209–216] by employing the identity for the imaginary part of the Green tensor:[93]

$$\left\langle \hat{\mathbf{E}}(\mathbf{r}, \omega)\hat{\mathbf{E}}^\dagger(\mathbf{r}', \omega')\right\rangle_{\mathrm{vac}} = \frac{\hbar}{\pi\epsilon_0}\frac{\omega^2}{c^2}\mathrm{Im}\{\mathbf{G}(\mathbf{r}, \mathbf{r}', \omega)\}\delta(\omega - \omega'), \quad (88)$$

where $\left\langle \hat{\mathbf{E}}(\mathbf{r}, \omega)\hat{\mathbf{E}}^\dagger(\mathbf{r}', \omega')\right\rangle_{\mathrm{vac}}$ stands for the vacuum expectation value of the (antinormally ordered) fields. By considering a single-mode field given as $\hat{\mathbf{E}}(\mathbf{r}, \omega) = \delta(\omega - \omega_0)\boldsymbol{\mathcal{E}}(\mathbf{r})a$, where a is the bosonic annihilation operator, and using $\langle aa^\dagger\rangle_{\mathrm{vac}} = 1$, we find the (total) probability (see the supplementary material, Sec. SI16 for derivation),

$$p_{\mathrm{EELS}} = \left|\frac{e}{\hbar\omega_0}\int dz e^{-i\frac{\omega_0}{v}z}\mathcal{E}_z(\mathbf{r}_T, z)\right|^2 = |g_Q|^2. \quad (89)$$

That is, the probability for (first-order) spontaneous emission into a single-mode field is given by the modulus squared of the quantum coupling g_Q (also named β_0 in several works[216]). This is the linearization of the nonperturbative result giving the Poissonian distribution, $p(n) = e^{-|g_Q|^2}|g_Q|^{2n}/n!$, which, as expected, approaches $p(1) \cong |g_Q|^2$ whenever $|g_Q|^2 \ll 1$.

E. Calculation of second-order processes using transition currents

Here, we show that the TCF can incorporate two-photon emission processes, which have garnered recent interest due to the potential for enhancing these normally weak transitions using confined fields in plasmonic and polaritonic systems[13,21,22,24–26] (Fig. 10). These processes have also been investigated with free electrons, leading to novel entanglement between infrared and x-ray photons.[23] The derived power expressions, Eqs. (95) and (96), perfectly match the established outcome for two-photon emission in a lossy medium, as derived through macroscopic QED[27,93] within second-order time-dependent perturbation theory[13] [see Supplemental Materials of Ref. 5 and Eq. (S18)].

The derivation here should provide a blueprint for including even higher-order emission phenomena and may also aid in the extension of the TCF to describe energy shifts such as Lamb shifts (and corresponding Casimir–Polder forces). The conceptual crux is to consider the two-photon process in two steps: in the first step, a vacuum fluctuation "polarizes" an emitter, creating a fluctuating current. This polarization is associated with emission of one of the two photons. This "induced" current then leads to the emission of the second photon. The current that is created in the first step is associated with a transition from the initial matter state i to an intermediate matter state n, while the second step involves a transition from n to the final matter state f.

Consider two-photon emission in which the initial state of the light and matter is $|i, 0\rangle$ (with $|i\rangle$ the initial eigenstate of the matter system and $|0\rangle$ the vacuum state of the electromagnetic field) and the final state is $|f, 1_{\boldsymbol{\kappa}}, 1_{\boldsymbol{\kappa}'}\rangle$ (with $|f\rangle$ the final eigenstate of the matter system and $|1_{\boldsymbol{\kappa}}, 1_{\boldsymbol{\kappa}'}\rangle$ a two-photon state with one photon in mode $\boldsymbol{\kappa}$ and one in mode $\boldsymbol{\kappa}'$). Let us consider the case in which the transition from i to f is one-photon forbidden (in the dipole approximation) and two-photon allowed. In this case, for example, the transition dipole moment is $d_{fi} = 0$, naively predicting zero dipolar emission according to the framework developed in this work. However, what this argument neglects is that the transition current is in fact a dynamic quantity, and can change in the presence of an electric field $\boldsymbol{\mathcal{E}}(t)$ that couples to the matter system. To accurately describe two-photon processes using the minimal coupling Hamiltonian, it is important to consider the gauge-invariant form of the current operator in the presence of an electromagnetic field $\hat{\mathbf{J}}(\mathbf{r}, t) = \frac{e}{2m}\hat{\psi}^\dagger(\mathbf{r}, t)\left(-i\hbar\boldsymbol{\nabla} - e\boldsymbol{\mathcal{A}}(\mathbf{r}, t)\right)\hat{\psi}(\mathbf{r}, t) + h.c.$, where we use second-quantization notation and introduce a classical vector potential field $\boldsymbol{\mathcal{A}}(\mathbf{r}, t)$.

Using linear response theory, as derived in Sec. SI26 of the supplementary material, the frequency-domain transition current reduces to

$$\mathbf{J}_{fi}(\mathbf{r}, \omega) = \mathbf{j}_{fi}(\mathbf{r}, \omega) + \int d\omega' \int d^3\mathbf{r}' \boldsymbol{\sigma}_{fi}(\mathbf{r}, \mathbf{r}', \omega, \omega')\boldsymbol{\mathcal{E}}^*(\mathbf{r}', \omega'), \quad (90)$$

where $\mathbf{j}_{fi}(\mathbf{r}, \omega)$ denotes the conventional (field-free) transition current, $\boldsymbol{\mathcal{E}}(\mathbf{r}, \omega) = i\omega\boldsymbol{\mathcal{A}}(\mathbf{r}, \omega)$ is the corresponding classical field, which we associate with vacuum fluctuations, and we introduce the "transition conductivity tensor"

$$\boldsymbol{\sigma}_{fi}(\mathbf{r}, \mathbf{r}', \omega, \omega') = \frac{2\pi i}{\omega'}\left[-\frac{e^2}{m}\mathbf{I}\, n_{fi}(\mathbf{r})\delta(\mathbf{r} - \mathbf{r}') + \frac{1}{\hbar}\sum_m \frac{\mathbf{j}_{mi}(\mathbf{r})\mathbf{j}_{fm}(\mathbf{r}')}{\omega - \omega_{im} - i\Gamma} - \frac{\mathbf{j}_{fm}(\mathbf{r})\mathbf{j}_{mi}(\mathbf{r}')}{\omega - \omega_{mf} + i\Gamma}\right]\delta(\omega + \omega' - \omega_{if}). \quad (91)$$

Here, $n_{fi}(\mathbf{r}) = \langle f|\hat{\psi}^\dagger(\mathbf{r})\hat{\psi}(\mathbf{r})|i\rangle = \psi_f^*(\mathbf{r})\psi_i(\mathbf{r})$ is the transition density, $\mathbf{I}$ is the identity operator, $\omega_{\alpha\beta} = \omega_\alpha - \omega_\beta$, and the sum is over all matter states $|m\rangle$. A phenomenological linewidth[217–219] Γ is introduced in

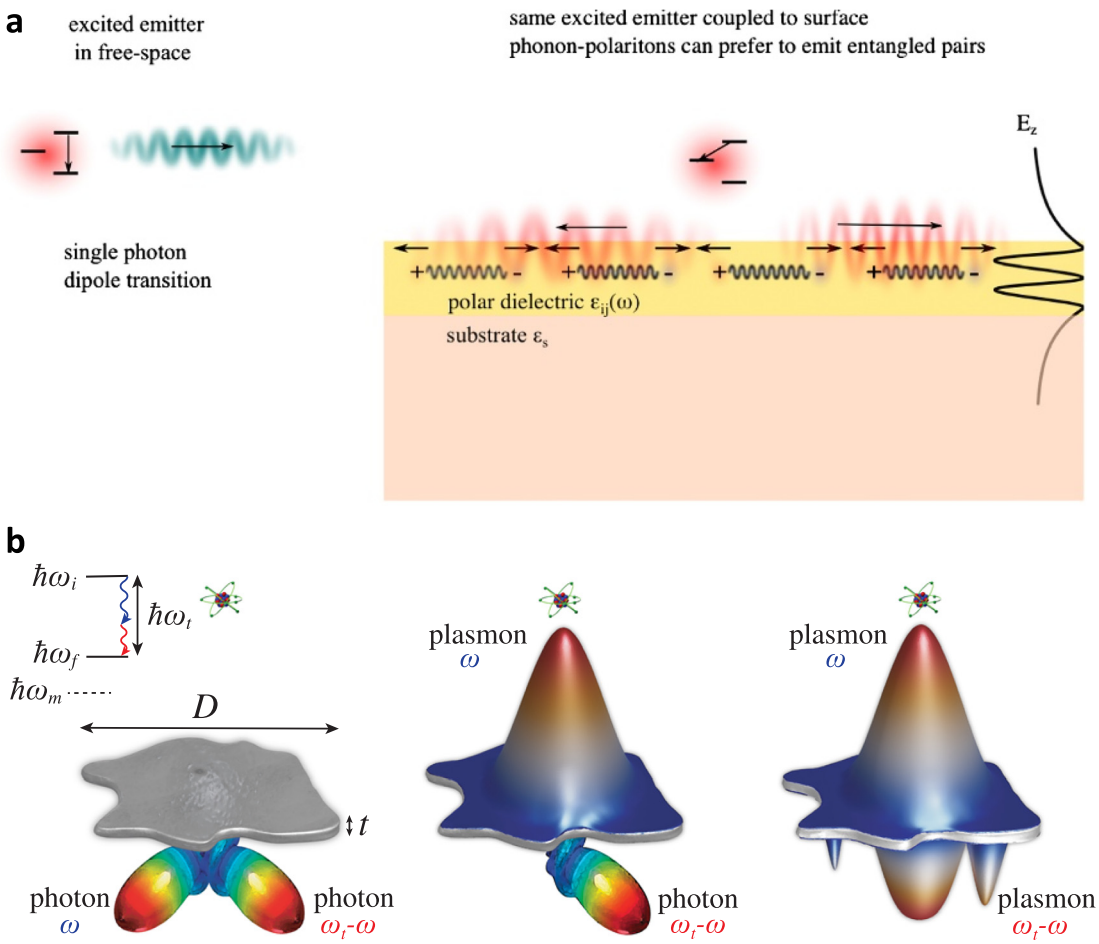

FIG. 10. Two-photon transitions mediated by nanophotonic environments. (a) dominant two-photon transitions in the presence of mid-IR phonon polariton modes for emitters placed near polar dielectric materials.[21] Reproduced with permission from Rivera *et al.*, Proc. Natl. Acad. Sci. U. S. A. **114**, 13607 (2017). Copyright 2017 Authors, licensed under a Creative Commons Attribution (CC BY) License. (b) Two-photon spontaneous emission in 2D plasmonic materials, leading to different outcomes: two photons, a plasmon and a photon, and two plasmons, as depicted in the sketches.[22] Reproduced with permission from Muniz *et al.*, Phys. Rev. Lett. **125**, 033601 (2020). Copyright 2020 the American Physical Society.

the intermediate states $|m\rangle$ such that $\omega_m \to \omega_m - i\Gamma$, assuming the states $|\mathrm{i}\rangle$ and $|\mathrm{f}\rangle$ are otherwise long-lived, recovering the correct pole positions of the exact perturbation-theory expression (see discussions in Secs. SI26 and SI29; a possible estimate for the linewidth Γ could be a typical single-photon transition lifetime for the system). As shown in Sec. SI25 of the supplementary material, the exact transition matrix element of second-order time-dependent perturbation theory leads to the conductivity tensor of Eq. (91), even without the phenomenological linewidths Γ. We also note that most calculations in the literature considering two-photon emission where the intermediate states lie above the energy levels ($\omega_\mathrm{m} > \omega_\mathrm{i} > \omega_\mathrm{f}$) do not depend on Γ, which in that case is usually set to $\Gamma \to 0$. From the requirement that the number of photons at frequency ω equals that at frequency $\omega_\mathrm{if} - \omega$, we show in Sec. SI29 that the transition conductivity tensor satisfies $\boldsymbol{\sigma}_\mathrm{fi}(\mathbf{r}, \mathbf{r}', \omega, \omega')/\omega = \boldsymbol{\sigma}_\mathrm{fi}^T(\mathbf{r}', \mathbf{r}, \omega', \omega)/\omega'$.

As shown in Sec. SI.27 of the supplementary material, taking the dipole limit $\mathbf{j}_\mathrm{fi}(\mathbf{r}) = -ie\omega_\mathrm{if}\mathbf{d}_\mathrm{fi}\delta(\mathbf{r} - \mathbf{r}_0)$ of Eq. (16), we find

$$\boldsymbol{\sigma}_\mathrm{fi}(\mathbf{r}, \mathbf{r}', \omega, \omega') \to -2\pi i\omega e\delta(\mathbf{r}' - \mathbf{r}_0)\delta(\mathbf{r} - \mathbf{r}_0)\delta(\omega + \omega' - \omega_\mathrm{if})\boldsymbol{\alpha}_\mathrm{fi}(\omega), \tag{92}$$

where we introduce the "transition polarizability tensor"

$$\boldsymbol{\alpha}_\mathrm{fi}(\omega) = -\frac{e}{\hbar}\sum_m \frac{\mathbf{d}_\mathrm{fm}\mathbf{d}_\mathrm{mi}}{\omega - \omega_\mathrm{mf} + i\Gamma} - \frac{\mathbf{d}_\mathrm{mi}\mathbf{d}_\mathrm{fm}}{\omega - \omega_\mathrm{im} - i\Gamma}, \tag{93}$$

satisfying $\boldsymbol{\alpha}_\mathrm{fi}(\omega_\mathrm{if} - \omega) = \boldsymbol{\alpha}_\mathrm{fi}^T(\omega)$. We consider the case where the field $\boldsymbol{\mathcal{E}}$ inducing the transition current in Eq. (90) is the vacuum noise field, expanded in eigenmodes $\mathbf{u}_\boldsymbol{\kappa}(\mathbf{r})$, such that $\boldsymbol{\mathcal{E}}_\mathrm{vac}(\mathbf{r}, \omega) = \sum_\boldsymbol{\kappa}\sqrt{\frac{\hbar\omega_\boldsymbol{\kappa}}{2\epsilon_0}}\mathbf{u}_\boldsymbol{\kappa}(\mathbf{r})\delta(\omega - \omega_\boldsymbol{\kappa})\alpha_\boldsymbol{\kappa}$, with $\alpha_\boldsymbol{\kappa}$ denoting uncorrelated noise amplitudes such that $\langle\alpha_\boldsymbol{\kappa}\alpha_{\boldsymbol{\kappa}'}\rangle = \delta_{\boldsymbol{\kappa}\boldsymbol{\kappa}'}$. The physical meaning is that the

vacuum field noise at frequency $\omega_{\boldsymbol{\kappa}}$ can induce a transition current at frequency $\omega - \omega_{\boldsymbol{\kappa}}$, and vice versa.

Given this transition current, we now compute the total emission according to the usual framework, while remembering to average over the vacuum field noise, as contributions from different modes are incoherent with each other. The total emission rate due to a transition current $\mathbf{J}_{\mathrm{fi}}(\mathbf{r},\omega)$ is given from Eq. (72) by

$$\Gamma_{\mathrm{fi}} = \int d\omega \frac{1}{\hbar\omega}\frac{dP_{\mathrm{fi}}}{d\omega} = \frac{1}{T}\frac{\mu_0}{\pi\hbar}\int d\omega \int d^3\mathbf{r}\int d^3\mathbf{r}'\mathbf{J}^*_{\mathrm{fi}}(\mathbf{r},\omega)\mathrm{Im}\mathbf{G}(\mathbf{r},\mathbf{r}',\omega)\mathbf{J}_{\mathrm{fi}}(\mathbf{r}',\omega). \quad (94)$$

By substituting the current of Eq. (90), and excluding a direct transition such that $\mathbf{j}_{\mathrm{fi}}(\mathbf{r},\omega) = 0$, we find

$$\Gamma_{\mathrm{fi}} = \frac{1}{T}\frac{\mu_0^2}{\pi^2}\int d\omega \int d^3\mathbf{r}\int d^3\mathbf{r}'\int d^3\mathbf{s}\int d^3\mathbf{s}'\int d\omega'\omega'\omega \times \mathrm{Tr}\left[\boldsymbol{\sigma}^*_{\mathrm{fi}}(\mathbf{r},\mathbf{s}',\omega,\omega')\mathrm{Im}\mathbf{G}(\mathbf{s}',\mathbf{s},\omega')\boldsymbol{\sigma}_{\mathrm{fi}}(\mathbf{s},\mathbf{r}',\omega',\omega)\mathrm{Im}\mathbf{G}(\mathbf{r}',\mathbf{r},\omega)\right], \quad (95)$$

and, in the dipole limit,

$$\Gamma_{\mathrm{fi}} = \frac{2q^2}{\pi\epsilon_0^2 c^4}\int_0^{\omega_{\mathrm{if}}} d\omega(\omega_{\mathrm{if}}-\omega)^2\omega^2 \times \mathrm{Tr}\left[\boldsymbol{\alpha}^*_{\mathrm{fi}}(\omega)\mathrm{Im}\mathbf{G}(\mathbf{r}_0,\mathbf{r}_0,\omega_{\mathrm{if}}-\omega)\boldsymbol{\alpha}^T_{\mathrm{fi}}(\omega)\mathrm{Im}\mathbf{G}(\mathbf{r}_0,\mathbf{r}_0,\omega)\right], \quad (96)$$

where in the last step we use $\boldsymbol{\alpha}_{\mathrm{fi}}(\omega_{\mathrm{if}}-\omega) = \boldsymbol{\alpha}^T_{\mathrm{fi}}(\omega)$.

The result for the decay rate exactly coincides with previously derived results (see, for example, Refs. 13 and 21) indicating that two-photon emission can indeed be described by the TCF. In particular, we see that two-photon emission can be thought of as emission from an induced transition current. The current is induced by the vacuum field itself. Importantly, the induced current is not at the same frequency as the inducing field and, therefore, cannot be thought of as arising from the linear conductivity (or polarizability). The relationship between the current and the field (unsurprisingly) is more akin to a nonlinear process, in which a field at some frequency causes polarization at a different lower frequency (e.g., difference-frequency generation).

We can also calculate the second-order correlations of the electric field, as shown in Sec. SI25 in the supplementary material, to find

$$\left\langle\widehat{\mathbf{E}}^\dagger(\mathbf{r},\omega)\widehat{\mathbf{E}}^\dagger(\mathbf{r}',\omega')\widehat{\mathbf{E}}(\mathbf{r}',\omega')\widehat{\mathbf{E}}(\mathbf{r},\omega)\right\rangle = \hbar^2\sum_{\mathrm{f}}\left|\int d^3\mathbf{s}'\int d^3\mathbf{s}\mu_0^2\omega'^2\omega\mathbf{G}(\mathbf{r},\mathbf{s},\omega)\boldsymbol{\sigma}_{\mathrm{fi}}(\mathbf{s},\mathbf{s}',\omega,\omega')\mathbf{G}(\mathbf{s}',\mathbf{r}',\omega')\right|^2, \quad (97)$$

and, in the dipole limit

$$\left\langle\widehat{\mathbf{E}}^\dagger(\mathbf{r},\omega)\widehat{\mathbf{E}}^\dagger(\mathbf{r}',\omega')\widehat{\mathbf{E}}(\mathbf{r}',\omega')\widehat{\mathbf{E}}(\mathbf{r},\omega)\right\rangle = 2\pi\hbar^2e^2T\delta(\omega+\omega'-\omega_{\mathrm{if}}) \times \sum_{\mathrm{f}}\left|\mu_0^2\omega'^2\omega^2\mathbf{G}(\mathbf{r},\mathbf{r}_0,\omega)\boldsymbol{\alpha}_{\mathrm{fi}}(\omega)\mathbf{G}(\mathbf{r}_0,\mathbf{r}',\omega_{\mathrm{if}}-\omega)\right|^2, \quad (98)$$

where we used $\delta(0) = T/2\pi$. In a similar manner to Eq. (69), we can use Plancherel's identity to write the free-space two-photon emission as

$$\Gamma_{2\mathrm{ph}} = \frac{1}{T}\int d\Omega\int d\Omega'\int d\omega\int d\omega'\frac{2r^2\epsilon_0 c\,2r'^2\epsilon_0 c}{2\pi\hbar\omega\,2\pi\hbar\omega'} \times \mathrm{Tr}\mathrm{Tr}\left\langle\widehat{\mathbf{E}}^\dagger(r\widehat{\mathbf{n}},\omega)\widehat{\mathbf{E}}^\dagger(r'\widehat{\mathbf{n}}',\omega')\widehat{\mathbf{E}}(r'\widehat{\mathbf{n}}',\omega')\widehat{\mathbf{E}}(r\widehat{\mathbf{n}},\omega)\right\rangle, \quad (99)$$

recovering the known result for the free-space two-photon emission rate in the dipole limit

$$\Gamma_{2\mathrm{ph}} = \frac{e^4}{18\pi^3\hbar^2c^6\epsilon_0^2}\int d\omega\sum_{\mathrm{f}}(\omega_{\mathrm{if}}-\omega)^3\omega^3 \times\left|\sum_m d_{\mathrm{fm}}d_{\mathrm{mi}}\left(\frac{1}{\omega-\omega_{\mathrm{mf}}+i\Gamma}-\frac{1}{\omega-\omega_{\mathrm{im}}-i\Gamma}\right)\right|^2. \quad (100)$$

Although we have focused for concreteness on emission from a bound electron system (e.g., an atom), the logic that leads to this result extends to other systems. In fact, a very similar line of reasoning was applied in Ref. 23 to describe two-photon emission from relativistic free electrons. There, the two-photon emission (one in the infrared domain and the other at an x-ray frequency) could be explained as a type of scattering process in which the electron scatters off the infrared field, causing it to emit an x-ray (due to relativistic energy-momentum conservation considerations). In this picture, the infrared field is inducing a (virtual) current in the electron system, which can then emit at x-ray frequencies. This picture was shown to be in line with a direct calculation of the two-photon emission from the standard second-order perturbation-theory formalism—similar to how Eqs. (95) and (96) above match the more direct calculation.

Before we move to the examples of Sec. V, we summarize the main results of the TCF in Table III.

V. APPLICATIONS OF TRANSITION CURRENTS TO BOUND-ELECTRON SYSTEMS

In this and the ensuing section, we shall employ the tools outlined in Secs. II–IV to derive a few results for several emitter systems and optical environments, with the focus on transitions beyond the dipole approximation, quantum coherence transfer, and quantum recoil corrections. For the sake of practical applications, we also employ a numerical solver, with transition-current sources as its inputs. Calculations are performed for both bound and free electron systems, to exemplify the broad validity of the transition-current method. We begin with the bound-electron case.

A. The hydrogen atom beyond the dipole approximation

Below, we propose an alternative derivation for the textbook example of the hydrogen atom, which recovers all multipole orders via a single calculation of the transition current. In this manner, the reader can gain further insight on the notion of forbidden transitions and the possibilities to enhance them, as well as on the transversal and longitudinal contributions to the current. We note that in this section we choose, for the sake of simplicity, to calculate the currents with respect to the uncoupled basis $|n,l,m,m_s\rangle$, where n,l,m,m_s are the principal, orbital angular momentum, z-component of the angular momentum, and z-component of the spin quantum numbers, respectively. The case of fine-structure quantum beats with respect to the coupled basis $|n,l,j,m_j\rangle$, where j,m_j are the total angular momentum and z-component of the total angular momentum quantum numbers, respectively, is

TABLE III. Main formulas of the transition-current formalism (TCF). The TCF allows for the calculation of correlations, radiation patterns, and transition rates associated with both first- and second-order processes.

First-order correlations	$\left\langle \widehat{\mathbf{E}}^{\dagger}(\mathbf{r},\omega)\widehat{\mathbf{E}}(\mathbf{r}',\omega')\right\rangle = \mu_0^2\omega^2\int d^3\mathbf{R}\int d^3\mathbf{R}'\mathbf{G}^*(\mathbf{R},\mathbf{r},\omega)\mathbf{G}(\mathbf{r}',\mathbf{R}',\omega')\left\langle \widehat{\mathbf{j}}^{\dagger}(\mathbf{R},\omega)\widehat{\mathbf{j}}(\mathbf{R}',\omega')\right\rangle$
Radiation pattern	$\frac{d^2P}{d\Omega d\omega} = \frac{r^2\epsilon_0 c}{\pi T}\mathrm{Tr}\left\langle \widehat{\mathbf{E}}^{\dagger}(r\widehat{\mathbf{n}},\omega)\widehat{\mathbf{E}}(r\widehat{\mathbf{n}},\omega)\right\rangle$
Transition rates	$\Gamma_{\mathrm{fi}} = \frac{2}{\hbar\epsilon_0 c^2}\int d^3\mathbf{r}\int d^3\mathbf{r}'\mathbf{j}_{\mathrm{fi}}^*(\mathbf{r})\mathrm{Im}\{\mathbf{G}(\mathbf{r},\mathbf{r}',\omega_{\mathrm{fi}})\}\mathbf{j}_{\mathrm{fi}}(\mathbf{r}')$
Second-order correlations	$\left\langle \widehat{\mathbf{E}}^{\dagger}(\mathbf{r},\omega)\widehat{\mathbf{E}}^{\dagger}(\mathbf{r}',\omega')\widehat{\mathbf{E}}(\mathbf{r}',\omega')\widehat{\mathbf{E}}(\mathbf{r},\omega)\right\rangle = \hbar^2\sum_{\mathrm{f}}\left\lvert\int d^3\mathbf{s}'\int d^3\mathbf{s}\mu_0^2\omega'^2\omega\mathbf{G}(\mathbf{r},\mathbf{s},\omega)\boldsymbol{\sigma}_{\mathrm{fi}}(\mathbf{s},\mathbf{s}',\omega,\omega')\mathbf{G}(\mathbf{s}',\mathbf{r}',\omega')\right\rvert^2$
Two-photon decay rate	$\Gamma_{\mathrm{fi}} = \frac{1}{T}\frac{\mu_0^2}{\pi^2}\int d\omega\int d^3\mathbf{r}\int d^3\mathbf{r}'\int d^3\mathbf{s}\int d^3\mathbf{s}'\int d\omega'\omega'\omega\mathrm{Tr}\left[\boldsymbol{\sigma}_{\mathrm{fi}}^*(\mathbf{r},\mathbf{s}',\omega,\omega')\mathrm{Im}\mathbf{G}(\mathbf{s}',\mathbf{s},\omega')\boldsymbol{\sigma}_{\mathrm{fi}}(\mathbf{s},\mathbf{r}',\omega',\omega)\mathrm{Im}\mathbf{G}(\mathbf{r}',\mathbf{r},\omega)\right]$

considered in Sec. V B. For the sake of simplicity we also neglect hyperfine and relativistic corrections to the hydrogen atom.

The transition current accounting for spin is given by Eq. (4), where we can choose to substitute the desired eigenfunctions of the hydrogen atom to describe some selected transitions. For example, the $2p,0\uparrow\rightarrow 1s,0\uparrow$ transition has a transition current,

$$\mathbf{j}_{\mathrm{fi}}(\mathbf{r}) = \frac{e}{m}\psi_{1s}^*(\mathbf{r})(-i\hbar\boldsymbol{\nabla})\psi_{2p}(\mathbf{r}) + \mu_B\boldsymbol{\nabla}\left[\psi_{1s}^*(\mathbf{r})\psi_{2p}(\mathbf{r})\right]\times\widehat{\mathbf{z}}, \quad (101)$$

where $\mu_B = e\hbar/2m$ is the Bohr magneton. Through explicit calculation, detailed in the supplementary material, Secs. SI17–SI21, we find for the $2p0\uparrow\rightarrow 1s\uparrow$ transition the result:

$$\boldsymbol{\mathcal{J}}_{\mathrm{fi}}(\mathbf{q}) = -i\omega e\frac{2^7}{3^5}\sqrt{2}a_0\frac{1}{\left(1+\bar{q}^2\right)^2}\left[\widehat{\mathbf{z}} + \frac{\bar{q}^2}{1+\bar{q}^2}\cos\theta\left(2\widehat{\mathbf{q}} - 3i\sin\theta\widehat{\boldsymbol{\phi}}\right)\right]. \quad (102)$$

Here and onwards, we define

$$\bar{q} = \frac{n_{\mathrm{i}}n_{\mathrm{f}}}{n_{\mathrm{i}}+n_{\mathrm{f}}}a_0 q, \quad (103)$$

as the small parameter characterizing the emission orders, with a_0 standing for the Bohr radius. While for the hydrogen atom a_0 is four orders of magnitude smaller than the emitted wavelength, it is instructive to observe that this small parameter scales as $a_0 q$, proportional to the ratio between the emitter dimension a_0 and the emission wavelength λ. Consequently, by using nontrivial optical environments and dispersion relations to shrink the emitted wavelength, small parameters such as $\bar{q}$ may become comparable to unity, thus breaking the dipole approximation. Table IV summarizes the results for different transitions. All derivations can be found in the supplementary material, Secs. SI17–SI21.

We exemplify the radiation patterns in free space for the four cases considered in Table IV:

$$\boldsymbol{\mathcal{E}}_{\mathrm{fi}}(r\widehat{\mathbf{n}},\omega_{\mathrm{fi}}) = \frac{e^{i\frac{\omega_{\mathrm{fi}}}{c}r}}{4\pi r}e\mu_0\omega_{\mathrm{fi}}^2\begin{cases} -\left|\boldsymbol{d}_{\mathrm{fi}}\right|\left[\frac{1}{\left(1+\bar{q}_{\mathrm{fi}}^2\right)^2}\sin\theta\widehat{\boldsymbol{\theta}} + 3i\frac{\bar{q}_{\mathrm{fi}}^2}{\left(1+\bar{q}_{\mathrm{fi}}^2\right)^3}\sin\theta\cos\theta\widehat{\boldsymbol{\phi}}\right], & 2p\uparrow\rightarrow 1s\uparrow \\ i\frac{\omega_{\mathrm{fi}}}{2c}\left|\boldsymbol{\mathcal{Q}}'_{\mathrm{fi}}\cdot\widehat{\mathbf{n}}\right|\left[\frac{1}{\left(1+\bar{q}_{\mathrm{fi}}^2\right)^3}\cos\theta\sin\theta\widehat{\boldsymbol{\theta}} + 2i\frac{\bar{q}_{\mathrm{fi}}^2}{\left(1+\bar{q}_{\mathrm{fi}}^2\right)^4}\sin\theta\left(\cos^2\theta-\frac{1}{3}\right)\widehat{\boldsymbol{\phi}}\right], & 3d0\uparrow\rightarrow 1s\uparrow \\ \frac{\omega_{\mathrm{fi}}}{2c}\left|\boldsymbol{\mathcal{Q}}'_{\mathrm{fi}}\cdot\widehat{\mathbf{n}}\right|\left[\frac{3\bar{q}_{\mathrm{fi}}^2}{\left(1+\bar{q}_{\mathrm{fi}}^2\right)^3}\sin\theta\widehat{\boldsymbol{\phi}}\right], & 2s\uparrow\rightarrow 1s\uparrow \\ \frac{i\hbar}{2mc}\left(\frac{1}{\left(1+\bar{q}_{\mathrm{fi}}^2\right)^3} - \frac{6\bar{q}_{\mathrm{fi}}^2}{\left(1+\bar{q}_{\mathrm{fi}}^2\right)^4}\cos^2\theta\right)\left[\cos\theta(\widehat{\mathbf{x}}+i\widehat{\mathbf{y}}) - e^{i\phi}\sin\theta\widehat{\mathbf{z}}\right], & 2p\uparrow\rightarrow 2p\downarrow, \end{cases} \quad (104)$$

where $\bar{q}_{\mathrm{fi}}$ is defined as in Eq. (103), with q replaced by ω_{fi}/c. The corresponding radiation patterns in free space are summarized in Fig. 11.

B. Quantum beats

This subsection demonstrates how to use transition currents to describe quantum beat phenomena and how to obtain quantitative results. We exemplify this derivation on the hydrogen atom, to obtain analytical expressions. We specifically examine the $3d\rightarrow 2p$ transition. The fine structure energy is given by[220]

$$E_{nj} = E_n\left[1 + \frac{\alpha^2}{n}\left(\frac{1}{j+\frac{1}{2}} - \frac{3}{4n}\right)\right], \quad (105)$$

where $j = l\pm 1/2$ is the total angular momentum number. To proceed, we need to write the coupled $|n,l,j,m_j\rangle$ eigenstates in terms of the uncoupled basis states $|n,l,m,m_s\rangle$ according to the angular momentum summation rules. For simplicity of notation, we define the two excited states $|e1\rangle = |3d_{3/2},3/2\rangle$ and $|e2\rangle = |3d_{5/2},5/2\rangle$, such that the emitter is prepared in a coherent superposition of them written as

TABLE IV. Momentum-space currents for different hydrogen atom transitions.

Transition	Momentum-space transition current	Leading multipole ($\bar{q} \to 0$)
$2p0\uparrow \to 1s\uparrow$	$\boldsymbol{\jmath}_{\rm fi}(\mathbf{q}) = -i\omega e \frac{2^7}{3^5}\sqrt{2}a_0 \frac{1}{(1+\bar{q}^2)^2}\left[\hat{\mathbf{z}} + \frac{\bar{q}^2}{1+\bar{q}^2}\cos\theta\left(2\hat{\mathbf{q}} - 3i\sin\theta\hat{\boldsymbol{\phi}}\right)\right]$	$\boldsymbol{\jmath}_{\rm fi}(0) \cong -i\omega e \boldsymbol{d}_{\rm fi}$ $\boldsymbol{d}_{\rm fi} = \frac{2^7}{3^5}\sqrt{2}a_0\hat{\mathbf{z}}$
$3d0\uparrow \to 1s\uparrow$	$\boldsymbol{\jmath}_{\rm fi}(\mathbf{q}) = -\frac{e\omega^2}{2c}\frac{1}{\sqrt{6}}\frac{3^5}{2^7}a_0^2\frac{1}{(1+\bar{q}^2)^3}\left[\cos\theta\hat{\mathbf{z}} - \frac{1}{3}\hat{\mathbf{q}} + \frac{\bar{q}^2}{1+\bar{q}^2}\left(\cos^2\theta - \frac{1}{3}\right)\left(\hat{\mathbf{q}} - 2i\sin\theta\hat{\boldsymbol{\phi}}\right)\right]$	$\boldsymbol{\jmath}_{\rm fi}(0) \cong -\frac{e\omega^2}{2c}\boldsymbol{\mathcal{Q}}'_{\rm fi}\cdot\hat{\mathbf{q}}$ $\boldsymbol{\mathcal{Q}}'_{\rm fi}\cdot\hat{\mathbf{q}} = \frac{1}{\sqrt{6}}\frac{3^5}{2^7}a_0^2\left(\cos\theta\hat{\mathbf{z}} - \frac{1}{3}\hat{\mathbf{q}}\right)$
$2s\uparrow \to 1s\uparrow$	$\boldsymbol{\jmath}_{\rm fi}(\mathbf{q}) = \frac{e\omega^2}{2c}\frac{2^9}{3^6}\sqrt{2}a_0^2\left[\frac{1+3\bar{q}^2}{(1+\bar{q}^2)^3}\hat{\mathbf{q}} - i\frac{3\bar{q}^2}{(1+\bar{q}^2)^3}\sin\theta\hat{\boldsymbol{\phi}}\right]$	$\boldsymbol{\jmath}_{\rm fi}(0) \cong -\frac{e\omega^2}{2c}\boldsymbol{\mathcal{Q}}'_{\rm fi}\cdot\hat{\mathbf{q}}$ $\boldsymbol{\mathcal{Q}}'_{\rm fi}\cdot\hat{\mathbf{q}} = -\frac{2^9}{3^6}\sqrt{2}a_0^2\hat{\mathbf{q}}$
$2p0\uparrow \to 2p0\downarrow$	$\boldsymbol{\jmath}_{\rm fi}(\mathbf{q}) = \frac{e\omega}{2mc}\left(\frac{1}{(1+\bar{q}^2)^3} - \frac{6\bar{q}^2}{(1+\bar{q}^2)^4}\cos^2\theta\right)\hbar e^{i\phi}\left(\hat{\boldsymbol{\theta}} + i\cos\theta\hat{\boldsymbol{\phi}}\right)$	$\boldsymbol{\jmath}_{\rm fi}(\mathbf{q}) \cong -\frac{ie\omega}{2mc}\boldsymbol{\mathcal{M}}_{\rm fi}\times\hat{\mathbf{q}}$ $\boldsymbol{\mathcal{M}}_{\rm fi}\times\hat{\mathbf{q}} = \hbar(\hat{\mathbf{x}} + i\hat{\mathbf{y}})\times\hat{\mathbf{q}}$
	$e^{i\phi}\left(\hat{\boldsymbol{\theta}} + i\cos\theta\hat{\boldsymbol{\phi}}\right) = \cos\theta(\hat{\mathbf{x}} + i\hat{\mathbf{y}}) - e^{i\phi}\sin\theta\hat{\mathbf{z}}$	$(\hat{\mathbf{x}} + i\hat{\mathbf{y}})\times\hat{\mathbf{q}} = ie^{i\phi}\left(\hat{\boldsymbol{\theta}} + i\cos\theta\hat{\boldsymbol{\phi}}\right)$

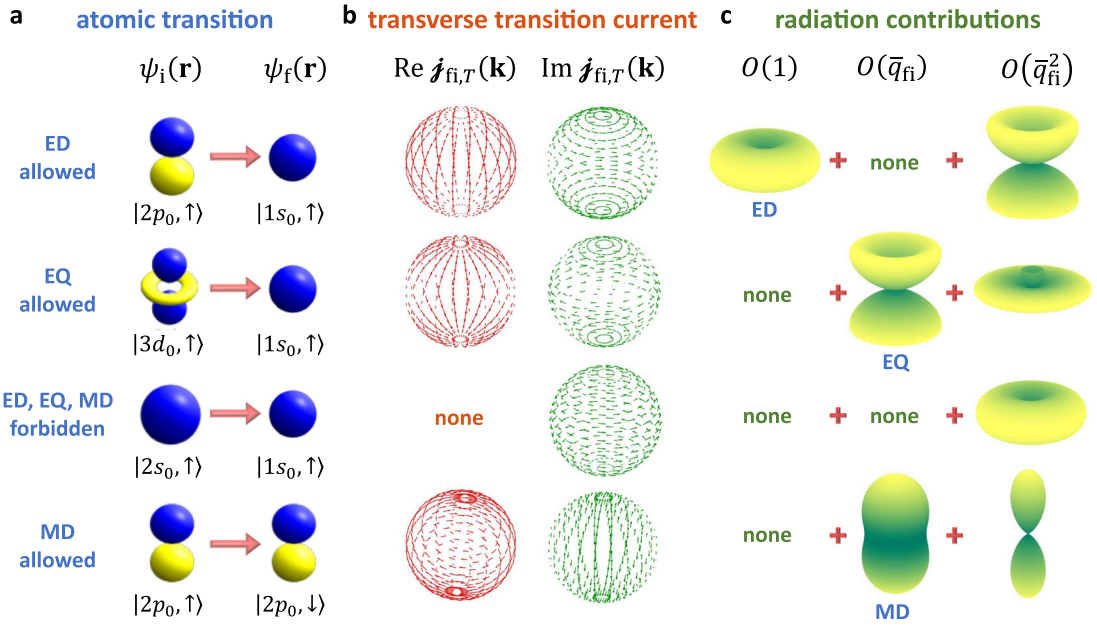

FIG. 11. Currents and radiation patterns in hydrogen atom transitions. (a) The $|2p_0\uparrow\rangle \to |1s_0\uparrow\rangle$, $|3d_0\uparrow\rangle \to |1s_0\uparrow\rangle$, $|2s_0\uparrow\rangle \to |1s_0\uparrow\rangle$ and $|2p_0\uparrow\rangle \to |2p_0\downarrow\rangle$ transitions, along with depictions of their respective wave functions and the leading-order of allowed radiative transition in free space. (b) Vectorial depiction of the transverse part of the Fourier-space transition currents appearing in Table I. (c) Depiction of the free-space radiation patterns described by Eq. (104), decomposed into leading orders in $\bar{q}_{\rm fi}$. Contributions are labeled by their multipole order.

$$|\psi_i\rangle = c_1|e1\rangle + c_2|e2\rangle. \tag{106}$$

The dipole-allowed transitions to ground states in the $n = 2$ orbital involve three states $|g1\rangle = |2p_{3/2}, 3/2\rangle$, $|g2\rangle = |2p_{3/2}, 1/2\rangle$ and $|g3\rangle = |2p_{1/2}, 1/2\rangle$ (see full details in the supplementary material, Sec. SI22), as depicted in Fig. 12. The process, therefore, comprises a Λ-system and a V-system, and, as discussed in Sec. III E, the QED prediction suggests that quantum beats will originate from the V-system only.

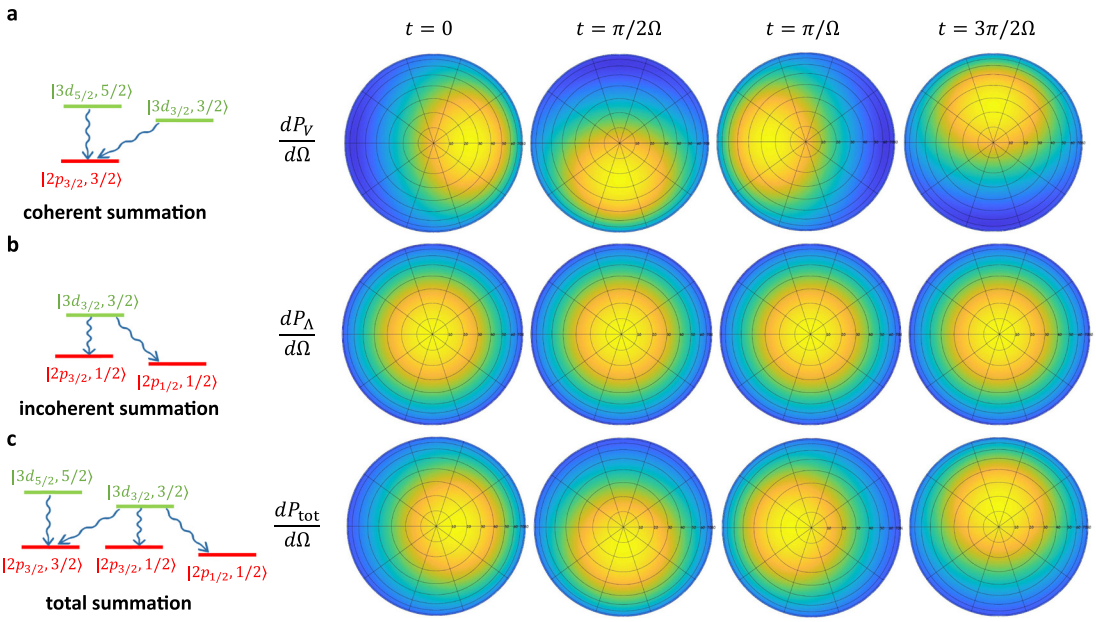

FIG. 12. Quantum beats in the emission pattern from the hydrogen atom. The atom is prepared in a coherent superposition of two initial states, $|3d_{3/2},3/2\rangle$ and $|3d_{5/2},5/2\rangle$, while three possible final states are considered: $|2p_{3/2},3/2\rangle$, $|2p_{3/2},1/2\rangle$ and $|2p_{1/2},1/2\rangle$. In this configuration, the atom comprises both a V-type and a Λ-type system. Right: depiction of the radiation pattern from each subsystem and the total system, for different times within one beat period. (a) For the V-type system, the two initial states share the same final state, and thus their field amplitudes are summed coherently; the radiation pattern thus exhibits quantum beats. (b) For the Λ-type system, the initial state decays to two distinct final states and the field amplitudes are summed incoherently; the radiation pattern is then constant in time. (c) The total system displays quantum beats with limited visibility.

The slowly varying instantaneous power emitted to the far field in vacuum is, according to Eq. (56) and applying the dipole approximation,

$$\frac{dP(t)}{d\Omega} = \frac{e^2\epsilon_0 c\mu_0^2\omega_0^4}{8\pi^2}\sum_{ii'}\sum_{f\sigma}\rho_e(i,i')e^{i(\omega_{fi}-\omega_{fi'})\left(t-\frac{r}{c}\right)}\boldsymbol{d}_{fi}^*\cdot\hat{\boldsymbol{\epsilon}}_\sigma\hat{\boldsymbol{\epsilon}}_\sigma\cdot\boldsymbol{d}_{fi'}, \tag{107}$$

with $\omega_0 = (E_3 - E_2)/\hbar = 5E_R/36\hbar$ where E_R is the Rydberg energy. The corresponding transition dipole moments are $\boldsymbol{d}_{e1\to g1} = -\frac{1}{\sqrt{5}}d\hat{\mathbf{z}}$, $\boldsymbol{d}_{e1\to g2} = \sqrt{\frac{2}{3}}d\hat{\mathbf{e}}_R$, $\boldsymbol{d}_{e2\to g1} = \sqrt{2}d\hat{\mathbf{e}}_R$, and $\boldsymbol{d}_{e1\to g3} = \sqrt{\frac{5}{3}}d\hat{\mathbf{e}}_R$, where $\hat{\mathbf{e}}_R = (\hat{\mathbf{x}} + i\hat{\mathbf{y}})/\sqrt{2}$ and $d = \frac{2^{11}3^4}{5^7}a_0$. The instantaneous power spectrum due to the Λ-system is constant in time,

$$\frac{dP_\Lambda}{d\Omega} = \hbar\omega_0\frac{\omega_0^3\alpha d^2}{2\pi c^2}\frac{7}{6}|c_1|^2(1+\cos^2\theta), \tag{108}$$

as expected. The V-system, however, displays a temporally-varying spectrum

$$\frac{dP_V}{d\Omega} = \hbar\omega_0\frac{\omega_0^3\alpha d^2}{2\pi c^2}\left[\frac{1+4|c_2|^2}{5} + \frac{6|c_2|^2-1}{5}\cos^2\theta + \frac{|c_1c_2|}{\sqrt{5}}\cos(\Omega t+\varphi_{21}+\phi)\sin 2\theta\right], \tag{109}$$

where $\varphi_{21} = \arg(c_1^*c_2)$. The beat frequency is then

$$\Omega = \omega_{e2\to g1} - \omega_{e1\to g1} = \frac{2\alpha^2}{45}\omega_0. \tag{110}$$

Finally, the total time-varying power for $|c_1| = |c_2| = 1/\sqrt{2}$ is

$$\frac{dP}{d\Omega} = \frac{dP_\Lambda}{d\Omega} + \frac{dP_V}{d\Omega} = \hbar\omega_0\frac{\omega_0^3\alpha d^2}{4\pi c^2}\left[\frac{67}{20} + \frac{59}{60}\cos 2\theta + \frac{1}{\sqrt{5}}\sin 2\theta\cos(\Omega t+\varphi_{21}+\phi)\right]. \tag{111}$$

C. Purcell enhancement of a general emitter near a material boundary

In this subsection, we exemplify the use of the TCF to derive the Purcell factor of a general emitter near a material boundary, allowing for corrections beyond the dipole approximation.

Consider an emitter situated at a height h above a planar boundary. We are now interested in how the transition rate is altered by the presence of the boundary compared to its free-space transition rate, or in other words, we wish to calculate the Purcell factor. For this calculation, we shall employ the angular spectrum decomposition of the reflected part of the dyadic Green function, derived in Ref. 96 in Cartesian coordinates, and overviewed in the supplementary material, Secs. SI30–SI31. As the medium in question is rotationally invariant around the z axis, a more transparent form of the reflected Green function can be obtained using cylindrical coordinates:

$$\mathbf{G}_{ref}(\mathbf{r},\mathbf{r}',\omega) = \frac{i}{8\pi^2}\int d^2\mathbf{k}_T\frac{e^{i\mathbf{k}_T\cdot(\mathbf{r}_T-\mathbf{r}_T')+i\sqrt{k_0^2-k_T^2}(z+z')}}{\sqrt{k_0^2-k_T^2}}\boldsymbol{\mathcal{G}}_{ref}(\mathbf{k}_T), \tag{112}$$

with the momentum-space tensor

$$\mathcal{G}_{\text{ref}}(\mathbf{k}_T) = \curlyvee_s(k_T)\widehat{\boldsymbol{\phi}}\widehat{\boldsymbol{\phi}} - \curlyvee_p(k_T)\left(\frac{\sqrt{k_0^2-k_T^2}}{k_0}\widehat{\boldsymbol{\rho}} - \frac{k_T}{k_0}\widehat{\mathbf{z}}\right)\left(\frac{\sqrt{k_0^2-k_T^2}}{k_0}\widehat{\boldsymbol{\rho}} + \frac{k_T}{k_0}\widehat{\mathbf{z}}\right), \tag{113}$$

where $\curlyvee_s$ and $\curlyvee_p$ are the s- and p-polarized Fresnel reflection coefficients. Since the total Green function in the upper half-space is $\mathbf{G}(\mathbf{r},\mathbf{r}',\omega) = \mathbf{G}^{(0)}(\mathbf{r},\mathbf{r}',\omega) + \mathbf{G}_{\text{ref}}(\mathbf{r},\mathbf{r}',\omega)$, the Purcell factor becomes (see the supplementary material, Sec. SI31 for derivation)

$$F_P = 1 + \frac{\alpha}{\pi c e^2 \Gamma_{\text{fi},0}}\text{Re}\int d^2\mathbf{k}_T \frac{e^{2ih\sqrt{k_{\text{fi}}^2-k_T^2}}}{\sqrt{k_{\text{fi}}^2-k_T^2}} \boldsymbol{\jmath}_{\text{fi}}^*\left(\mathbf{k}_T, \sqrt{k_{\text{fi}}^2-k_T^2}\right) \cdot \mathcal{G}_{\text{ref}}(\mathbf{k}_T)\cdot \boldsymbol{\jmath}_{\text{fi}}\left(\mathbf{k}_T, -\sqrt{k_{\text{fi}}^2-k_T^2}\right), \tag{114}$$

where $\boldsymbol{\jmath}_{\text{fi}}(\mathbf{k})$ are the momentum-space transition currents given in Eq. (14), and $k_{\text{fi}} = \omega_{\text{fi}}/c$. It is important to emphasize that Eq. (114) is general, for any emitter transition—especially those that are beyond the dipole approximation—and any boundary material characterized by its reflection coefficients, $\curlyvee_s$ and $\curlyvee_p$ [as in Fig. 4(b)]. For completeness, we include the known result for a transition dipole moment $\boldsymbol{d}_{\text{fi}}$,

$$F_P = 1 + \frac{3}{4}\frac{|d_{\text{fi},x}|^2 + |d_{\text{fi},y}|^2}{|d_{\text{fi}}|^2}\text{Re}\int_0^\infty dx e^{2ihk_{\text{fi}}\sqrt{1-x^2}}\left[\frac{x}{\sqrt{1-x^2}}\curlyvee_s(x) - x\sqrt{1-x^2}\curlyvee_p(x)\right] + \frac{3}{2}\frac{|d_{\text{fi},z}|^2}{|d_{\text{fi}}|^2}\text{Re}\int_0^\infty dx e^{2ihk_{\text{fi}}\sqrt{1-x^2}}\frac{x^3}{\sqrt{1-x^2}}\curlyvee_p(x), \tag{115}$$

for $x = k_T/k_{\text{fi}}$, recovering the result in Ref. 96.

D. Interband transitions of excitons in quantum dots

The purpose of this subsection is to employ the TCF for a solid-state emitter, such as quantum wells or quantum dots. Excitonic transitions in quantum dots with mesoscopic dimensions[40,46,98] as well as those in quantum wells[45,160] have gained interest in the past decade due to their ability to break the dipole approximation, thus altering the emission rate and patterns, and even shifting the emission frequencies (see Fig. 5).

To formally describe a transition in a condensed-matter system, it is sometimes useful to use the second-quantization formalism for the transition current, Eq. (9), especially when a many-body state is involved. For example, in order to describe the recombination of a single electron–hole pair (that is, a single electron placed in the conduction band and a single hole in the valence band), one formally needs to consider a many-body state. We define the initial state as

$$|\text{i}\rangle \equiv |\chi\rangle = \sum_{\mathbf{k}_c,\mathbf{k}_v}\chi(\mathbf{k}_c,\mathbf{k}_v)c_{v,\mathbf{k}_v}c^\dagger_{c,\mathbf{k}_c}|\mathcal{F}\rangle, \tag{116}$$

denoting an exciton eigenstate, expanded in terms of single-electron excitations of the conduction (c) and valence (v) bands, where $\chi(\mathbf{k}_c,\mathbf{k}_v)$ are the expansion coefficients and $|\mathcal{F}\rangle$ is the Fermi Sea state $|\mathcal{F}\rangle = |1_{v,\mathbf{q}_1},1_{v,\mathbf{q}_2},\ldots,1_{v,\mathbf{q}_N}\rangle \otimes |0_{c,\mathbf{q}_1},0_{c,\mathbf{q}_2},\ldots,0_{c,\mathbf{q}_N}\rangle$ where all electrons are in the valence band. The final state is then the Fermi sea, which is the ground state of the system

$$|\text{f}\rangle \equiv |\mathcal{F}\rangle = |1_{v,\mathbf{q}_1},1_{v,\mathbf{q}_2},\ldots,1_{v,\mathbf{q}_N}\rangle \otimes |0_{c,\mathbf{q}_1},0_{c,\mathbf{q}_2},\ldots,0_{c,\mathbf{q}_N}\rangle. \tag{117}$$

We now employ the well-known envelope function approximation,[46,47,221,222] and use the symmetries of the Bloch functions,[222] under which the transition current becomes (see derivation in the supplementary material, Sec. SI23)

$$\mathbf{j}_{\text{fi}}(\mathbf{r}) = \frac{e}{m}\left\langle u^*_{0,v}(-i\hbar\nabla)u_{0,c}\right\rangle_{UC}\chi(\mathbf{r},\mathbf{r}), \tag{118}$$

where $\chi(\mathbf{r}_e,\mathbf{r}_h)$ is the so-called envelope function, which is an eigenfunction of the Electron–hole effective mass Hamiltonian:[46]

$$H_{\text{exc}} = \frac{\mathbf{p}_e^2}{2m_e^*} + \frac{\mathbf{p}_h^2}{2m_h^*} + V_e(\mathbf{r}_e) + V_h(\mathbf{r}_h) - \frac{q^2}{4\pi\epsilon_0\epsilon_r|\mathbf{r}_e-\mathbf{r}_h|}. \tag{119}$$

Here, $m^*_{e(h)}$ is the effective electron (hole) mass, $V_{e(h)}(\mathbf{r})$ is the external confining potential of the quantum dot felt by the electron (hole), $u_{\mathbf{k}_{v/c}}(\mathbf{r})$ are Bloch functions, and $\langle\cdot\rangle_{UC}$ denotes a unit cell expectation value.

Importantly, under the envelope function approximation, the transition current corresponding to Electron–hole recombination is dominated by the transition matrix element of the momentum operator between the conduction and valence Bloch functions:[46]

$$\mathbf{p}_{\text{cv}} = \left\langle u^*_{0,v}(-i\hbar\nabla)u_{0,c}\right\rangle_{UC}. \tag{120}$$

Usually, one considers different regimes for the calculation of $\chi(\mathbf{r}_e,\mathbf{r}_h)$: the unconfined regime [bulk exciton with $V_e = V_h = 0$, wherein $\chi(\mathbf{r}_e,\mathbf{r}_h)$ is just the hydrogen-like wave function], strong confinement [$V_e, V_h \gg$ Coulomb attraction, wherein $\chi(\mathbf{r}_e,\mathbf{r}_h) = \chi_e(\mathbf{r}_e)\chi_h(\mathbf{r}_h)$ and the electron and hole wave functions are separable], and weak confinement (both the confining and Coulomb potentials are dominant). In this section, we focus on the latter.

For the special case of a parabolic confinement, we can write

$$V_{e(h)} = \frac{1}{2}m^*_{e(h)}\Omega_x^2x^2_{e(h)} + \frac{1}{2}m^*_{e(h)}\Omega_y^2y^2_{e(h)} + \frac{1}{2}m^*_{e(h)}\Omega_z^2z^2_{e(h)}, \tag{121}$$

and then decompose $\chi(\mathbf{r}_e,\mathbf{r}_h)$ into a center-of-mass (cm) part and a relative motion part as

$$\chi(\mathbf{r}_e,\mathbf{r}_h) = \chi_{\text{cm}}(\mathbf{r}_{\text{cm}})\chi_{\text{rel}}(\mathbf{r}_{\text{rel}}), \tag{122}$$

where $\mathbf{r}_{\text{cm}}, \mathbf{r}_{\text{rel}}$ are the center-of-mass and relative coordinates, respectively. Then, the wave functions $\chi_{\text{cm}}(\mathbf{r}_{\text{cm}})$ and $\chi_{\text{rel}}(\mathbf{r}_{\text{rel}})$ are, respectively, eigenstates of the quantum harmonic oscillator (with total mass $M^* = m_e^* + m_h^*$) and the hydrogen-like potential (with relative mass $\mu^* = m_e^*m_h^*/(m_e^*+m_h^*)$). The combined energy ladder of the harmonic and hydrogen potentials define the exciton subbands of energies

$$E_{n_xn_yn_z;n} = E_c + \hbar\Omega_x\left(n_x+\frac{1}{2}\right) + \hbar\Omega_y\left(n_y+\frac{1}{2}\right) + \hbar\Omega_z\left(n_z+\frac{1}{2}\right) - \frac{E_R}{n^2}, \tag{123}$$

where E_c is the conduction band energy and E_R is the Rydberg energy corresponding to the hydrogen-like potential. In this case, the transition current simplifies to

$$\mathbf{j}_{\text{fi}}(\mathbf{r}) = \frac{e}{m}\mathbf{p}_{\text{cv}}\chi_{\text{rel}}(0)\chi_{\text{cm}}(\mathbf{r}). \tag{124}$$

Here, χ_{rel} is a hydrogenic wave function ψ_{nlm}, with l being the orbital angular momentum. Further, the value of $\chi_{\mathrm{rel}}(0)$ is nonzero only for $l = 0$, and hence, OAM-carrying transitions are forbidden; thus, we have

$$\chi_{\mathrm{rel}}(0) = \frac{\delta_{l,0}}{\sqrt{\pi} n^{\frac{5}{2}} n! a_{\mathrm{B}}^{\frac{3}{2}}}. \tag{125}$$

The center-of-mass wave function, χ_{cm}, corresponds to a three-dimensional Harmonic oscillator wave function

$$\chi_{\mathrm{cm}}(\mathbf{r}) = \prod_{i=1}^{3} \left(\frac{1}{2\pi\Delta r_i^2}\right)^{\frac{1}{4}} \frac{\exp\left(-\frac{1}{4}\frac{r_i^2}{\Delta r_i^2}\right)}{\sqrt{2^{n_{r_i}} n_{r_i}!}} H_{n_{r_i}}\left(\frac{r_i}{\sqrt{2}\Delta r_i}\right), \tag{126}$$

with $r_i = x, y, z$ and $\Delta r_i = \sqrt{\frac{\hbar}{2M^*\Omega_{r_i}}} = \Delta x, \Delta y, \Delta z$.

E. Emission patterns from mesoscopic quantum dots beyond the dipole approximation

In this subsection, we proceed with the quantum dot example and use transition currents to calculate—both analytically and numerically using an electromagnetic solver—the emission pattern from a mesoscopic quantum dot that breaks the dipole approximation. To this end, we consider the simple case of a recombination from the ground excitonic state $|000;0\rangle$ for an azimuthally symmetric, mesoscopic quantum dot: $\Delta x = \Delta y = \Delta r_T \neq \Delta z$, that is comparable to λ, the optical wavelength.[46] Assuming the conduction-to-valence transition dipole to be along the z direction, the corresponding transition current is then

$$\mathbf{j}_{\mathrm{fi}}(\mathbf{r}) = -ie\omega_{\mathrm{cv}} d_{\mathrm{cv}} \hat{\mathbf{z}} \frac{(2\pi)^{\frac{3}{4}}}{\sqrt{\pi V_{\mathrm{QD}} V_{\mathrm{B}}}} \exp\left(-\frac{1}{4}\frac{x^2+y^2}{\Delta r_T^2} - \frac{1}{4}\frac{z^2}{\Delta z^2}\right), \tag{127}$$

and its Fourier transform is

$$\boldsymbol{j}_{\mathrm{fi}}(k\hat{\mathbf{n}}) = -ie\omega_{\mathrm{cv}} d_{\mathrm{cv}} \hat{\mathbf{z}} \left(\frac{2}{\pi}\right)^{\frac{3}{4}} \sqrt{\frac{V_{\mathrm{QD}}}{\pi V_{\mathrm{B}}}} e^{-\frac{1}{4}\bar{k}_T^2 \sin^2\theta - \frac{1}{4}\bar{k}_z^2 \cos^2\theta}, \tag{128}$$

again denoting $\bar{k}_j = 2\Delta r_j k$ with $j = T, z$, where we have defined the quantum dot volume as $V_{\mathrm{QD}} = \Delta x \Delta y \Delta z$ and the Bohr volume $V_{\mathrm{B}} = a_{\mathrm{B}}^3$. When the values of $\bar{k}_j$ become comparable to or larger than unity, that is, for example, whenever $\Delta r_T, \Delta z \gtrsim \lambda/4\pi \sim 40$ nm for $\lambda = 500$ nm, the emission is strongly modified compared to a dipole emission pattern. We illustrate this by calculating and simulating the emission patterns from nonlocal quantum dots in both free space and near a boundary, as illustrated in Fig. 13.

VI. APPLICATIONS OF TRANSITION CURRENTS TO FREE-ELECTRON SYSTEMS

Most uses of transition currents in the literature were in bound-electron systems, but recent years have shown that the TCF can be useful in various problems involving free electrons, particularly in the context of optical excitations in electron microscopy.[74,85,86,90,188]

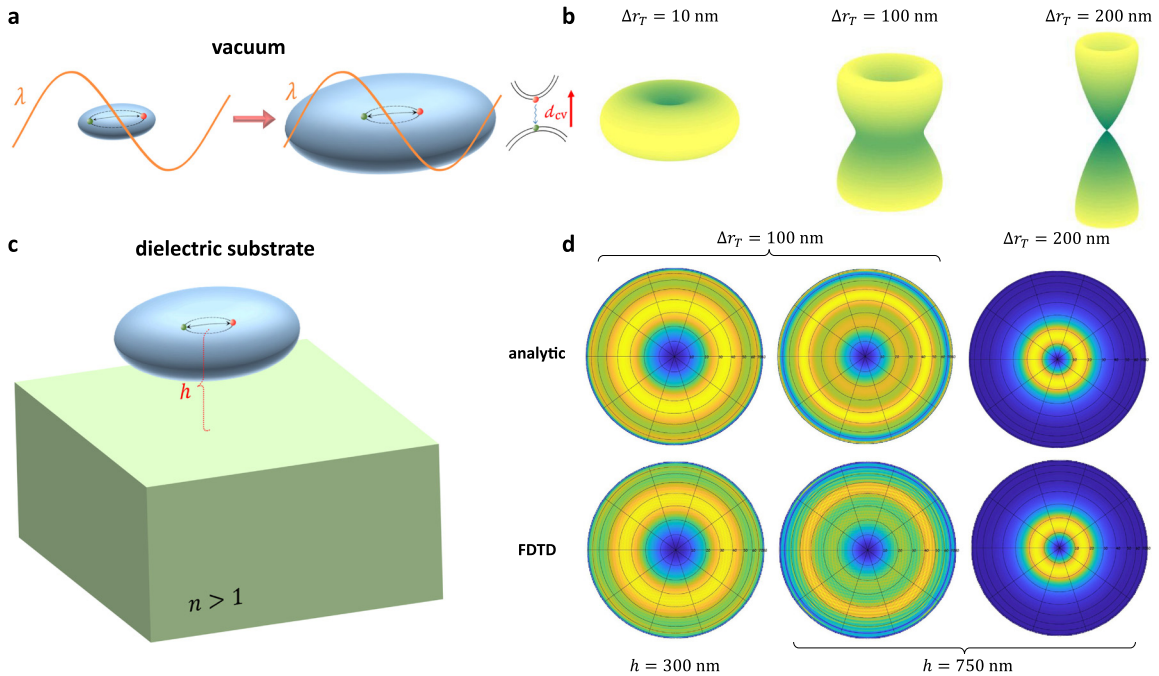

FIG. 13. Radiation patterns from mesoscopic quantum dots in vacuum and above a dielectric substrate. (a) Depiction of the scaling of quantum dot dimensions compared to the emitted wavelength, which already display considerable deviation from the dipole approximation even for emission in vacuum. (b) Analytic radiation patterns in free space for different transverse quantum dot dimensions. (c) Depiction of a mesoscopic quantum dot situated at a height h above a dielectric interface of refractive index n. (d) Analytically calculated and numerically simulated radiation patterns into the vacuum side for different transverse quantum dot size and height above the interface. We consider $\lambda = 500$ nm $\Delta z = \Delta r_T/4$, and a fused silica substrate with $n = 1.46$.

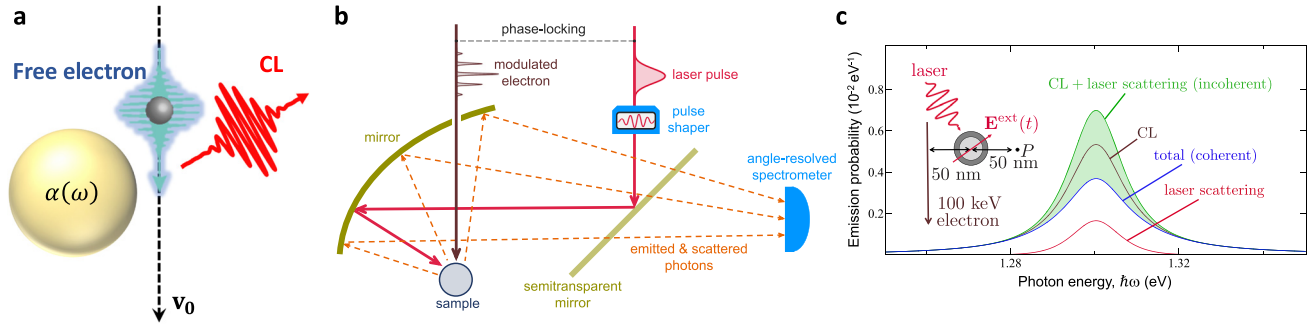

FIG. 14. Coherent light emission from free electrons interacting with a polarizable nanoparticle. (a) Depiction of coherent cathodoluminescence—spontaneous light emission by a free electron, here passing close to a nanoparticle of polarizability $\alpha(\omega)$. (b) Proposal for an experimental setup in which a free electron wave function, pre-modulated by a laser field, interacts with a sample driven by the same laser pulse, leading to coherent interference that alters the cathodoluminescence emission.[188] (c) Calculation of the light emission and scattering for the interaction depicted in panel (b), showing inhibition of the total field below the incoherent summation of the scattered and spontaneously emitted fields[188] (parameters are shown in the inset). Reproduced with permission from Di Giulio *et al.*, ACS Nano **15**, 7290 (2021). Copyright 2021 Authors, licensed under a Creative Commons Attribution (CC BY) License.

The places in which transition currents are of special importance in free-electron physics are where the electron wave function is manipulated, which is an area of relevance due to recent experimental advances.[69,89,223–227] As we shall demonstrate below, another important regime for transition currents is the recoiled regime of free-electron light emission,[141] which has recently become experimentally accessible.[178]

A. Electron interaction with a nanoparticle: Cathodoluminescence and energy-loss spectroscopy

To describe coherent cathodoluminescence light emission from a polarizable nanoparticle [Fig. 14(a)], we apply Eq. (48) for the case where the free electron travels aloof with respect to a nanoparticle of polarizability $\boldsymbol{\alpha}(\omega)$ located at $\mathbf{r}_0 = 0$ in vacuum. We use the Dyson expansion for the dyadic Green function, Eq. (32). By taking the nonretarded near-field approximation [Eq. (30)] for $\mathbf{G}^{(0)}(0, \mathbf{r}', \omega)$ on the right, and the far-field approximation [Eq. (39)] for $\mathbf{G}^{(0)}(\mathbf{r}, 0, \omega)$ on the left, we find the CL probability per unit frequency (see the supplementary material Sec. SI10 for derivation)

$$\frac{dp_{\mathrm{CL}}}{d\omega} = \frac{1}{(4\pi\epsilon_0)^3}\frac{8e^2\omega^5}{3\pi c^3\hbar v^4}\int d^2\mathbf{r}_T \left|\psi_{\mathrm{i},T}(\mathbf{r}_T)\right|^2 \left|\boldsymbol{\alpha}(\omega)\cdot\mathbf{F}(\mathbf{r}_T,\omega)\right|^2, \quad (129)$$

where

$$\mathbf{F}(\mathbf{r}_T,\omega) = K_1\left(\frac{\omega}{v}r_T\right)\hat{\mathbf{r}}_T + iK_0\left(\frac{\omega}{v}r_T\right)\hat{\mathbf{z}}, \quad (130)$$

and K_n denotes the modified Bessel function of the second kind. Up to relativistic corrections (i.e., for $c \to \infty$), the result derived in Ref. 74 is recovered for $\left|\psi_{\mathrm{i},T}(\mathbf{r}_T)\right|^2 = \delta(\mathbf{r}_T - \mathbf{r}_{T0})$.

To calculate the energy loss rate, we again employ the Dyson expansion for the dyadic Green function, Eq. (32), but this time take the nonretarded near-field approximation of Eq. (30) for $\mathbf{G}^{(0)}$ on both sides. This gives

$$\mathrm{Im}\mathbf{G}_{\mathrm{S}}(\mathbf{r},\mathbf{r}',\omega) = \frac{1}{(4\pi\epsilon_0)^2}\frac{\epsilon_0 c^2}{\omega^2}\frac{3\hat{\mathbf{r}}\hat{\mathbf{r}} - \mathbf{I}}{r^3}\cdot\mathrm{Im}\boldsymbol{\alpha}(\omega)\cdot\frac{3\hat{\mathbf{r}}'\hat{\mathbf{r}}' - \mathbf{I}}{r'^3}. \quad (131)$$

We use Eq. (85) to calculate the EELS probability, giving (see the supplementary material, Sec. SI15 for derivation)

$$\frac{dp_{\mathrm{EELS}}}{d\omega} = \frac{1}{(4\pi\epsilon_0)^2}\frac{4e^2\omega^2}{\pi\hbar v^4}\int d^2\mathbf{r}_T \left|\psi_{\mathrm{i},T}(\mathbf{r}_T)\right|^2 \mathbf{F}^*(\mathbf{r}_T,\omega)\cdot\mathrm{Im}\{\boldsymbol{\alpha}(\omega)\}\cdot\mathbf{F}(\mathbf{r}_T,\omega). \quad (132)$$

Again, up to relativistic corrections, the result derived in Ref. 74 is recovered for $\left|\psi_{\mathrm{i},T}(\mathbf{r}_T)\right|^2 = \delta(\mathbf{r}_T - \mathbf{r}_{T0})$.

B. Interference of cathodoluminescence with external light

In this subsection, we show how the TCF can capture experimental scenarios in free-electron light emission where an external, classical laser field interferes with the spontaneously emitted light. Whenever two or more sources of electromagnetic field are coherently coupled to the same system, interference effects start playing a role as a result of the simultaneous stimulation of absorption and emission processes between the levels constituting the sample. Practical examples are given by pump-probe scenarios in which a laser and an electron pulse illuminate simultaneously a sample[87,188] [Figs. 14(b) and 14(c)] as well as by situations when several electrons are sent together to interact with the same specimen[74,86] [Figs. 8(c) and 8(d)]. Recently, this concept was extended to include interference between a free-electron CL emission at two consecutive samples.[228]

From a theoretical point of view, the exploration of such phenomena can be readily performed by assuming that the total current is composed of a sum of a classical component $\mathbf{j}^{\mathrm{laser}}(\mathbf{r},\omega)$, responsible for the production of a classical external laser pulse, and a quantum current operator $\hat{\mathbf{j}}^{\mathrm{e}^-}(\mathbf{r},\omega)$, whose second-quantized form is able to directly capture the presence of multiple electrons,[74,86,188] as discussed in Sec. III F:

$$\hat{\mathbf{j}}(\mathbf{r},\omega) = \hat{\mathbf{j}}^{\mathrm{e}^-}(\mathbf{r},\omega) + \mathbf{j}^{\mathrm{laser}}(\mathbf{r},\omega). \quad (133)$$

This line of thought was first adopted in the context of homodyne detection to study the interference between the cathodoluminescence light emission produced by an electron compressed via the so-called photon-induced near-field electron microscopy (PINEM) interaction and a reference laser[87] (a component of the same laser used for PINEM). A similar approach explored the possibility to retrieve the quantum coherence of the shaped electron wave function through

spectral shear interferometry of the emitted light[85] [Figs. 7(c) and 7(d)]. In a related development, the possibility of performing pump-probe measurements with synchronized electron and laser pulses was explored as an approach to reach a combination of meV-nm-fs resolutions.[188] In these works, the probability of measuring a photon is obtained by multiplying Eq. (42) by the time of interaction T and dividing it by the emitted photon energy $\hbar\omega$, yielding

$$\frac{d^2p_{\mathrm{cl}}}{d\Omega d\omega} = \frac{r^2\epsilon_0 c}{\pi\hbar\omega}\left\langle \widehat{\mathbf{E}}^{\dagger}(r\hat{\mathbf{n}},\omega)\cdot\widehat{\mathbf{E}}(r\hat{\mathbf{n}},\omega)\right\rangle. \tag{134}$$

As we have seen in Eq. (12), the evaluation of this expression demands the calculation of the expectation value of the current correlations, which in our case becomes

$$\begin{aligned}\left\langle \widehat{\mathbf{j}}^{\dagger}(\mathbf{r},\omega)\widehat{\mathbf{j}}(\mathbf{r}',\omega')\right\rangle = &\left\langle \widehat{\mathbf{j}}^{\mathrm{e}^-\dagger}(\mathbf{r},\omega)\widehat{\mathbf{j}}^{\mathrm{e}^-}(\mathbf{r}',\omega')\right\rangle\\ &+\left\langle \widehat{\mathbf{j}}^{\mathrm{e}^-\dagger}(\mathbf{r},\omega)\right\rangle\mathbf{j}^{\mathrm{laser}}(\mathbf{r}',\omega')\\ &+\mathbf{j}^{\mathrm{laser}*}(\mathbf{r},\omega)\left\langle \widehat{\mathbf{j}}^{\mathrm{e}^-}(\mathbf{r}',\omega')\right\rangle\\ &+\mathbf{j}^{\mathrm{laser}*}(\mathbf{r},\omega)\mathbf{j}^{\mathrm{laser}}(\mathbf{r}',\omega'),\end{aligned} \tag{135}$$

involving two- and one-current operator expectation values, $\left\langle \widehat{\mathbf{j}}^{\mathrm{e}^-\dagger}(\mathbf{r},\omega)\widehat{\mathbf{j}}^{\mathrm{e}^-}(\mathbf{r}',\omega')\right\rangle$ and $\left\langle \widehat{\mathbf{j}}^{\mathrm{e}^-}(\mathbf{r},\omega)\right\rangle$ respectively. Remarkably, the TCF can reproduce the same results (see Refs. 87 and 188 for a proof based on macroscopic QED that the current formalism applies to this configuration). In particular, terms coming from the two-current averages account for photons that are incoherently emitted from every individual electron as well as for the coherent emission from each electron pair (as discussed in Sec. III F), while the remaining one-current terms include the effect of signal suppression or enhancement produced by the destructive or constructive interference of the emission coming from each electron and the external laser pulse.

The above result becomes more interesting when N electrons are involved: as we have seen in Eq. (60), the incoherent signal is proportional to N, while the mutual electron–electron emission leads to a coherent amplification of the total signal proportional to N^2 if the electrons are in phase,[74,147,229] an effect known as super-radiance. The amount of achievable modulation is determined by the so-called coherence factor,[87,188] defined in Eq. (57) as $M_\omega^j = \int_{-\infty}^{\infty} dz\,|\phi_j(z)|^2 e^{\frac{i\omega z}{v}}dz$ for an electron labeled by j. The absolute value of the coherence factor is constrained to $0 \le |M_\omega^j| \le 1$ due to wave function normalization, with the lower bound applying to unsynchronized electron beams with a well-defined momentum $\phi_j(z) \propto e^{ikz}$, and the upper limit of one reached for classical-point particle electrons $|\phi_j(z)|^2 = \delta(z)$. Interestingly, the interaction of an electron with light, either close to an interface in a PINEM setup[230,231] or in free space via stimulated Compton scattering,[232,233] followed by a macroscopic propagation of the order of millimeters, can produce a substantial coherence factor at multiple harmonics of the modulating laser frequency, while a combination of several PINEM interactions and macroscopic propagation leads to $|M_\omega^j| \sim 1$, as in Ref. 234.

C. Smith–Purcell radiation and quantum-recoil corrections

This subsection shows that transition currents can be applied to also capture quantum-optical phenomena that directly arise from the quantized nature of the photon—as in the recoil of a free electron due to the emission of a photon. This result helps to emphasize that despite not having to handle the electromagnetic field using second quantization, the transition-current approach does not miss such quantum effects.

As a representative type of radiation emission from free electrons, we consider Smith–Purcell radiation,[71] which is obtained whenever a free electron traverses a periodic structure (Fig. 15). This radiation emission is characterized by a distinctive dispersion relation connecting the emission angle with respect to the electron direction of motion, θ, the emitted wavelength, λ, and the period of the structure, Λ:

$$\lambda(\theta) = \frac{\Lambda}{n}\left(\beta^{-1} - \cos\theta\right). \tag{136}$$

Here, n is the diffraction order and $\beta = v/c$ the normalized electron velocity. We utilize this effect to exemplify both the use of numerical solvers for the calculation of SP radiation patterns and spectra, as well as for quantum corrections that go beyond the nonrecoil approximation.[64,141,178] As discussed in Sec. II D, these corrections are all encapsulated in the transition current.

We begin with a conventional case of SP radiation, employing the transition currents under the nonrecoil approximation, which is valid for most experimental conditions. Given an initial electron wave function envelope $\phi_i(\mathbf{r})$, the paraxial and nonrecoil approximations can be employed as in Eq. (22), giving the expression for the power spectrum as in Eq. (48). An FDTD solver could be used to calculate the Fourier integral over the far-field Green function, by placing an array of dipole emitters pointing along z, with a phase lag of $e^{i\frac{\omega}{v}z}$ between them[235,236] and recording the far field. An incoherent summation over different lateral positions of the dipole lines—weighted by the modulus squared of the transverse electron wave function $|\phi_{\mathrm{i},T}(\mathbf{r}_T)|^2$—is then required. The latter procedure is valid when only the light is measured, and the electron final state is traced out. This independence of coherent cathodoluminescence on the electron wave function (i.e., just a trivial dependence on the probability density, but not on the phase of the wave function) has been investigated and confirmed both theoretically and experimentally.[69,74]

Equivalently, one may choose to take advantage of the periodicity of the system and perform the simulation over a single unit cell instead. Owing to the periodicity of the structure, the far field Green function satisfies $\mathbf{G}_\infty(r\hat{\mathbf{n}},\mathbf{r}'-\hat{\mathbf{z}}n\Lambda,\omega) = e^{\frac{i\omega}{c}\hat{\mathbf{n}}\cdot\hat{\mathbf{z}}n\Lambda}\mathbf{G}_\infty(r\hat{\mathbf{n}},\mathbf{r}',\omega)$, and we can write Eq. (48) as (see the supplementary material, Sec. SI24 for derivation)

$$\frac{d^2P}{d\Omega d\omega} = \left|\frac{\sin\left[\left(\frac{\omega}{c}\cos\theta - \frac{\omega}{v}\right)\frac{N\Lambda}{2}\right]}{\sin\left[\left(\frac{\omega}{c}\cos\theta - \frac{\omega}{v}\right)\frac{\Lambda}{2}\right]}\right|^2 \int d^2\mathbf{r}_T\left|\phi_{\mathrm{i},T}(\mathbf{r}_T)\right|^2\left[\frac{d^2P(\mathbf{r}_T)}{d\Omega d\omega}\right]_{UC}, \tag{137}$$

where $\left[d^2P(\mathbf{r}_T)/d\Omega d\omega\right]_{UC}$ is the recorded far-field power spectrum for a portion of the electron beam current inside a single unit cell:

$$\left[\frac{d^2P(\mathbf{r}_T)}{d\Omega d\omega}\right]_{UC} = \frac{r^2\omega^2e^2}{\pi c^3\epsilon_0 T}\left|\int_{UC} dz e^{\frac{i\omega}{v}z}\mathbf{G}_\infty(r\hat{\mathbf{n}},\mathbf{r}_T,z,\omega)\cdot\hat{\mathbf{z}}\right|^2, \tag{138}$$

where $\int_{UC}\cdot$ denotes integration over the (longitudinal) unit cell, and N is the number of periodicities traversed by the electron.

Having established the non-recoil result, we now proceed to employ the TCF considering quantum recoil effects. In this manner, the transition-current approach can incorporate "quantum corrections" even

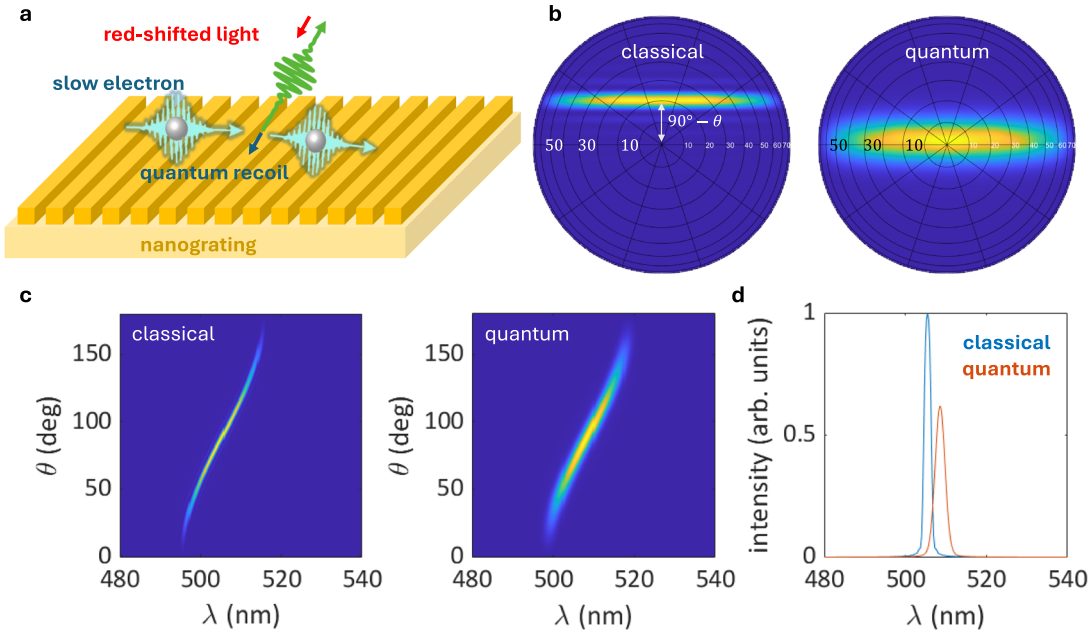

FIG. 15. Quantum corrections to Smith–Purcell radiation from slow quantum electrons traversing a nanograting—simulated via FDTD. (a) Depiction of Smith–Purcell radiation from a slow electron that experiences a considerable recoil, revealing quantum aspects of the electron; this results in a redshift of the emitted light spectrum. (b) Classical [Eq. (138)] and quantum-corrected [Eq. (140)] emission patterns for $\lambda = 509$ nm. In this example, the far-field angular plots are defined with respect to the grating normal, i.e., a situation where a detector is placed above and parallel to the grating surface. Hence the elevation angle corresponds in the highlighted case to $90°-\theta$, where θ is the observation angle with respect to the electron trajectory. We note, however, that in some experiments involving angle-resolved measurements of CL in grazing-angle incidence,[84] the detector plane is in fact perpendicular to the sample surface, and the polar angles can be defined with respect to the electron trajectory. (c) Classical and quantum Smith–Purcell dispersion, as a function of the observation angle θ and wavelength. (d) Classical and quantum spectra for an aperture $\Delta\theta = 10°$ around $\theta = 90°$. The expected redshift and additional uncertainty are clearly visible. We consider a grating with a pitch $\Lambda = 10$ nm, electron of energy $E = 100$ eV and energy uncertainty $\Delta E = 0.4$ eV.

when used as a source current for classical electromagnetic numerical solvers. To demonstrate this, we derive the transition current for a slow ($\gamma \sim 1$) Schrödinger free electron without neglecting quantum recoil and dispersion effects. In this case, we have, using Eqs. (18) and (21),

$$\mathbf{j}_{\mathrm{fi}}(\mathbf{r},\omega) = \frac{e\mathbf{v}_0}{\sqrt{V}}\int \frac{d^3\delta\mathbf{k}_{\mathrm{i}}}{(2\pi)^3}\tilde{\phi}_i(\delta\mathbf{k}_{\mathrm{i}})e^{i(\mathbf{q}+\delta\mathbf{k}_{\mathrm{i}})\cdot\mathbf{r}} \times 2\pi\delta\left(\omega - \mathbf{q}\cdot\mathbf{v}_0 - \delta\mathbf{k}_{\mathrm{i}}\cdot\mathbf{v}_0 - \frac{\hbar}{2m}\delta\mathbf{k}_{\mathrm{i}}^2 + \frac{\hbar}{2m}\mathbf{q}^2\right), \quad (139)$$

with $\mathbf{q} = \mathbf{k}_0 - \mathbf{k}_{\mathrm{f}}$. Using the recoiled transition current of Eq. (139), we obtain the quantum-corrected power spectrum of a localized transverse wave function [i.e., $|\phi_{i,T}(\mathbf{r}_T)|^2 \sim \delta(\mathbf{r}_T - \mathbf{r}_{T0})$ for focused electron beams] as (see the supplementary material, Sec. SI24 for derivation)

$$\frac{d^2P}{d\Omega d\omega} = \int dq_z \left|\tilde{\phi}_{iz}\left(\frac{\omega}{v} - q_z\right)\right|^2 \times \left|\frac{\sin\left[\left(\frac{\omega}{c}\cos\theta - \frac{\omega}{v} - \frac{\hbar\omega}{2E}q_z + \frac{\hbar\omega}{4E}\frac{\omega}{v}\right)\frac{N\Lambda}{2}\right]}{\sin\left[\left(\frac{\omega}{c}\cos\theta - \frac{\omega}{v} - \frac{\hbar\omega}{2E}q_z + \frac{\hbar\omega}{4E}\frac{\omega}{v}\right)\frac{\Lambda}{2}\right]}\right|^2 \times \left[\frac{d^2P(\mathbf{r}_{T0})}{d\Omega d\omega}\right]_{UC}, \quad (140)$$

where $E = mv^2/2$ is the kinetic energy of the incident electron. Remarkably, Eq. (140) suggests that the quantum limit can be obtained by simulating the classical unit-cell power spectrum $\left[d^2P(\mathbf{r}_T)/d\Omega d\omega\right]_{UC}$ and multiplying it by the quantum-corrected dispersion function, originating in the recoiled transition current of Eq. (139). It is seen that both the dependence on the longitudinal wave function, as well as the dispersion relation, are now changed. Specifically, there now exists a direct dependence on the spectral content of the longitudinal wave function, that was absent from the nonrecoil case. In the nonrecoil limit of $\hbar\omega/2E \to 0$ this relation recovers Eq. (138), since $\int dq_z \left|\tilde{\phi}_{iz}(q_z)\right|^2 = 1$. Fig. 15 compares the results of Eqs. (138) and (140) for a slow electron emitting SP radiation, showing a clear spectral redshift as well as shift in the emission angle for the more accurate quantum calculation.

VII. CONCLUSIONS AND OUTLOOK

We presented a method for the calculation of spontaneous emission in arbitrary photonic media that does not explicitly use quantized electromagnetic fields. Instead, the wave functions of quantum matter undergoing a transition between initial and final states prescribe transition currents, which are then treated as sources to the classical Maxwell equations. The response of the medium is contained in full in the dyadic Green function, which connects current sources and the resulting field amplitudes. These could then be found either analytically (upon knowledge or approximation of the Green function) or

numerically (by inserting the transition-current source into an electromagnetic solver). The former may be advantageous when the transition current spans over a continuous set of states, while the latter is more adequate when matter undergoes transitions only between a discrete subset of states. By formulating simple and intuitive sum rules over final and initial states, one obtains the relevant observables from the resulting classical field amplitudes without washing out quantum optical effects—as semiclassical models often do.

The transition-current picture allows for an intuitive understanding of various quantum aspects of spontaneous emission that go far beyond the single dipolar transition. For example, we show that the spatial structure of the transition currents holds information regarding all multipole orders and allows one to readily calculate both emission patterns and Purcell-enhanced rates beyond the dipole approximation. This regime has attracted interest owing to the ability to access and engineer forbidden transitions for emitters in the vicinity of nanophotonic media hosting polaritons with ultrashort wavelengths,[13,45] or when considering mesoscopic solid-state emitters.[40,98] A recurring scenario where the dipole approximation is broken happens in free-electron systems, due to the extended nature of free-electron wave functions. We further apply the TCF to free electrons to calculate cathodoluminescence emission and electron energy-loss probabilities. Such processes serve as important analytical tools in electron microscopy, e.g., for the characterization of nanophotonic systems.

Quantum coherence transfer between an emitter and light can also be correctly described, thus allowing for the calculation of quantum beat phenomena in bound-electron systems, as well as wave function-dependent optical coherence of cathodoluminescence in free-electron systems. Remarkably, the TCF captures more complex phenomena in spontaneous emission, such as many-body interference effects and super-radiance of both bound- and free-electron systems alike, in arbitrary settings, which can be appealing for recently developing fields such as waveguide QED;[237] subtle quantum recoil corrections to free-electron radiation; and even second-order processes such as two-photon emission. The TCF similarly applies for situations in which the radiation is dominated by ponderomotive terms[238] or, more generally, in any second-order process.

Albeit being vastly comprehensive, the validity of the TCF is eventually limited to the perturbative regime, which truncates the Dyson series after a small number of photon emissions. Specifically, the formalism assumes weak coupling between light and matter, and further neglects counter-rotating terms in the interaction Hamiltonian (negative frequencies in the dyadic Green function; see the supplementary material, Secs. SI2–SI3 for further discussion). Thus, the transition-current description of non-perturbative, strongly coupled dynamics (as in the Jaynes–Cummings model) or those that go beyond the rotating-wave approximation (as in the quantum Rabi model), is not yet known to be possible.

In this respect, we note that quantum phenomena up to second order in perturbation theory, such as photon statistics in the frequency domain, can be captured by the two-photon correlations derived herein. However, a full description of non-perturbative phenomena, such as ones often necessary for certain non-Gaussian states with negative-valued Wigner functions, is currently beyond the scope of this formalism.

It will be intriguing to investigate the extension of the formalism beyond the perturbative regime. For free-electron systems under the paraxial and nonrecoil approximation, one can show that since the current operators commute, it should be readily possible to extend the TCF to the nonperturbative regime[74,188] described by the theory of quantum photon-induced electron microscopy.[88,209,216] For bound electron systems, however, such generalizations should include time-ordered, higher-order current-current correlations of the form of Eq. (12), connecting the emitter dynamics with the quantum correlations and photon statistics of the emitted light. Thus, complex emitter dynamics, especially in many-body systems with arbitrary inter-atom couplings, cannot be readily simplified by the TCF. A strategy to cover dynamical effects in the non-perturbative regime is to integrate transition currents with the Wigner–Weisskopf method,[239] or generalize the TCF to dynamics of open quantum systems. This might be possible, for example, using a superoperator Dyson series expansion of the Lindblad equation in Liouville space,[240] and then deriving the corresponding form for transition currents.

We did not cover the full scope of phenomena that may be described by the TCF, so we leave this for future work or as a challenge for the interested reader. For example, one may consider further second-order processes such as Lamb shifts and Casimir–Polder forces, more complex photonic environments with nonlocal or anisotropic responses, the interaction of free electrons with bound electron systems,[229,241,242] and non-perturbative approaches to recover the quantum state of the electromagnetic field. The latter is of special interest as it tackles the nonclassical nature of light sources, which is considered a hallmark of quantum optics. The ability to theoretically describe nonclassical light generation with transition currents may provide a different perspective to quantum optics, connecting the observed nonclassical light statistics to correlations in the emitter.[86,243,244]

SUPPLEMENTARY MATERIAL

See the supplementary material for elaborate derivations of the different results contained in this paper.

ACKNOWLEDGMENTS

This work was supported by the European Research Council (ERC), Grant No. 789104-eNANO, and the European Commission (EC), Grant No. 101017720 FET-Proactive EBEAM. A.K. acknowledges support by the Urbanek-Chodorow postdoctoral fellowship of Stanford University, the VATAT-Quantum fellowship by the Israeli Ministry of Innovation, Science and Technology, the Viterbi fellowship of the Technion—Israel Institute of Technology, and the Zuckerman STEM leadership postdoctoral program. N.R. acknowledges the support of a Junior Fellowship from the Harvard Society of Fellows. V.D.G. thanks Francesco Andreoli for helpful and enjoyable discussions.

AUTHOR DECLARATIONS

Conflict of Interest

The authors have no conflicts to disclose.

Author Contributions

Aviv Karnieli: Conceptualization (equal); Formal analysis (equal); Investigation (equal); Visualization (equal); Writing — original draft (equal); Writing — review & editing (equal). **Nicholas Rivera:** Formal analysis (equal); Investigation (equal); Writing — original draft (equal); Writing — review & editing (equal). **Valerio Di Giulio:** Formal analysis (equal); Investigation (equal); Writing — original draft (equal);

Writing — review & editing (equal). **Ady Arie:** Supervision (equal); Writing — review & editing (equal). **F. Javier García de Abajo:** Conceptualization (equal); Supervision (equal); Writing — review & editing (equal). **Ido Kaminer:** Conceptualization (equal); Supervision (equal); Writing — review & editing (equal).

DATA AVAILABILITY

The data that supports the findings of this study are available within the article and its supplementary material.

REFERENCES

[1]C. Cohen-Tannoudji, J. Dupont-Roc, and G. Grynberg, *Atom-Photon Interactions* (Wiley, 1998).
[2]C. M. Dodson and R. Zia, "Magnetic dipole and electric quadrupole transitions in the trivalent lanthanide series: Calculated emission rates and oscillator strengths," Phys. Rev. B **86**, 125102 (2012).
[3]M. Furno, R. Meerheim, S. Hofmann, B. Lüssem, and K. Leo, "Efficiency and rate of spontaneous emission in organic electroluminescent devices," Phys. Rev. B **85**, 115205 (2012).
[4]C. Girard, O. J. F. Martin, and A. Dereux, "Molecular lifetime changes induced by nanometer scale optical fields," Phys. Rev. Lett. **75**, 3098 (1995).
[5]R. G. Hulet, E. S. Hilfer, and D. Kleppner, "Inhibited spontaneous emission by a Rydberg atom," Phys. Rev. Lett. **55**, 2137–2140 (1985).
[6]T. H. Taminiau, S. Karaveli, N. F. Van Hulst, and R. Zia, "Quantifying the magnetic nature of light emission," Nat. Commun. **3**, 979 (2012).
[7]F. Le Kien, S. Dutta Gupta, V. I. Balykin, and K. Hakuta, "Spontaneous emission of a cesium atom near a nanofiber: Efficient coupling of light to guided modes," Phys. Rev. A **72**, 032509 (2005).
[8]M. Kosik, O. Burlayenko, C. Rockstuhl, I. Fernandez-Corbaton, and K. Słowik, "Interaction of atomic systems with quantum vacuum beyond electric dipole approximation," Sci. Rep. **10**(1), 5879 (2020).
[9]D. N. Chigrin, D. Kumar, D. Cuma, and G. Von Plessen, "Emission quenching of magnetic dipole transitions near a metal nanoparticle," ACS Photonics **3**, 27–34 (2016).
[10]B. Rolly, B. Bebey, S. Bidault, B. Stout, and N. Bonod, "Promoting magnetic dipolar transition in trivalent lanthanide ions with lossless Mie resonances," Phys. Rev. B **85**, 245432 (2012).
[11]G. Rosolen and B. Maes, "Strong multipolar transition enhancement with graphene nanoislands," APL Photonics **6**, 086103 (2021).
[12]D. G. Baranov, R. S. Savelev, S. V. Li, A. E. Krasnok, and A. Alù, "Modifying magnetic dipole spontaneous emission with nanophotonic structures," Laser Photonics Rev. **11**, 1600268 (2017).
[13]N. Rivera, I. Kaminer, B. Zhen, J. D. Joannopoulos, and M. Soljačić, "Shrinking light to allow forbidden transitions on the atomic scale," Science **353**, 263–269 (2016).
[14]T. Neuman, R. Esteban, D. Casanova, F. J. García-Vidal, and J. Aizpurua, "Coupling of molecular emitters and plasmonic cavities beyond the point-dipole approximation," Nano Lett. **18**, 2358–2364 (2018).
[15]A. Cuartero-González and A. I. Fernández-Domínguez, "Light-forbidden transitions in plasmon-emitter interactions beyond the weak coupling regime," ACS Photonics **5**, 3415–3420 (2018).
[16]E. M. Purcell, "Spontaneous emission probabilities at radio frequencies," Phys. Rev. **69**, 681 (1946).
[17]E. Yablonovitch, "Inhibited spontaneous emission in solid-state physics and electronics," Phys. Rev. Lett. **58**, 2059–2062 (1987).
[18]G. M. Akselrod *et al.*, "Probing the mechanisms of large Purcell enhancement in plasmonic nanoantennas," Nat. Photonics **8**(11), 835–840 (2014).
[19]M. Pelton, "Modified spontaneous emission in nanophotonic structures," Nat. Photonics **9**, 427–435 (2015).
[20]J. J. Baumberg, J. Aizpurua, M. H. Mikkelsen, and D. R. Smith, "Extreme nanophotonics from ultrathin metallic gaps," Nat. Mater. **18**(7), 668–678 (2019).
[21]N. Rivera, G. Rosolen, J. D. Joannopoulos, I. Kaminer, and M. Soljačić, "Making two-photon processes dominate one-photon processes using mid-IR phonon polaritons," Proc. Natl. Acad. Sci. U. S. A. **114**, 13607–13612 (2017).
[22]Y. Muniz, A. Manjavacas, C. Farina, D. A. R. Dalvit, and W. J. M. Kort-Kamp, "Two-photon spontaneous emission in atomically thin plasmonic nanostructures," Phys. Rev. Lett. **125**, 033601 (2020).
[23]N. Rivera, L. J. Wong, J. D. Joannopoulos, M. Soljačić, and I. Kaminer, "Light emission based on nanophotonic vacuum forces," Nat. Phys. **15**(12), 1284–1289 (2019).
[24]P. A. D. Gonçalves *et al.*, "Plasmon–emitter interactions at the nanoscale," Nat. Commun. **11**(1), 366 (2020).
[25]S. Ghosh, N. Rivera, G. Eisenstein, and I. Kaminer, "Creating heralded hyperentangled photons using Rydberg atoms," Light **10**(1), 100 (2021).
[26]F. Hu *et al.*, "Two-plasmon spontaneous emission from a nonlocal epsilon-near-zero material," Commun. Phys. **4**(1), 84 (2021).
[27]N. Rivera and I. Kaminer, "Light–matter interactions with photonic quasiparticles," Nat. Rev. Phys. **2**, 538–561 (2020).
[28]M. Lewenstein, P. Balcou, M. Y. Ivanov, A. L'Huillier, and P. B. Corkum, "Theory of high-harmonic generation by low-frequency laser fields," Phys. Rev. A **49**, 2117–2132 (1994).
[29]L. A. Blanco and F. J. García de Abajo, "Spontaneous light emission in complex nanostructures," Phys. Rev. B **69**, 205414 (2004).
[30]M. C. Kohler *et al.*, "High harmonic generation via continuum wave-packet interference," Phys. Rev. Lett. **105**, 203902 (2010).
[31]S. M. Barnett, B. Huttner, and R. Loudon, "Spontaneous emission in absorbing dielectric media," Phys. Rev. Lett. **68**, 3698–3701 (1992).
[32]H. R. Xia, C. Y. Ye, and S. Y. Zhu, "Experimental observation of spontaneous emission cancellation," Phys. Rev. Lett. **77**, 1032–1034 (1996).
[33]S. Y. Zhu and M. O. Scully, "Spectral line elimination and spontaneous emission cancellation via quantum interference," Phys. Rev. Lett. **76**, 388–391 (1996).
[34]G. Bjork, S. Machida, Y. Yamamoto, and K. Igeta, "Modification of spontaneous emission rate in planar dielectric microcavity structures," Phys. Rev. A **44**, 669 (1991).
[35]P. Goy, J. M. Raimond, M. Gross, and S. Haroche, "Observation of cavity-enhanced single-atom spontaneous emission," Phys. Rev. Lett. **50**, 1903–1906 (1983).
[36]J. J. Sanchez-Mondragon, N. B. N, and J. H. E, "Theory of spontaneous-emission line shape in an ideal cavity," Phys. Rev. Lett. **51**, 550 (1983).
[37]D. Kleppner, "Inhibited spontaneous emission," Phys. Rev. Lett. **47**, 233–236 (1981).
[38]S. Fan, P. R. Villeneuve, J. D. Joannopoulos, and E. F. Schubert, "High extraction efficiency of spontaneous emission from slabs of photonic crystals," Phys. Rev. Lett. **78**, 3294–3297 (1997).
[39]S. Noda, M. Fujita, and T. Asano, "Spontaneous-emission control by photonic crystals and nanocavities," Nat. Photonics **1**, 449–458 (2007).
[40]M. L. Andersen, S. Stobbe, A. S. Sørensen, and P. Lodahl, "Strongly modified plasmon-matter interaction with mesoscopic quantum emitters," Nat. Phys. **7**, 215–218 (2011).
[41]S. Chichibu, T. Azuhata, T. Sota, and S. Nakamura, "Spontaneous emission of localized excitons in InGaN single and multiquantum well structures," Appl. Phys. Lett. **69**, 4188–4190 (1996).
[42]W. W. Chow and S. W. Koch, "Theory of semiconductor quantum-dot laser dynamics," IEEE J. Quantum Electron. **41**, 495–505 (2005).
[43]I. Kaminer *et al.*, "Efficient plasmonic emission by the quantum Čerenkov effect from hot carriers in graphene," Nat. Commun. **7**, ncomms11880 (2016).
[44]M. Kira, F. Jahnke, W. Hoyer, and S. W. Koch, "Quantum theory of spontaneous emission and coherent effects in semiconductor microstructures," Prog. Quantum Electron. **23**, 189–279 (1999).
[45]Y. Kurman *et al.*, "Control of semiconductor emitter frequency by increasing polariton momenta," Nat. Photonics **12**, 423–429 (2018).
[46]S. Stobbe *et al.*, "Spontaneous emission from large quantum dots in nanostructures: Exciton-photon interaction beyond the dipole approximation," Phys. Rev. B **86**, 085304 (2012).
[47]M. Sugawara, "Wannier excitons Theory," Phys. Rev. B **51**, 10743–10754 (1995).
[48]T. B. Hoang *et al.*, "Ultrafast spontaneous emission source using plasmonic nanoantennas," Nat. Commun. **6**, 7788 (2015).
[49]F. Jahnke *et al.*, "Giant photon bunching, superradiant pulse emission and excitation trapping in quantum-dot nanolasers," Nat. Commun. **7**, 11540 (2016).

[50]L. Li, W. Wang, T. S. Luk, X. Yang, and J. Gao, "Enhanced quantum dot spontaneous emission with multilayer metamaterial nanostructures," ACS Photonics **4**, 501–508 (2017).
[51]P. Senellart, G. Solomon, and A. White, "High-performance semiconductor quantum-dot single-photon sources," Nat. Nanotechnol. **12**, 1026–1039 (2017).
[52]D. Englund *et al.*, "Controlling the spontaneous emission rate of single quantum dots in a two-dimensional photonic crystal," Phys. Rev. Lett. **95**, 013904 (2005).
[53]K. F. Mak and J. Shan, "Photonics and optoelectronics of 2D semiconductor transition metal dichalcogenides," Nat. Photonics **10**, 216 (2016).
[54]D. Y. Qiu, F. H. Da Jornada, and S. G. Louie, "Optical spectrum of **MoS2**: Many-body effects and diversity of exciton states," Phys. Rev. Lett. **111**, 216805 (2013).
[55]G. D. Shepard *et al.*, "Trion-species-resolved quantum beats in $MoSe_2$," ACS Nano **11**, 11550–11558 (2017).
[56]S. Sim *et al.*, "Ultrafast quantum beats of anisotropic excitons in atomically thin ReS_2," Nat. Commun. **9**, 351 (2018).
[57]P. A. M. Dirac, "The quantum theory of the emission and absorption of radiation," Proc. R. Soc. London, Ser. A **114**, 243–265 (1927).
[58]A. Einstein, "Strahlungs-Emission und -Absorption nach der Quantentheorie," in *Berlin Years: Writings, 1914–1917* (Princeton University Press, 1916), Vol. 6, p. 212.
[59]P. A. Cerenkov, "Visible radiation produced by electrons moving in a medium with velocities exceeding that of light," Phys. Rev. **52**, 378–379 (1937).
[60]A. Friedman, A. Gover, G. Kurizki, S. Ruschin, and A. Yariv, "Spontaneous and stimulated emission from quasifree electrons," Rev. Mod. Phys. **60**, 471–535 (1988).
[61]J. Nelayah *et al.*, "Mapping surface plasmons on a single metallic nanoparticle," Nat. Phys. **3**(5), 348–353 (2007).
[62]F. J. García de Abajo *et al.*, "Cherenkov effect as a probe of photonic nanostructures," Phys. Rev. Lett. **91**, 143902 (2003).
[63]J. V. Jelley, "Čerenkov radiation and its applications," J. Appl. Phys. **6**, 227 (1955).
[64]I. Kaminer *et al.*, "Quantum Čerenkov radiation: Spectral cutoffs and the role of spin and orbital angular momentum," Phys. Rev. X **6**, 011006 (2016).
[65]X. Lin *et al.*, "Controlling Cherenkov angles with resonance transition radiation," Nat. Phys. **14**, 816 (2018).
[66]C. Luo, M. Ibanescu, S. G. Johnson, and J. D. Joannopoulos, "Čerenkov radiation in photonic crystals," Science **299**, 368–371 (2003).
[67]V. L. Ginzburg, "Radiation by uniformly moving sources (Vavilov–Čerenkov effect, transition radiation, and other phenomena)," Phys.-Usp. **39**, 973 (1996).
[68]A. Polman, M. Kociak, and F. J. García de Abajo, "Electron-beam spectroscopy for nanophotonics," Nat. Mater. **18**, 1158–1171 (2019).
[69]R. Remez *et al.*, "Observing the Quantum Wave Nature of Free Electrons through Spontaneous Emission," Phys. Rev. Lett. **123**, 060401 (2019).
[70]R. Remez *et al.*, "Spectral and spatial shaping of Smith–Purcell radiation," Phys. Rev. A **96**, 061801 (2017).
[71]S. J. Smith and E. M. Purcell, "Visible light from localized surface charges moving across a grating," Phys. Rev. **92**, 1069 (1953).
[72]Z. Wang, K. Yao, M. Chen, H. Chen, and Y. Liu, "Manipulating Smith–Purcell emission with Babinet metasurfaces," Phys. Rev. Lett. **117**, 157401 (2016).
[73]Y. Yang *et al.*, "Maximal spontaneous photon emission and energy loss from free electrons," Nat. Phys. **14**, 894–899 (2018).
[74]F. J. García de Abajo and V. Di Giulio, "Optical excitations with electron beams: Challenges and opportunities," ACS Photonics **8**(4), 945–974 (2021).
[75]E. J. R. Vesseur, R. de Waele, M. Kuttge, and A. Polman, "Direct observation of plasmonic modes in Au nanowires using high-resolution cathodoluminescence spectroscopy," Nano Lett. **7**, 2843–2846 (2007).
[76]T. Coenen, D. T. Schoen, B. J. M. Brenny, A. Polman, and M. L. Brongersma, "Combined electron energy-loss and cathodoluminescence spectroscopy on individual and composite plasmonic nanostructures," Phys. Rev. B **93**, 195429 (2016).
[77]T. Coenen, F. Bernal Arango, A. Femius Koenderink, and A. Polman, "Directional emission from a single plasmonic scatterer," Nat. Commun. **5**, 3250 (2014).
[78]C. I. Osorio, T. Coenen, B. J. M. Brenny, A. Polman, and A. F. Koenderink, "Angle-resolved cathodoluminescence imaging polarimetry," ACS Photonics **3**, 147–154 (2016).
[79]O. Nicoletti *et al.*, "Three-dimensional imaging of localized surface plasmon resonances of metal nanoparticles," Nature **502**(7469), 80–84 (2013).
[80]R. B. Pettit, J. Silcox, and R. Vincent, "Measurement of surface-plasmon dispersion in oxidized aluminum films," Phys. Rev. B **11**, 3116 (1975).
[81]A. Horl *et al.*, "Tomographic imaging of the photonic environment of plasmonic nanoparticles," Nat. Commun. **8**(1), 37 (2017).
[82]G. Adamo *et al.*, "Light well: A tunable free-electron light source on a chip," Phys. Rev. Lett. **103**, 113901 (2009).
[83]X. Bendaña, A. Polman, and F. J. García de Abajo, "Single-photon generation by electron beams," Nano Lett. **11**, 5099–5103 (2011).
[84]A. Karnieli *et al.*, "Cylindrical metalens for generation and focusing of free-electron radiation," Nano Lett. **22**, 5641–5650 (2022).
[85]A. Karnieli, N. Rivera, A. Arie, and I. Kaminer, "The coherence of light is fundamentally tied to the quantum coherence of the emitting particle," Sci. Adv. **7**, eabf8096 (2021).
[86]A. Karnieli, N. Rivera, A. Arie, and I. Kaminer, "Superradiance and subradiance due to quantum interference of entangled free electrons," Phys. Rev. Lett. **127**, 060403 (2021).
[87]O. Kfir, V. Di Giulio, F. J. García de Abajo, and C. Ropers, "Optical coherence transfer mediated by free electrons," Sci. Adv. **7**, eabf6380 (2021).
[88]A. Ben Hayun *et al.*, "Shaping quantum photonic states using free electrons," Sci. Adv. **7**, eabe4270 (2021).
[89]G. Guzzinati *et al.*, "Probing the symmetry of the potential of localized surface plasmon resonances with phase-shaped electron beams," Nat. Commun. **8**, 14999 (2017).
[90]F. J. García de Abajo, "Optical excitations in electron microscopy," Rev. Mod. Phys. **82**, 209–275 (2010).
[91]N. Talebi, "Schrödinger electrons interacting with optical gratings: Quantum mechanical study of the inverse Smith–Purcell effect," New J. Phys. **18**, 123006 (2016).
[92]J. C. Garrison and R. Y. Chiao, *Quantum Optics* (Oxford University Press, 2014).
[93]S. Scheel and S. Y. Buhmann, "Macroscopic QED—concepts and applications," Acta Phys. Slovaca **58**, 675 (2008), http://www.physics.sk/aps/pub.php?y=2008&pub=aps-08-05
[94]M. O. Scully and M. S. Zubairy, *Quantum Optics* (Cambridge University Press, 1997).
[95]J. Garrison and R. Chiao, *Quantum Optics* (Oxford University Press, 2008).
[96]L. Novotny and B. Hecht, *Principles of Nano-Optics* (Cambridge University Press, 2006).
[97]Y. Xu, R. K. Lee, and A. Yariv, "Quantum analysis and the classical analysis of spontaneous emission in a microcavity," Phys. Rev. A **61**, 033807 (2000).
[98]P. Tighineanu, A. S. Sørensen, S. Stobbe, and P. Lodahl, "Unraveling the mesoscopic character of quantum dots in nanophotonics," Phys. Rev. Lett. **114**, 247401 (2015).
[99]G. S. Solomon, M. Pelton, and Y. Yamamoto, "Single-mode spontaneous emission from a single quantum dot in a three-dimensional microcavity," Phys. Rev. Lett. **86**, 3903–3906 (2001).
[100]S. Hughes, "Enhanced single-photon emission from quantum dots in photonic crystal waveguides and nanocavities," Opt. Lett. **29**, 2659 (2004).
[101]P. Lodahl *et al.*, "Controlling the dynamics of spontaneous emission from quantum dots by photonic crystals," Nature **430**, 654–657 (2004).
[102]S. Ogawa, M. Imada, S. Yoshimoto, M. Okano, and S. Noda, "Control of light emission by 3D photonic crystals," Science **305**, 227–229 (2004).
[103]V. S. C. M. Rao and S. Hughes, "Single quantum dot spontaneous emission in a finite-size photonic crystal waveguide: Proposal for an efficient 'on chip' single photon gun," Phys. Rev. Lett. **99**, 193901 (2007).
[104]Y. Chen, T. R. Nielsen, N. Gregersen, P. Lodahl, and J. Mørk, "Finite-element modeling of spontaneous emission of a quantum emitter at nanoscale proximity to plasmonic waveguides," Phys. Rev. B **81**, 125431 (2010).
[105]M. Liu, T. W. Lee, S. K. Gray, P. Guyot-Sionnest, and M. Pelton, "Excitation of dark plasmons in metal nanoparticles by a localized emitter," Phys. Rev. Lett. **102**, 107401 (2009).

[106]M. Ringler *et al.*, "Shaping emission spectra of fluorescent molecules with single plasmonic nanoresonators," Phys. Rev. Lett. **100**, 203002 (2008).
[107]K. J. Russell, T. L. Liu, S. Cui, and E. L. Hu, "Large spontaneous emission enhancement in plasmonic nanocavities," Nat. Photonics **6**, 459–462 (2012).
[108]S. Kühn, U. Håkanson, L. Rogobete, and V. Sandoghdar, "Enhancement of single-molecule fluorescence using a gold nanoparticle as an optical nanoantenna," Phys. Rev. Lett. **97**, 017402 (2006).
[109]P. Ginzburg *et al.*, "Spontaneous emission in non-local materials," Light **6**, e16273 (2017).
[110]Z. Jacob *et al.*, "Engineering photonic density of states using metamaterials," Appl. Phys. B **100**, 215–218 (2010).
[111]Z. Jacob, I. I. Smolyaninov, and E. E. Narimanov, "Broadband Purcell effect: Radiative decay engineering with metamaterials," Appl. Phys. Lett. **100**, 181105 (2012).
[112]D. Lu, J. J. Kan, E. E. Fullerton, and Z. Liu, "Enhancing spontaneous emission rates of molecules using nanopatterned multilayer hyperbolic metamaterials," Nat. Nanotechnol **9**, 48–53 (2014).
[113]M. A. Noginov *et al.*, "Controlling spontaneous emission with metamaterials," Opt Lett. **35**, 1863 (2010).
[114]T. Tumkur *et al.*, "Control of spontaneous emission in a volume of functionalized hyperbolic metamaterial," Appl. Phys. Lett. **99**, 151115 (2011).
[115]R. Beams, P. Bharadwaj, and L. Novotny, "Electroluminescence from graphene excited by electron tunneling," Nanotechnology **25**, 055206 (2014).
[116]M. Engel *et al.*, "Light–matter interaction in a microcavity-controlled graphene transistor," Nat. Commun. **3**, 906 (2012).
[117]V. D. Karanikolas and E. Paspalakis, "Localized exciton modes and high quantum efficiency of a quantum emitter close to a **MoS2** nanodisk," Phys. Rev. B **96**, 41404 (2017).
[118]W. J. M. Kort-Kamp *et al.*, "Active magneto-optical control of spontaneous emission in graphene," Phys. Rev. B **92**, 205415 (2015).
[119]F. Rana, J. H. Strait, H. Wang, and C. Manolatou, "Ultrafast carrier recombination and generation rates for plasmon emission and absorption in graphene," Phys. Rev. B **84**, 045437 (2011).
[120]I. Thanopulos, V. Karanikolas, N. Iliopoulos, and E. Paspalakis, "Non-Markovian spontaneous emission dynamics of a quantum emitter near a **MoS_2** nanodisk," Phys. Rev. B **99**, 195412 (2019).
[121]Y. Xu, R. K. Lee, and A. Yariv, "Finite-difference time-domain analysis of spontaneous emission in a microdisk cavity," Phys. Rev. A **61**, 033808 (2000).
[122]S. M. Barnett, B. Huttner, R. Loudon, and R. Matloob, "Decay of excited atoms in absorbing dielectrics," J. Phys. B **29**, 3763 (1996).
[123]A. V. Bogatskaya, E. A. Volkova, V. Y. Kharin, and A. M. Popov, "Polarization response in extreme nonlinear optics: When can the semiclassical approach be used?," Laser Phys. Lett. **13**, 045301 (2016).
[124]W. W. Chow, M. O. Scully, and J. O. Stoner, "Quantum-beat phenomena described by quantum electrodynamics and neoclassical theory," Phys. Rev. A **11**, 1380–1388 (1975).
[125]M. D. Crisp and E. T. Jaynes, "Radiative effects in semiclassical theory," Phys. Rev. **179**, 1253–1261 (1969).
[126]R. M. Herman, H. Grotch, R. Kornblith, and J. H. Eberly, "Quantum electrodynamic and semiclassical interference effects in spontaneous radiation," Phys. Rev. A **11**, 1389–1396 (1975).
[127]E. T. Jaynes and F. W. Cummings, "Comparison of quantum and semiclassical radiation theories with application to the beam maser," Proc. IEEE **51**, 89–109 (1963).
[128]E. Lorin, S. Chelkowski, and A. Bandrauk, "A numerical Maxwell–Schrödinger model for intense laser–matter interaction and propagation," Comput. Phys. Commun. **177**, 908–932 (2007).
[129]P. W. Milonni, "Semiclassical and quantum-electrodynamical approaches in nonrelativistic radiation theory," Phys. Rep. **25**, 1–81 (1976).
[130]R. K. Nesbet, "Spontaneous emission in semiclassical radiation theory," Phys. Rev. A **4**, 259–264 (1971).
[131]R. K. Nesbet, "Where semiclassical radiation theory fails," Phys. Rev. Lett. **27**, 553 (1971).
[132]H. Rigneault and S. Monneret, "Modal analysis of spontaneous emission in a planar microcavity," Phys. Rev. A **54**, 2356–2368 (1996).
[133]G. S. Agarwal, "Anisotropic vacuum-induced interference in decay channels," Phys. Rev. Lett. **84**, 5500–5503 (2000).
[134]D. A. Cardimona, "Effect of atomic-state coherence and spontaneous emission on three-level dynamics," Phys. Rev. A **41**, 5016–5025 (1990).
[135]S. Evangelou, V. Yannopapas, and E. Paspalakis, "Simulating quantum interference in spontaneous decay near plasmonic nanostructures: Population dynamics," Phys. Rev. A **83**, 055805 (2011).
[136]G. C. Hegerfeldt and M. B. Plenio, "Macroscopic dark periods without a metastable state," Phys. Rev. A **46**, 373–379 (1992).
[137]P. Zhou and S. Swain, "Ultranarrow spectral lines via quantum interference," Phys. Rev. Lett. **77**, 3995–3998 (1996).
[138]S. Y. Zhu, R. C. F. Chan, and C. P. Lee, "Spontaneous emission from a three-level atom," Phys. Rev. A **52**, 710–716 (1995).
[139]S. Y. Zhu, H. Chen, and H. Huang, "Quantum interference effects in spontaneous emission from an atom embedded in a photonic band gap structure," Phys. Rev. Lett. **79**, 205–208 (1997).
[140]M. A. Schlosshauer, *Decoherence and the Quantum-To-Classical Transition* (Springer, Berlin Heidelberg, 2007).
[141]S. Tsesses, G. Bartal, and I. Kaminer, "Light generation via quantum interaction of electrons with periodic nanostructures," Phys. Rev. A **95**, 013832 (2017).
[142]S. E. Economou, R. B. Liu, L. J. Sham, and D. G. Steel, "Unified theory of consequences of spontaneous emission in a Λ system," Phys. Rev. B **71**, 195327 (2005).
[143]A. K. Patnai and G. S. Agarwal, "Laser-field-induced quantum beats in correlations in cascade emission," J. Mod. Opt **45**, 2131–2138 (1998).
[144]S. Karaveli and R. Zia, "Spectral tuning by selective enhancement of electric and magnetic dipole emission," Phys. Rev. Lett. **106**, 193004 (2011).
[145]F. Krausz and M. Ivanov, "Attosecond physics," Rev. Mod. Phys. **81**, 163–234 (2009).
[146]R. H. Dicke, "Coherence in spontaneous radiation processes," Phys. Rev. **93**, 99–110 (1954).
[147]A. Gover *et al.*, "Superradiant and stimulated-superradiant emission of bunched electron beams," Rev. Mod. Phys. **91**, 035003 (2019).
[148]M. Gross and S. Haroche, "Superradiance: An essay on the theory of collective spontaneous emission," Phys. Rep. **93**, 301–396 (1982).
[149]F. J. García de Abajo, "Interaction of radiation and fast electrons with clusters of dielectrics: A multiple scattering approach," Phys. Rev. Lett. **82**, 2776–2779 (1999).
[150]F. J. García de Abajo, "Smith–Purcell radiation emission in aligned nanoparticles," Phys. Rev. E **61**, 5743–5752 (2000).
[151]F. J. García de Abajo and A. Howie, "Relativistic electron energy loss and electron-induced photon emission in inhomogeneous dielectrics," Phys. Rev. Lett. **80**, 5180–5183 (1998).
[152]E. O. Göbel *et al.*, "Quantum beats of excitons in quantum wells," Phys. Rev. Lett. **64**, 1801–1804 (1990).
[153]E. A. Wolf, D. M. Finton, V. Zoutenbier, and I. Biaggio, "Quantum beats of a multiexciton state in rubrene single crystals," Appl. Phys. Lett. **112**, 083301 (2018).
[154]R. J. Glauber, "The quantum theory of optical coherence," Phys. Rev. **130**, 2529 (1963).
[155]J. D. Jackson, *Classical Electrodynamics* (Wiley, 1999).
[156]B. R. Judd, "Optical absorption intensities of rare-Earth ions," Phys. Rev. **127**, 750 (1962).
[157]C. Qian *et al.*, "Enhanced strong interaction between nanocavities and p -shell excitons beyond the dipole approximation," Phys. Rev. Lett. **122**, 087401 (2019).
[158]M. Cotrufo and A. Fiore, "Spontaneous emission from dipole-forbidden transitions in semiconductor quantum dots," Phys. Rev. B **92**, 125302 (2015).
[159]I. D. Rukhlenko *et al.*, "Spontaneous emission of guided polaritons by quantum dot coupled to metallic nanowire: Beyond the dipole approximation," Opt. Express **17**(20), 17570–17581 (2009).
[160]M. K. Svendsen *et al.*, "Combining density functional theory with macroscopic QED for quantum light–matter interactions in 2D materials," Nat. Commun. **12**(1), 2778 (2021).
[161]T. Coenen, E. J. R. Vesseur, and A. Polman, "Angle-resolved cathodoluminescence spectroscopy," Appl. Phys. Lett. **99**, 143103 (2011).
[162]V. L. Ginzburg and I. M. Frank, "Radiation of a uniformly moving electron due to its transition from one medium into another," Zh. Eksp. Teor. Fiz. **9**, 353–362 (1945).

[163]Y. N. Dnestrovskii and D. P. Kostomarov, "Radiation of a modulated beam of charged particles in passing through a round opening in a flat screen," Sov. Phys. Doklady **4**, 132 (1959).
[164]H. Motz, W. Thon, and R. N. Whitehurst, "Experiments on radiation by fast electron beams," J. Appl. Phys. **24**, 826–833 (1953).
[165]I. Kaminer *et al.*, "Spectrally and spatially resolved Smith–Purcell radiation in plasmonic crystals with short-range disorder," Phys. Rev. X **7**, 011003 (2017).
[166]N. Talebi *et al.*, "Merging transformation optics with electron-driven photon sources," Nat. Commun. **10**, 599 (2019).
[167]N. Van Nielen *et al.*, "Electrons generate self-complementary broadband vortex light beams using chiral photon sieves," Nano Lett. **20**, 5975–5981 (2020).
[168]J. Christopher *et al.*, "Electron-driven photon sources for correlative electron-photon spectroscopy with electron microscopes," Nanophotonics **9**, 4381–4406 (2020).
[169]A. Massuda *et al.*, "Smith–Purcell radiation from low-energy electrons," ACS Photonics **5**, 3513–3518 (2018).
[170]C. Roques-Carmes, S. E. Kooi, Y. Yang, A. Massuda, P. D. Keathley, A. Zaidi, Y. Yang, J. D. Joannopoulos, K. K. Berggren, I. K, and M. S, "Towards integrated tunable all-silicon free-electron light sources," Nat. Commun. **10**, 3176 (2019).
[171]C. Roques-Carmes *et al.*, "Free-electron–light interactions in nanophotonics," Appl. Phys. Rev. **10**, 011303 (2023).
[172]Y. Pan and A. Gover, "Spontaneous and stimulated radiative emission of modulated free-electron quantum wavepackets—semiclassical analysis," J. Phys. Commun. **2**, 115026 (2018).
[173]Y. Pan and A. Gover, "Spontaneous and stimulated emissions of a preformed quantum free-electron wave function," Phys. Rev. A **99**, 052107 (2019).
[174]A. Gover and Y. Pan, "Dimension-dependent stimulated radiative interaction of a single electron quantum wavepacket," Phys. Lett. A **382**, 1550–1555 (2018).
[175]L. J. Wong, N. Rivera, C. Murdia, T. Christensen, J. D. Joannopoulos, M. Soljačić, and I. Kaminer, "Control of quantum electrodynamical processes by shaping electron wavepackets," Nat. Commun. **12**, 1700 (2021).
[176]C. Mechel *et al.*, "Quantum correlations in electron microscopy," Optica **8**, 70 (2021).
[177]S. Huang *et al.*, "Quantum recoil in free electron-driven spontaneous emission from van der Waals crystals," in *Conference on Lasers and Electro-Optics (2022), Paper FF4C.4 FF4C.4* (Optica Publishing Group, 2022).
[178]S. Huang *et al.*, "Quantum recoil in free-electron interactions with atomic lattices," Nat. Photonics **17**, 224–230 (2023).
[179]W. C. Chew, *Waves and Fields in Inhomogenous Media* (Wiley-IEEE Press, 1995).
[180]F. J. García de Abajo and A. Howie, "Retarded field calculation of electron energy loss in inhomogeneous dielectrics," Phys. Rev. B **65**, 115418 (2002).
[181]H. S. Han, A. Lee, K. Sinha, F. K. Fatemi, and S. L. Rolston, "Observation of vacuum-induced collective quantum beats," Phys. Rev. Lett. **127**, 073604 (2021).
[182]R. J. Glauber and M. Lewenstein, "Quantum optics of dielectric media," Phys. Rev. A **43**, 467 (1991).
[183]V. Di Giulio, "Nanophotonics with charged particles," Ph.D. thesis (Institut de Ciències Fotòniques, 2023).
[184]A. Rustagi and A. F. Kemper, "Coherent excitonic quantum beats in time-resolved photoemission measurements," Phys. Rev. B **99**, 125303 (2019).
[185]P. Kling, E. Giese, C. M. Carmesin, R. Sauerbrey, and W. P. Schleich, "High-gain quantum free-electron laser: Emergence and exponential gain," Phys. Rev. A **99**, 053823 (2019).
[186]P. Kling, E. Giese, R. Endrich, P. Preiss, R. Sauerbrey, and W. P. S, "What defines the quantum regime of the free-electron laser?," New J. Phys. **17**, 123019 (2015).
[187]C. M. Carmesin, P. Kling, E. Giese, R. Sauerbrey, and W. P. Schleich, "Quantum and classical phase-space dynamics of a free-electron laser," Phys. Rev. Res. **2**(2), 023027 (2020).
[188]V. Di Giulio, O. Kfir, C. Ropers, and F. J. García de Abajo, "Modulation of cathodoluminescence emission by interference with external light," ACS Nano **15**, 7290–7304 (2021).
[189]A. Goban *et al.*, "Superradiance for atoms trapped along a photonic crystal waveguide," Phys. Rev. Lett. **115**, 063601 (2015).
[190]M. Scheibner *et al.*, "Superradiance of quantum dots," Nat. Phys. **3**, 106–110 (2007).
[191]F. Damanet, D. Braun, and J. Martin, "Cooperative spontaneous emission from indistinguishable atoms in arbitrary motional quantum states," Phys. Rev. A **94**, 33838 (2016).
[192]K. Cong, Q. Zhang, Y. Wang, G. T. Noe, A. Belyanin, and J. K, "Dicke superradiance in solids [Invited]," J. Opt. Soc. Am. B **33**(7), C80–C101 (2016).
[193]S. J. Masson and A. Asenjo-Garcia, "Universality of Dicke superradiance in arrays of quantum emitters," Nat. Commun. **13**(1), 2285 (2022).
[194]V. V. Kocharovsky, V. V. Zheleznyakov, E. R. Kocharovskaya, and V. V. Kocharovsky, "Superradiance: The principles of generation and implementation in lasers," Phys.-Usp. **60**, 345 (2017).
[195]R. G. Devoe and R. G. Brewer, "Observation of superradiant and subradiant spontaneous emission of two trapped ions," Phys. Rev. Lett. **76**, 2049 (1996).
[196]S. E. Korbly, A. S. Kesar, J. R. Sirigiri, and R. J. Temkin, "Observation of frequency-locked coherent terahertz Smith–Purcell radiation," Phys. Rev. Lett. **94**, 054803 (2005).
[197]A. M. Cook *et al.*, "Observation of narrow-band terahertz coherent Cherenkov radiation from a cylindrical dielectric-lined waveguide," Phys. Rev. Lett. **103**, 095003 (2009).
[198]C. Bostedt *et al.*, "Linac coherent light source: The first five years," Rev. Mod. Phys. **88**, 015007 (2016).
[199]C. Pellegrini, A. Marinelli, and S. Reiche, "The physics of x-ray free-electron lasers," Rev. Mod. Phys. **88**, 015006 (2016).
[200]C. J. Hirschmugl, M. Sagurton, and G. P. Williams, "Multiparticle coherence calculations for synchrotron-radiation emission," Phys. Rev. A **44**, 1316–1320 (1991).
[201]A. Angioi, A. Piazza, and A. Di, "Quantum limitation to the coherent emission of accelerated charges," Phys. Rev. Lett. **121**, 010402 (2018).
[202]S. Liu *et al.*, "Light-emitting metasurfaces: Simultaneous control of spontaneous emission and far-field radiation," Nano Lett. **18**, 6906–6914 (2018).
[203]Y. Luo *et al.*, "Purcell-enhanced quantum yield from carbon nanotube excitons coupled to plasmonic nanocavities," Nat. Commun. **8**(1), 1413 (2017).
[204]J. L. Zhang *et al.*, "Strongly cavity-enhanced spontaneous emission from silicon-vacancy centers in diamond," Nano Lett. **18**, 1360–1365 (2018).
[205]O. Bitton, S. N. Gupta, and G. Haran, "Quantum dot plasmonics: From weak to strong coupling," Nanophotonics **8**, 559–575 (2019).
[206]T. Hümmer, F. J. García-Vidal, L. Martín-Moreno, and D. Zueco, "Weak and strong coupling regimes in plasmonic QED," Phys. Rev. B **87**, 115419 (2013).
[207]R. H. Ritchie and A. Howie, "Inelastic scattering probabilities in scanning transmission electron microscopy," Philos. Mag. A **58**, 753–767 (1988).
[208]F. J. García de Abajo and M. Kociak, "Probing the photonic local density of states with electron energy loss spectroscopy," Phys. Rev. Lett. **100**, 106804 (2008).
[209]O. Kfir, "Entanglements of electrons and cavity photons in the strong-coupling regime," Phys. Rev. Lett. **123**, 103602 (2019).
[210]V. Di Giulio and F. J. García de Abajo, "Free-electron shaping using quantum light," Optica **7**, 1820–1830 (2020).
[211]R. Dahan *et al.*, "Imprinting the quantum statistics of photons on free electrons," Science **373**, eabj7128 (2021).
[212]A. Gorlach *et al.*, "Ultrafast non-destructive measurement of the quantum state of light using free electrons," arXiv:2012.12069 (2020).
[213]A. Feist *et al.*, "Cavity-mediated electron-photon pairs," arXiv:2202.12821 (2022).
[214]J.-W. Henke *et al.*, "Integrated photonics enables continuous-beam electron phase modulation," Nature **600**(7890), 653–658 (2021).
[215]Y. Adiv, H. Hu, S. Tsesses, R. Dahan, K. Wang, Y. Kurman, A. Gorlach, H. Chen, X. Lin, G. Bartal, and I. Kaminer, "Observation of 2D Cherenkov Radiation," Phys. Rev. X **13**, 011002 (2023).
[216]V. Di Giulio, M. Kociak, and F. J. García de Abajo, "Probing quantum optical excitations with fast electrons," Optica **6**, 1524 (2019).
[217]A. N. Poddubny, P. Ginzburg, P. A. Belov, A. V. Zayats, and Y. S. Kivshar, "Tailoring and enhancing spontaneous two-photon emission using resonant plasmonic nanostructures," Phys. Rev. A **86**, 033826 (2012).
[218]A. Hayat, P. Ginzburg, and M. Orenstein, "Observation of two-photon emission from semiconductors," Nat. Photonics **2**(4), 238–241 (2008).
[219]R. W. Boyd, *Nonlinear Optics* (Academic Press, 2008).

[220]V. B. Berestetskii, E. M. Lifshitz, and L. P. Pitaevskii, *Quantum Electrodynamics* (Butterworth-Heinemann (Elsevier), 1982), Vol. 4.
[221]L. A. Coldren, S. W. Corzine, and M. L. Mašanović, *Diode Lasers and Photonic Integrated Circuits* (John Wiley & Sons, Inc., 2012).
[222]S. Ayari, A. Smiri, A. Hichri, S. Jaziri, and T. Amand, "Radiative lifetime of localized excitons in transition-metal dichalcogenides," Phys. Rev. B **98**, 205430 (2018).
[223]I. Madan *et al.*, "Ultrafast transverse modulation of free electrons by interaction with shaped optical fields," ACS Photonics **9**, 3215–3224 (2022).
[224]S. Tsesses *et al.*, "Tunable photon-induced spatial modulation of free electrons," Nat. Mater. **22**(3), 345–352 (2023).
[225]R. Shiloh, Y. Lereah, Y. Lilach, and A. Arie, "Sculpturing the electron wave function using nanoscale phase masks," Ultramicroscopy **144**, 26–31 (2014).
[226]A. H. Tavabi *et al.*, "Experimental demonstration of an electrostatic orbital angular momentum sorter for electron beams," Phys. Rev. Lett. **126**, 094802 (2021).
[227]J. Verbeeck *et al.*, "Demonstration of a 2×2 programmable phase plate for electrons," Ultramicroscopy **190**, 58–65 (2018).
[228]M. Taleb, M. Hentschel, K. Rossnagel, H. Giessen, and N. Talebi, "Phase-locked photon–electron interaction without a laser," Nat. Phys. **19**, 869–876 (2023).
[229]A. Gover and A. Yariv, "Free-electron-bound-electron resonant interaction," Phys. Rev. Lett. **124**, 064801 (2020).
[230]K. E. Priebe *et al.*, "Attosecond electron pulse trains and quantum state reconstruction in ultrafast transmission electron microscopy," Nat. Photonics **11**, 793–797 (2017).
[231]Y. Morimoto and P. Baum, "Attosecond control of electron beams at dielectric and absorbing membranes," Phys. Rev. A **97**, 033815 (2018).
[232]P. Baum and A. H. Zewail, "Attosecond electron pulses for 4D diffraction and microscopy," Proc. Natl. Acad. Sci. U. S. A. **104**, 18409–18414 (2007).
[233]M. Kozák, T. Eckstein, N. Schönenberger, and P. Hommelhoff, "Inelastic ponderomotive scattering of electrons at a high-intensity optical travelling wave in vacuum," Nat. Phys. **14**(2), 121–125 (2017).
[234]S. V. Yalunin, A. Feist, and C. Ropers, "Tailored high-contrast attosecond electron pulses for coherent excitation and scattering," Phys. Rev. Res **3**, L032036 (2021).
[235]P. Chaturvedi *et al.*, "Imaging of plasmonic modes of silver nanoparticles using high-resolution cathodoluminescence spectroscopy," ACS Nano **3**, 2965–2974 (2009).
[236]P. Das, T. K. Chini, and J. Pond, "Probing higher order surface plasmon modes on individual truncated tetrahedral gold nanoparticle using cathodoluminescence imaging and spectroscopy combined with FDTD simulations," J. Phys. Chem. C **116**, 15610–15619 (2012).
[237]A. S. Sheremet, M. I. Petrov, I. V. Iorsh, A. V. Poshakinskiy, and A. N. Poddubny, "Waveguide quantum electrodynamics: Collective radiance and photon-photon correlations," Rev. Mod. Phys. **95**, 015002 (2023).
[238]V. Di Giulio and F. J. García de Abajo, "Optical-cavity mode squeezing by free electrons," Nanophotonics **11**, 4659–4670 (2022).
[239]V. Weisskopf and E. Wigner, "Berechnung der natürlichen Linienbreite auf Grund der Diracschen Lichttheorie," Z. Phys. **63**, 54–73 (1930).
[240]D. Manzano, "A short introduction to the Lindblad master equation," AIP Adv. **10**, 025106 (2020).
[241]R. Ruimy, A. Gorlach, C. Mechel, N. Rivera, and I. Kaminer, "Toward atomic-resolution quantum measurements with coherently shaped free electrons," Phys. Rev. Lett. **126**, 233403 (2021).
[242]Z. Zhao, X. Q. Sun, and S. Fan, "Quantum entanglement and modulation enhancement of free-electron-bound-electron interaction," Phys. Rev. Lett. **126**, 233402 (2021).
[243]A. Pizzi, A. Gorlach, N. Rivera, A. Nunnenkamp, and I. Kaminer, "Light emission from strongly driven many-body systems," Nat. Phys. **19**, 551–561 (2023).
[244]O. Tziperman *et al.*, "Spontaneous emission from correlated emitters," arXiv:2306.11348 (2023).